PETROPHYSICAL INVESTIGATIONS OF THE ATZBACHER SAND, MOLASSE ZONE

2002

WURMBAUER KARIN

SUBMITTED TO THE INSTITUTE OF GEOPHYSICS
UNIVERSITY OF LEOBEN

DIPLOMA-THESIS FOR THE DEGREE DIPLOM-INGENIEUR
IN APPLIED GEOSCIENCES,
SPECIALISING IN APPLIED GEOPHYSICS

SUPERVISOR:

PROF. DR. J. SCHÖN

LEOBEN, NOVEMBER 2002

I DECLARE IN LIEU OF OATH THAT I DID THIS DIPLOMA
THESIS IN HAND AND BY MYSELF USING ONLY
LITERATURE CITED AT THE END OF THIS VOLUME

KARIN WURMBAUER

LEOBEN, NOVEMBER 2002

Acknowledgements

While working on this diploma thesis I have been supported by many people. I express my gratitude to all who helped me doing this work.

First of all, I would like to express my sincere gratitude towards my supervisor Prof. Dr. Jürgen Schön. I benefited substantially from his guidance and advice. I was supported when ever and where ever he could and thank him very much for his comprehension. I am very thankful that I had the opportunity to work with him.

Additionally, I would like to thank the department of Applied Geophysics of the JOANNEUM RESEARCH for giving me the opportunity to consolidate my knowledge in geophysics and work in a professional and friendly environment.

Many thanks to my family, in particular Mum and Dad for the financial, mental and loving encouragement to study 'Applied Geophysics'.
Special thanks to Claudia for her friendship, encouragement and supporting during my whole study.
I am grateful to all of my friends for support and friendship in all circumstances.

DIPLOMA-THESIS

INDEX OF CONTENTS

FIGURE INDEX

TABLE INDEX

Summary of results and interpretation

The problem of this thesis was if the Atzbacher Sands consist of one connected sedimentological and reservoir-physical unit or several independent hydrological units exist. An analyse of log data, petrophysical data and seismic data was necessary to answer the question and results in the following contributions:

a) There is an exact defined and by borehole measurements detectable boundary of the Ottnanger Schlier and the Atzbacher Sand. Thus the top of the Atzbacher Sand is exactly defined and is separated from the base of the Ottnanger Schlier by a huge clay package which leads to the ideal conditions of sealing the water from above as well as the Vöckla layers do this at the bottom of the Atzbacher Sand. Therefore the water is trapped in between the sand layers and reaching this enormous potential of an aquifer.

b) The Atzbacher Sands do not only consist of clean sand due to the sedimentary deposition.
The upper part of the Atzbacher Sands can be interpreted as a sequence deposited in subtidal sandwaves and muddy areas. The lower part of the Atzbacher Sands was deposited in fields covered by small sandwaves and ripples. The lowermost sections against the underlying Vöckla beds show sedimentary features of shallow subtidal to intertidal environments. The whole section of the Atzbacher Sands exhibits a transgressional sequence overlain by the muddy shelf sedimentations of the Ottnanger Schlier.

c) The diversity of the sedimentary characteristic of the Atzbacher Sands was investigated by statistical analyse using Semi-Variograms which show a clear evidence for clay layers in the sand packages. Especially the hole effect, which occurs very often when analysing the Atzbacher Sands, describe the periodicity of similar and less similar layers. Therefore it was possible to classify the wells into three different groups distinguished between the rate of dissimilarity at a lag-distance of 3m and the hole effect. A high dissimilarity value with a hole effect shows the well w03 and the wells w01, w20, w07 show lower dissimilarities without an hole effect. Low dissimilarity values with a hole effect are represented by the wells w06, w10, w12, w05.

d) Petrophysical measurements of the single Atzbacher facies A1, A2, A3, A4, B1, B2, C1, C2, C3 were determined. Good quality sands without too much influence and interbedding of clay are represented by the facies A2, A4, B1, B2 and C1. The others show much more layers of clay in the sand packages. Due to the petrophysical measurements and analysis three groups can be distinguished. There is on the one hand the Ottnanger Schlier facies and the Atzbacher Sand facies C3 with an high amount of clay in the samples, as well as high gamma-ray values and low resistivity values. The other group consists of the Atzbacher Sand facies A1, A2, A3, B1, B2, C1 and C2 with a medium amount of clay, gamma-ray values as well as medium resistivity values. The last group consists only of one Atzbacher Sand facies named A4 representing a nearly clean sand with a low amount of clay as well as a low amount of gamma-ray values and the resistivity value is very high.

e) The Ottnanger clay is compared to the Atzbacher Sand facies much more homogenous and this is confirmed by the variograms which show no hole effect at all and lower dissimilarities as the Atzbacher Sand facies does.

f) The Ottnanger Schlier facies contains sand lenses of hydrological importance.
This would explain the fact why some wells do not reach the Atzbacher Sand horizon and nevertheless receive water from an aquifer.
The borehole interpretation, especially the measurement of the gamma ray and the resistivity curves, shows the results of sand rich parties above the Ottnanger clay facies, most likely still belonging to the Ottnanger Schlier facies. This could not have been confessed because in that work the upper top of the Ottnanger Schlier has not been defined. These sand parties are not as constant compared to the sand of the Atzbacher facies and often pinch out in the lateral extension but giving the potential for a usable water horizon in a reasonable dimension.
An aquifer condition could be possible because the water has no chance to escape due to the sealing up property of the clay and marl rich layers and facies, so that there is a good chance for building a potential aquifer with all its requirements and ideal properties.

Zusammenfassung und Interpretation

Die Atzbacher Sande stellen im Bereich der oberösterreichischen Arteserprovinzen den wichtigsten Aquifer dar und dieser ist durch zahlreiche Hausbrunnen erschlossen. Es stellt sich die Frage ob die Atzbacher Sande aus einer sedimentologischen und reservoir-physikalischen Einheit bestehen oder aus mehreren unabhängig von einander existierenden Einheiten.
Dazu wurde im Rahmen der Diplomarbeit eine Analyse von Bohrlochdaten, petrophysikalischen Daten und seismischen Daten durchgeführt mit dem folgenden Ergebnis:

a) Es existiert eine exakt definierte und von den Bohrlochmessungen detektierte Grenze zwischen dem Ottnanger Schlier und den Atzbacher Sanden. Die Atzbacher Sande sind von der Sedimentabfolge des Ottnanger Schliers durch einen Tonhorizont getrennt, der lithologisch die Basis des Ottnanger Schliers bildet. Weiters sind die Atzbacher Sande an der Basis von den Vöckla Schichten begrenzt, die sehr tonführend sind. Diese Tonpakete stellen ideale Begrenzungen für die Atzbacher Sande dar und bilden damit die Grundlage für einen potentiellen Aquifer.

b) Die Atzbacher Sande selbst bestehen nicht nur aus reinem Sand sondern mächtige Lagen von Sand wechseln sich mit weniger mächtigen Tonhorizonten ab.
Die Atzbacher Sande bestehen aus drei sich lateral verzahnenden Lithofaziesgruppen. Die erste Faziesgruppe, die den hangenden Abschnitt der Atzbacher Sande einnimmt, wird als subtidale Rinnenfazies mit longitudinalen Sandbecken und dazwischen auftretenden subtidalen Sandwellenfeldern sowie pelitreichen Flächen interpretiert. Die zweite Lithofaziesgruppe, die den liegenden Abschnitt repräsentiert, scheint überwiegend von kleineren subtidalen Sandwellen- und Rippelfeldern aufgebaut zu sein, während die dritte Gruppe im unmittelbaren Übergangsbereich zu den liegenden Vöcklaschichten Hinweise auf ein seichtes subtidales bis intertidales Milieu aufweist. Das Gesamtprofil der Atzbacher Sande lässt sich als transgressive Serie interpretieren, die von der Schelfschlammfazies des Ottnanger Schliers überlagert wird.

c) Bestätigt wird diese lithologische Abfolge mit Semi-Variogrammen durch das Auftreten der sogenannten ‚hole effects', die generell ein Charakteristikum der Atzbacher Sande darstellen und damit die Periodizität der mehr oder weniger unterschiedlichen Schichten darstellen. Es war aufgrund dieser Analyse möglich die Brunnen in drei verschiedene Gruppen einzuteilen abhängig von der Größe der Unähnlichkeit in einem Lag-Abstand von drei Metern und dem Auftreten von 'hole effects'. Hohe Unähnlichkeitswerte mit einem 'hole effect' zeigte der Brunnen w03 und niedrigere Unähnlichkeitswerte ohne 'hole effect' repräsentieren die Brunnen w01, w20 und w07. Die Brunnen w06, w10, w12 und w05 zeigen ebenfalls niedrige Unähnlichkeitswerte jedoch weisen sie alle einen sehr deutlichen 'hole effect' auf.

d) Mittels der petrophysikalischen Messungen wurden die einzelnen Faziesproben A1, A2, A3, A4, B1, B2, C1, C2 und C3 untersucht. Gute Sande ohne übermäßigem Einfluss von Mergel oder Ton stellen die Faziestypen A2, A4, B1, B2 und C1 dar. Bei allen anderen ist eine rege Schichtung zwischen Sand und Tonlagen zu erkennen. Aufgrund von Korngrössenanalysen, Gamma-ray- und Widerstandsanalysen war es möglich die Atzbacher Sande und den Ottnanger Schlier in drei Gruppen einzuteilen. Die erste Gruppe wird repräsentiert von der Ottnanger Schlier Fazies und der Atzbacher Sand Fazies C3. Da sie einen hohen Tonanteil aufweisen zeigt die Gamma-ray Analyse hohe Werte an und die Widerstandswerte sind relativ gering. Die zweite

Gruppe besteht aus der Atzbacher Sand Fazies A1, A2, A3, B1, B2, C1 und C2. Sie weisen einen mittleren Tongehalt auf mit mittleren Gamma-ray Werten und wie zu erwarten mittlere Widerstandswerte. Die letzte Gruppe besteht nur aus einer Atzbacher Sand Fazies A4 und sie repräsentiert einen fast reinen Sand. Die Gamma-ray Werte sind dementsprechend niedrig und die Widerstandswerte erreichen ein Maximum.

e) Analysiert man die Variogramme des Ottnanger Tons, die die Atzbacher Sande am Top lithologisch von dem Paket des Ottnanger Schliers begrenzen, so sind keine Anzeichen von diesen 'hole effects' zu erkennen. Das bedeutet das der Ottnanger Ton ein mehr oder weniger homogenes Schichtpaket darstellt ohne lithologischem Fazieswechsel.

f) Die Ottnanger Schlier Fazies beinhaltet Sand Linsen von hydrologischer Wichtigkeit. Das würde die Tatsache erklären, warum seichtere Brunnen, die den Atzbacher Horizont nicht erbohren, trotzdem Wasser fördern können.
Die Bohrlochinterpretation, speziell die Gamma-Ray-Messungen und die Widerstandsmessungen, gibt eindeutig Hinweise auf Sandhorizonte, die sich überhalb der Atzbacher Sande befinden und wahrscheinlich noch zu der Fazies des Ottnanger Schliers gestellt werden können. Das konnte aber nicht sicher gesagt werden, da die Oberkante des Ottnanger Schliers nicht interpretiert wurde.
Diese Sandpakete sind nicht so konstant wie die der Atzbacher Sande sondern keilen nach mehr oder weniger großen Distanzen aus. Einige aber würden aufgrund ihrer analysierten Mächtigkeit sicherlich das Potential zu einem Aquifer erreichen, da diese Horizonte von Ton und Mergel Schichten begrenzt sind.

1 Conceptual Formulation

The Atzbacher Sands represent an important aquifer system in the artesian province in Upper Austria. The aquifer system has been made available for numerous of house-wells to get the water from. Therefore the hydro-geological characterization is necessary for a classification of the Atzbacher Sands due to securing the water-consumption in the next future.
The project is supported by the Oberösterreichischen Landesregierung.
The key-questions are if the Atzbacher Sands consist of one connected sedimentological and reservoir-physical unit or the case occurs that several independent hydrogeological units exist. It has to be worked out if it is possible to give an answer of the question on hydrological connection with petrophysical experiments and evaluations.

Due to the several productive wells in Upper Austria it is known that the depths of the wells are very variable and the question is if all the wells produce their water from the Atzbacher Sand horizon or from a horizon lying on the top of the Atzbacher Sands belonging to the Ottnanger Schlier facies. It is the case that the Atzbacher Sands show vertical splitting ups and therefore it has not been found an answer yet if all the wells really reach this horizon to take the water from. Some wells in the artesian province are already dry or it happened that some wells only give little water anymore in the last few years.

The next thing that has to be answered if the Ottnanger Schlier has the potential for an aquifer horizon due to the fact of clay rich lithology. The Atzbacher Sands are sealed up by the Ottnanger clay at the top and therefore leading to a potential aquifer horizon. But as I have mentioned before that the problem is not that easy due to irregularities concerning splitting up of the Atzbacher Sands.

For answering this hydrogeological problem it was necessary to take samples for petrophysical analysis. Different methods for characterizing the Atzbacher Sands as well as the Ottnanger Schlier came into operation like grain size distribution, electrical methods, gamma-ray investigations, Oedometer application, borehole-investigations and seismic analysis with already available data. With this methods different questions about porosity, electrical properties, seismic properties or the amount of radioactivity due to the occurrence of clay had to be answered as a contribution for sedimentological classification.

The measurement of borehole data like the resistivity and the gamma-ray depending on different lithology was necessary to distinguish between different facies to determine the border between the Atzbacher Sand to the Ottnanger Schlier or clay. Crossplots, restistivity versus gamma ray, give an additional information on the different lithologies that have to be distinguished and on the affiliation to a certain sedimentological horizon.
Due to the availability of seismic data in that area and the interaction with the borehole correlation it was possible to generate a stratigraphical model for giving a broad idea of the depth of the Atzbacher boundary to the upper lying Ottnanger Schlier for answering the question which well takes its water from the Atzbacher horizon and which does not even reach this special aquifer.
That evaluation was possible with a special program called RC$^{2®}$ and variograms were created with the use of the borehole data to give auxiliary information on the characterization of the Atzbacher Sand as well as the Ottnanger Schlier.

2 Geology: Tertiary area of the Molasse basin

In the Tertiary area, from the late Eocene period, the Molasse basin of the alpine-Carpathian foredeep was formed between Upper Austria and Salzburg.
The assymetric Molasse trough gets broader in the west and increasingly deep in the south. Under the Molasse basin lies the cristalline basin with paleocene and mesocene sediments. The Molasse basin has a thickness of more than 3500 m consisting of tertiary sediments. The Molasse basin in Upper Austria and Salzburg consists of the autochthonous Molasse, which proceeds in the south beneath the Alpine napes of the Flysch zone and Helvet zone. The Molasse basin is tectonically structured, with many intensive, polyphasic thrust faults until Lower Miocene.
The history of sedimentation of the Molasse basin started at Upper Miocene with the transgression of the sea to the north due to basin drawdown. Thereafter different facies types were formed. Above the Fischschiefer facies of Lower Oligocene marl lime was deposited in marine pelagic facies, followed by clay-marls and schlier sedimentations. At the same time sedimentation from the alpine zone concentrated in the south. Due to alpine uplifting in the Upper Oligocene the sedimentation in the west Parathetis was interrupted. In the east part of Bavaria and Austria the marine facies continued into the Upper Oligocene and much facies differentiation can be seen. In the north of the Molasse basin the clastical Linzer Sands were created.
To the south the Linzer Sands interlocked with the pelagic basin facies of the so called 'Älteren Schlier'. On the southern margin alpine gravel clastical, submarine boulder fans slid into the basin. At the beginning of the Miocene period the transgression of the Eggenburg started coming from the east. Above the Puchkirchner Series the Haller Series sediments were deposited. The Haller Series consist of pelite sediments from a basin facies with turbidite-like, sandy interstratification deposited in a shallow marine facies.
In Lower Miocene period the sea started transgressing once again, and the marine sediments of the Innviertler Group were formed. These were deposited above the Haller Series. The deposition took place in a sand-rich subtidal shallow marine environment with strong tidal activity. In eastern Upper Austria pelite- sediments from the Lower Ottnangium area were deposited, in contrast to the deposition on the western and northern Molasse basin margins. Here pelites, sands and gravels with strong vertical and lateral interlocking were deposited. During the Lower Ottnangium area the Robulus Schlier s.str. formed in the east and the Vöckla layers formed in the west part of the Molasse basin.
The Atzbacher Sands are located above the Vöckla layers, and these sands are connected to the Robulus Schlier s.str through a lithological transition. The Vöckla layers, the Atzbacher Sands and the Ottnanger Schlier are called Robulus Schlier s.l.. Transition and lateral interlocking occurs between these layers. At the same time the phosphorite-rich sands and fossil-rich gravel-sands were deposited in the north. The Rieder layers, the Mehrnbacher Sands, the Braunauer Schlier and the Treubacher Sands, all of which were deposited in the Middle Ottnangium period, are located above the Robulus Schlier s.l.. After the regression of the sea, brackish Oncophora layers were deposited during the Upper Ottnangium area. After the process of alluviation the erosion-phase began in Karpatium period and the surface-relief was created. Coal-rich lacustrine deposites were formed.
In Pliocene the deposition of the Molasse sediments restarted and the recent surface-morphology was formed.

2.1 OTTNANGIUM

The boundary between Eggenburg and Ottnang period is not determined precisely. In Ottnang the Hall formation was totally eroded in the north. Sandy-silty, mica pelite of the "Schlierfazies" were interrupted from sandy segments and erosions and strong tides dominated. When examining those sands they can be described as subtidal sandwaves influenced by tides.
The basis of the Atzbacher formation lies in the east. Two porous sand packages lie above the Vöckla formation and these are called the Atzbacher Sands. Submarine erosions are typical for the Atzbacher Sands and the Ottnanger Schlier.

Litoral and inner shelf:
Atzbacher Sands in north and northeast: subtidal sands influenced by strong tides

Shelf and slope:
Atzbacher Sands in south-west: sands and sliding of sands in channels
Ottnanger Schlier: sandy-silty, mica-like marl clay

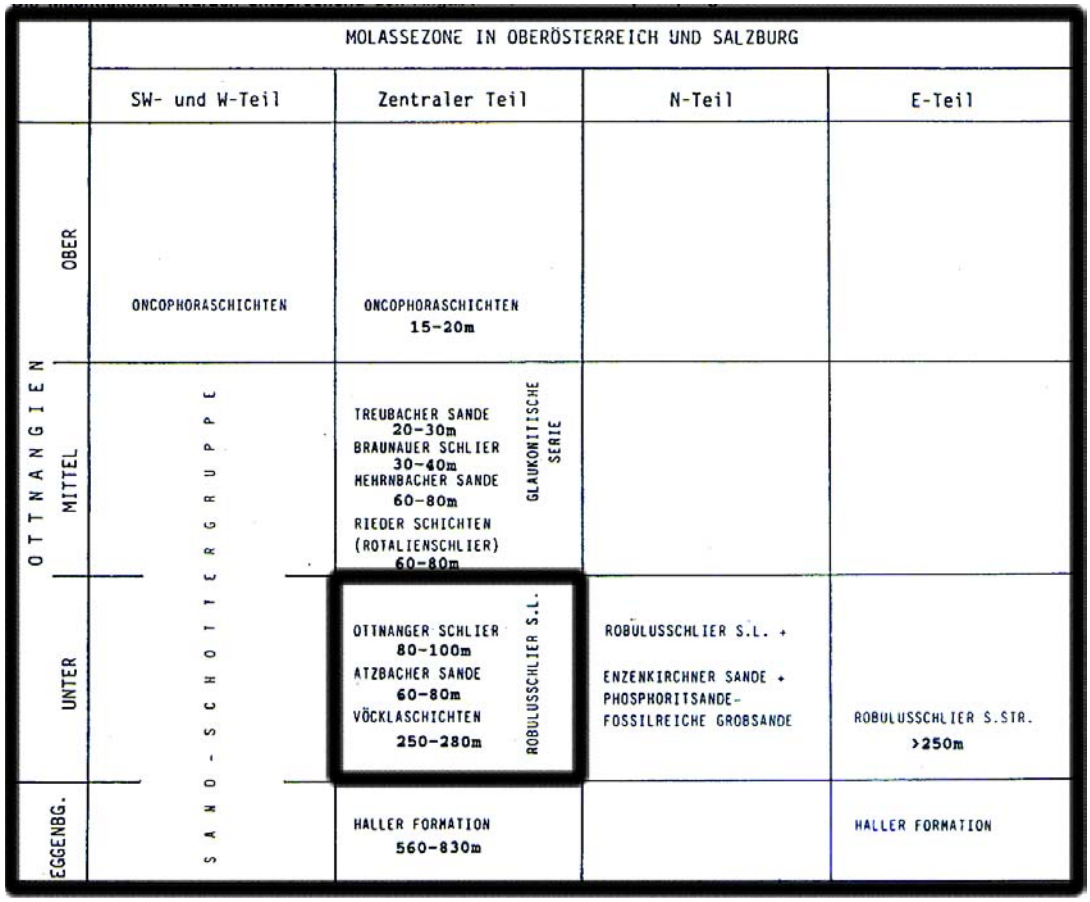

Figure 2.1: Timetable

The sedimentation of the Innviertler Group started at Lower Ottnangium and ended at Mittle Ottnangium (see Figure 2.1).
The Innviertler Group consists of the Vöckla layers, followed by the Atzbacher Sands, Ottnanger Schlier, Rieder beds, Mehrnbacher Sands, Braunauer Schlier, and finally Treubacher Sands.
The Vöckla layers, the Atzbacher Sands and the Ottnanger Schlier are respectively about 250 m, 80-100 m and 150 m thick.

2.1.1 VÖCKLA LAYERS

Powerful outcrops between the area of Vöcklamarkt and Alltang give a good insight into the petrophysical texture of the 250-280 m spanking rock series. It consists of grey marly, mica, sometimes strongly glauconitical, fine to middle grained sands with 20 cm thick lime-sand-stone concretions and single layers of clay-marl. To the east the sands become increasingly marly and a sand-clay-marl-sediment was formed, but the sands are still predominant.
The Vöckla layers are of local character.
The microfauna is fairly rare and in the marly deposition there are Robulus inornatus, Cibicides, Elphidium, Globigerina, and Nodosaria. The microfauna shows a marine character and the occurrence of the Rotalia beccarii shows a brackish touch (Krenmayr, 1991).

2.1.2 ATZBACHER SANDS

Concordant above the Vöckla layers bounded through transitions come the Atzbacher Sands. The thickness of the crossover is about 20 m and more and more sand layers occur and finally the Atzbacher Sands were formed.
They consist of light gray to greenish gray, fine to middle grained quartz-sands. Nearby both, 2-3 cm thin lime-sandstone-layers and thick lime-sandstone-concretions can be found. Thin clay-marl-layers are recognized, and they occur between the transition of the Atzbacher Sands and Vöckla layers and also between the Atzbacher Sands and the Ottnanger Schlier. Nearby, clay-marl pieces can be found in the sands, sometimes interspersed at random, and sometimes in layers. Isolated gravelstones and fine roadstones can be observed. The dipping of the layers can be determined by the thin clay-marl-layers. Mostly the sands show distinctive cross-bedding and false-bedding and sometimes the sands are strongly deformed due to subaquatic shear slides.
Shark´s teeth can sometimes be found as macrofossils and the microfauna consists of Foraminiferes and Globigerines.
Between the Atzbacher Sands and the Ottnanger Schlier no tectonic structure could be found.

2.1.3 OTTNANGER SCHLIER

The Ottnanger Schlier has a thickness of about 80-100 m. Characteristic for the Ottnanger Schlier are gray-greenishgray, bluegray, fine grained- mica clay-marls containing thin fine sand-layers and fine sand-clay-marls. These layers show very good bedding. That series represents the claymarl highest step of the whole miocene. The microfauna consists of Molluscs, Scaphopoda, Bivalvia, Gastropoda, Cephalopoda, Echinodermata and Robulus inornatus.

2.2 TIDAL-INFLUENCED SEDIMENTAION OF THE INNVIERTLER GROUP

Between the Atzbacher Sands three groups can be distinguished: facies A, B and C (see Figure 2.2). The sedimentary environment of the Atzbacher Sands can be described as a tidal influenced, sand rich, subtidal shallow sea deposit. The main part of the facies consists of subtidal channels and sandwave fields. Only on the transition to the Vöckla layers is there evidence of a tidal low water line. The facies A1-A4, B1-B2 and C1 are participating on the structure of the Atzbacher Sands. Facies C responds to the Vöckla layers and the facies C1-C3 displaces the crossover between the Atzbacher Sands and the Vöckla layers. Concerning the distribution of the facies in Figure 2.2 the top part (A1-A4) consists of a channel facies with longitudinal sand banks. In that region the coarse fraction dominates. The middle part of Figure 2.2, facies B1-B2, consists of subtidal little sand waves and ripplefields. The base of the Atzbacher Sands, facies C1-C4, shows, as mentioned before, a shallow subtidal to intertidal milieu.
The whole profile can be interpreted as a transgressive serie, with lateral interlocking of the two lithofacies. Above the Atzbacher Sands the Ottnanger Schlier facies follows. By looking at the wave-ripples it is possible to see that the Atzbacher Sands were formed at a depth of 20-25 m. The polymodal-dispersed paleo flow of the Atzbacher Sands is assymetric concerning the intensity of the tidal flow. The main flow in E-NE direction is due to a flood-current. Generally a transportation from W to E can be distinguished.
An alpine origin of the sediments can be distinguished because of the composition of the heavy minerals.
The whole sedimentation took place in a time of maximal extension of the Parathetis (Roetzel & Krenmayr, 1996).

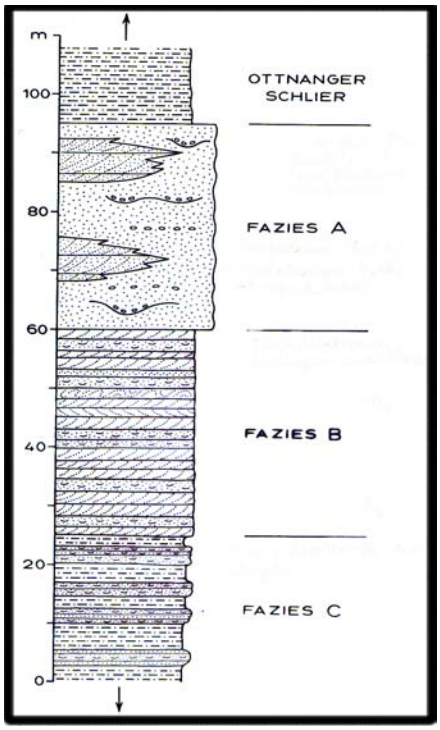

Figure 2.2: Facies classification of the Atzbacher Sands

3 Selection criteria of the different facies samples

For making petrophysical investigations on the different facies of the Atzbacher aquifer and the Ottnanger Schlier, samples had to be collected and examined.
The collection took place in Upper Austria (see Figure 3.1), where the Atzbacher Sand and the Ottnanger Schlier reach the surface and built some fantastic outcrops for taking samples to be examined. The outcrops were found due to the work of Peter Faupl and Reinhard Roetzel (1987) who marked the positions of the different facies types. Therefore it was possible to get a sample of each of the facies to examine the individual composition and other petrophysical properties.
The amount of the sample that was needed was a tup of about 10 l capacity. Due to the fact that the sand is not very compact the sample could simply be selected with a blade. I tried to collect the sample as representative as possible due to the inhomogenous composition. Sometimes it happened that the composition of the one facies outcrop was not homogenous. Small horizontal layers of compact clay material crosses the sand banks and therefore the collecting of a representative sample had to be careful. The fact of horizontal thin clay layers between the sand could not be considered in my laboratory experiments due to the fact that the structure gets destroyed when collecting a certain amount of sample into the tup. In this work no geophysical outcrop measurements were taken and so these horizontal and vertical petrophysical differences could not be taken into account but would not be of less importance.

Table 3.1 illustrates the sampling location of the different facies and a short description of the individual lithofacies.

LITHOFACIES	LOCATION	LITHOLOGY
A1	Sandpit Haslau	Sand of middle grainsize, fine-coarse gravel, peliteclasts, marl
A2	Sandpit Haslau	Sand of middle and coarse grainsize, pelitclasts, fragmental plant remains
A3	Sandpit Ottnang Fischer	Sand of middle and coarse grainsize, cm-mm thick marllayers, peliteclasts
A4	Sandpit Haslau SW Neue Welt	Peliteclasts (5-15cm)in a sandy matrix, clast-supported
B1	Sandpit W Roith	Sand of fine-middle grainsize, pelitelayers (cm-dm-range), peliteclasts
B2	Sandpit W Kogl	Sand of fine-middle grainsize, pelitelayers
C1	Sandpit Oberthumberg	Sand of fine grainsize with interbedding of silty marl in cm range
C2	Sandpit Kasberg	Sand of fine-middle grainsize with interbedding of silty marl in cm range
C3	Sandpit Timelkam	Sand of fine-middle grainsize with interbedding of silty marlin cm-dm range, sands in channels (0,4-1,5m)
Ottnanger Schlier	Sandpit Grieskirchen	Clay and marl with some local sandlayers

Table 3.1: Sampling location and lithofacies description

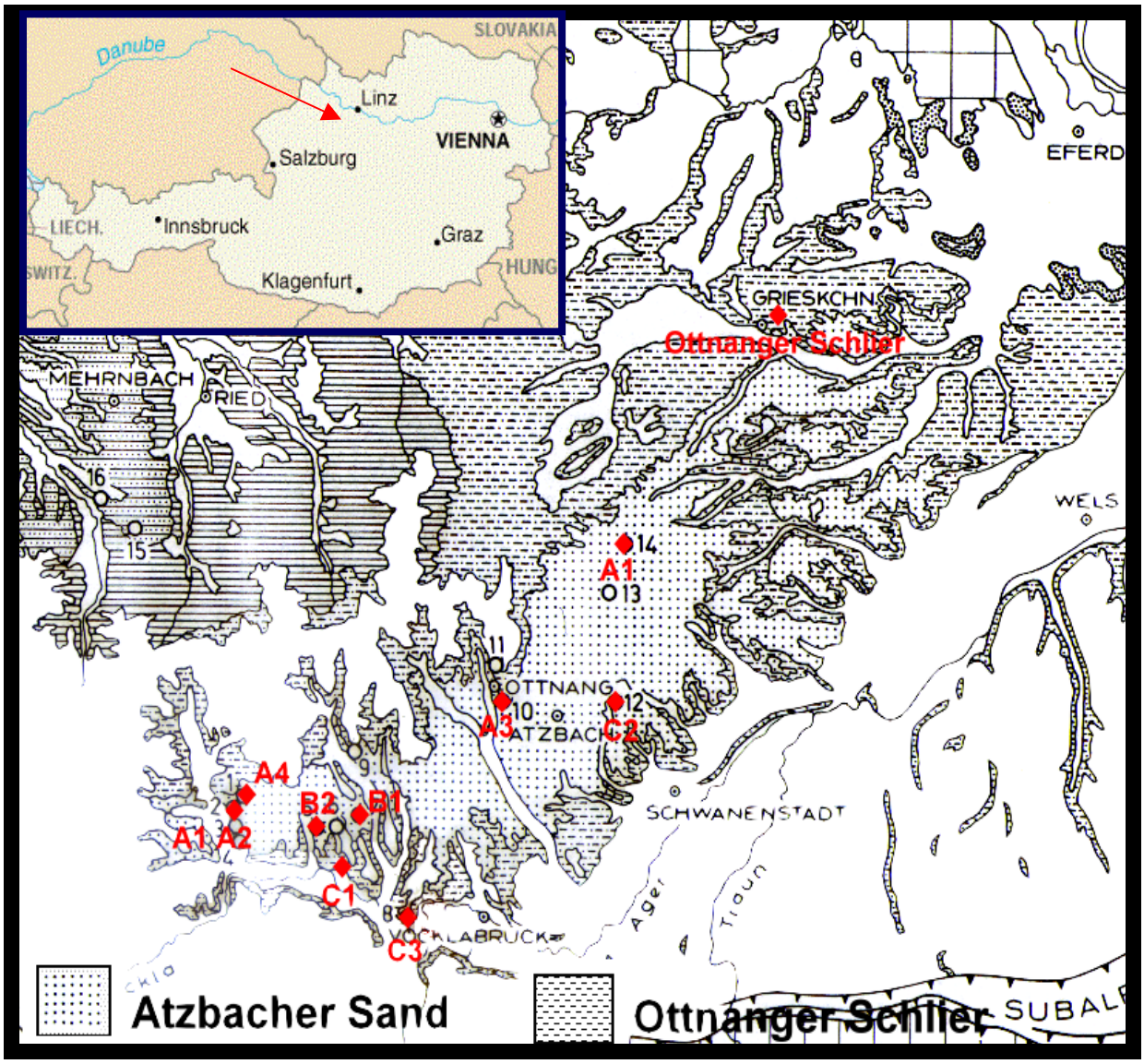

Figure 3.1: Stratigraphic map of the Molasse basin with its sampling locations

3.1 Description of the different facies locations

3.1.1 Location SP Haslau, facies A2 and A1

The lithofacies of A2 consists of massy sands with plain laminated mm-cm thick fragmental plant remains. These plant layers show a thickness of some dm but it is possible that they reach a thickness of over 90 cm. The sediments are mainly sands of middle grain-size with some gravelly sands and betimes peliteclastics occur (see Figure 3.2).

Figure 3.2: SP Haslau, facies A2

The south part of the SP Haslau consists of the facies A1 with its non structured massy sands. Predominantly they consist of glauconite- and mica-rich sands of middle grain size but fine and coarse grain sizes occur either. Remarkable are the broad erosive channel structures. Often the pelites are concentrated in those channel structures or occur in thin disconnected layers. If the pelite clasts reach a certain thickness then internal structures can be recognized. The bottom of the channel structure are often accompanied by cm large clastics. Sometimes intensive bioturbation and isolated coaly plantremains occur (see Figure 3.3).

Figure 3.3: SP Haslau, facies A1

3.1.2 Location SP Ottnang Fischer, facies A3

This facies consists of glauconite- and mica-rich sands of middle- and fine grainsize signed of wedge shaped cross stratification (sets). Secondarily trough-like sets can occur. The sets show a thickness ranging between 0,3-0,7m. The border between the sets are formed of the so called first-order or E1 surfaces, which consist of pelits with undulating or lense-like layers. These E1 layers cut off the top of the cross stratification in a erosive way and at the same time built the bottom set of the next cross stratification set. In between this set the so called E2 and E3 surfaces can be distinguished. The E3 surfaces bargain for the foreset beds and the E2 areas show a parallel trend or cut off the E3 surfaces in a discordant way. The E3 layers are very pelite rich and often show counter flow ripples and those of E2 consist mainly of mud drapes (see Figure 3.4 and Figure 3.5).

Figure 3.4: SP Ottnang Fischer, facies A3. Veritcal extension ~ 3m, horizontal extension ~ 4m

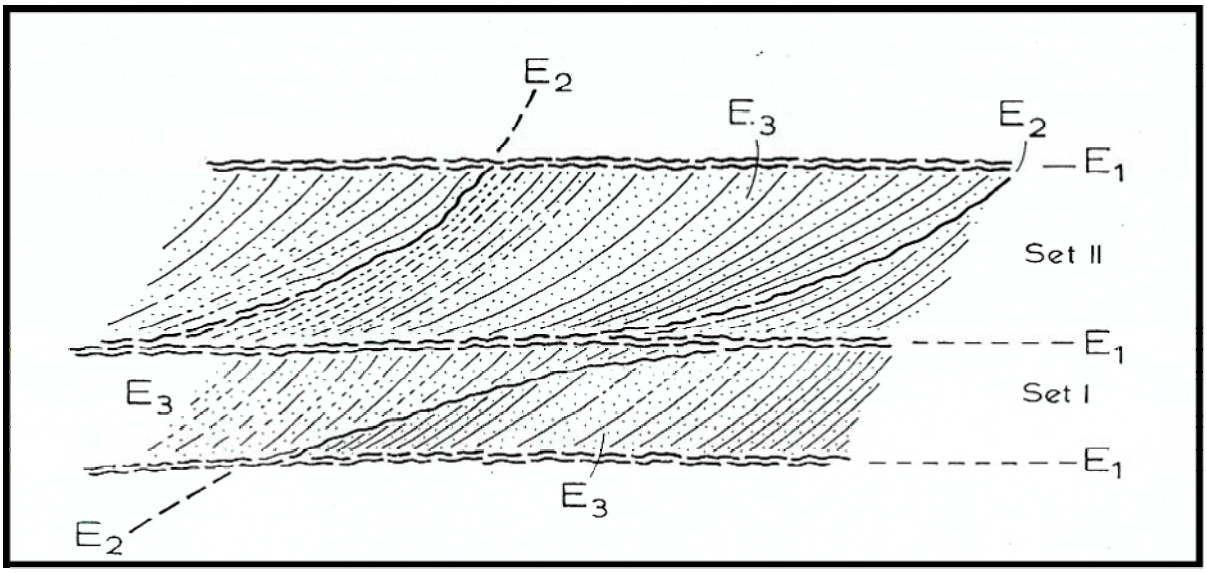

Figure 3.5: Schematical illustration of sandwave cross stratification (J.R.L. Allen ,1980)

3.1.3 Location SP Haslau SW Neue Welt, facies A4

That lithofacies consists of mica- and glauconite-rich, subrounded sands of middle and coarse grain sizes and sometimes sands of fine grainsizes occur. On the foreset beds of the cross stratification are incrustations of fine mica-rich sandy silts and subrounded silt-clasts. Remarkable are the coalify fossil wood rests which are enriched on the top of the foreset beds or when of larger sizes they occur isolated in the sediment.

3.1.4 Location SP Roith, facies B1

Lithofacies B1 consists of 5–30 cm thick mica-rich sands of middle and fine grain sizes with a high portion of glauconite. Between the sandbanks occur cm–dm thick silty marl-layers which are interrupted laterally or transform into petlite clastics. These marl-layers contain thin sandlayers or lenses of fine grainsize. Ripplelayers and cross stratification are typical for this facies. It is possible that dewatering structures occur and very often it happens that this leads to the destruction of the internal structures and that effect is called contorted bedding. Bioturbation only plays a secondary role but if they occur then they are mostly identified as mm thick tubes caused by worms (see Figure 3.6 and Figure 3.7).

Figure 3.6: SP Roith, facies B1

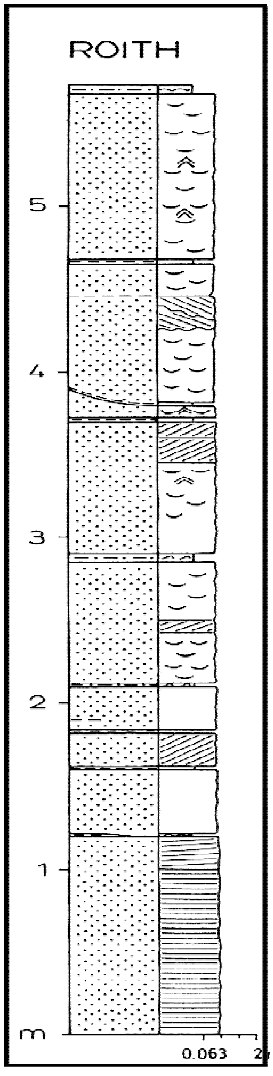

Figure 3.7: Detail profile and legend of the sand pit Roith (Faupl & Roetzel , 1987)

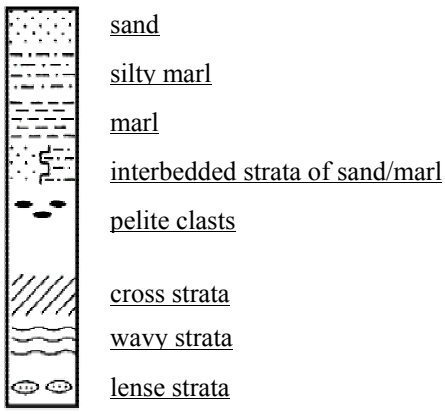

sand
silty marl
marl
interbedded strata of sand/marl
pelite clasts
cross strata
wavy strata
lense strata

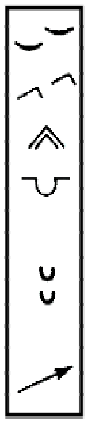

flaser strata
current ripples
wave ripples
convolute strata
bioturbation
direction of the paleo-current

3.1.5 Location SP W Kogl, facies B2

The facies B2 is very similar to facies B1. It consists as well of mica-rich and glauconite-rich sands of fine and middle grain sizes with inter-stratification of silty sands. In contrast to facies B1 the sand layers are hardly interrupted from silty marl-layers. Often ripple troughs and current ripple occur as well as herring bone bedding (see Figure 3.8).

Figure 3.8: SP W Kogl, facies B2

3.1.6 Location SP Oberthumberg, facies C1

This facies consists of intensive change between silty horizons and sands of fine grainsizes. Pelites are identified by their wavy layers and lense stratification. Bipolar internal structure could be observed in between the lense-like structures. The thickness of the finely grained mica-rich sands reaches a value of several cm and these structures are characterized by flaser bedding. When looking closer at the flaser structure they consist of pelite rich ripple troughs and current ripples. Isolated load casts have been noticed in those pelits. Bioturbation is very rare and this facies is very often in connection with facies A (see Figure 3.9).

Figure 3.9: SP Oberthumberg, facies C1

3.1.7 Location SP Kasberg, facies C2

Characterizing for this facies is an intensive change between mica-rich sands of fine grain sizes with silty marls. Strong bioturbation occurs very often. This facies is very similar to facies C1. The pelite horizons show a thickness of about 30 cm and show incrustions of sands. The pelite horizons show wavy bedding and lense stratification. Flaser bedding are characteristic for the sandy parts of the facies. Sometimes pelite clasts occur in the sands and also intensive bioturbation (see Figure 3.10 and Figure 3.11).

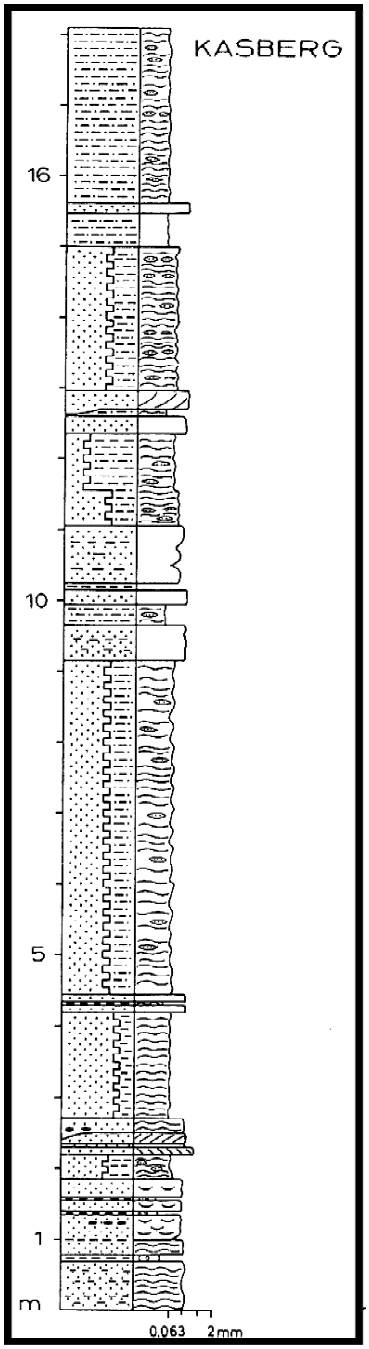

Figure 3.11: Detail profile and legend of the sand pit Kasberg (Faupl & Roetzel, 1987)

Figure 3.10: SP Kasberg, facies C2

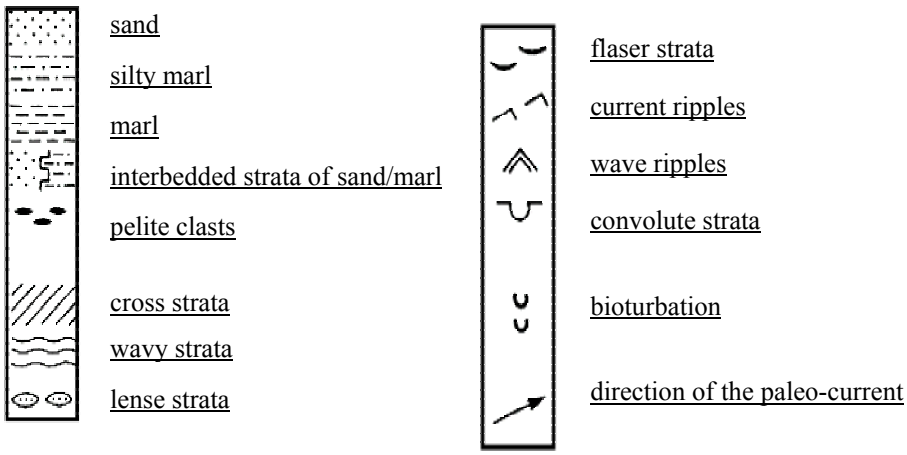

3.1.8 Location SP Timelkam, facies C3

The facies C3 is very similar to C2 and shows as well an intensive change between mica-rich sands of fine grain size with silty marls. The sedimentary structures contain flaser bedding and lense stratification. Sandy interbeds show ripple stratification. The big difference to facies C2 is the occurrence of erosive sand sections. The whole facies shows an intensive bioturbation like mm-thick tubes with pelitic walls (see Figure 3.12 and Figure 3.13).

Figure 3.12: SP Timelkam, facies C3. Vertical extension ~ 40 cm, horizontal extension ~ 30 cm

Figure 3.13: Detail profile and legend of the sand pit Timelkam (Faupl & Roetzel, 1987)

3.1.9 Location SP Grieskirchen, Ottnanger Schlier facies

The Ottnanger Schlier mainly consists of fine grained-mica claymarls containing fine grained sand-layers and fine grained sand-clay-marls. These layers show very good bedding and often smaller and larger sand-lenses can be seen (see Figure 3.14 and Figure 3.15).

Figure 3.14: SP Grieskirchen, Ottnanger Schlier facies

Figure 3.15: SP Grieskirchen, Ottnanger Schlier facies

4 Investigations on the collected samples

For investigations on the selected samples I used methods like granulometric evaluation, gamma ray spectrometry, resistivity measurements and Oedometer investigations.
With the granulometric evaluation it was possible to answer the question of grain size distribution for each single facies of the Atzbacher Sands as well as for the Ottnanger Schlier. This leads to important statements about the clay content in the samples.
The resistivity measurements lead to the determination of the electrical conductivity, the formation factor F, which is a hint for the porosity of the samples. It is also related to the affection of clay in the sample.
The gamma ray measurements give information about the intensity of radioactivity, which is affected by the amount of clay in the sample.
With the interaction between resistivity, gamma ray and granulometric measurements it is possible to classify the Atzbacher Sands and Ottnanger Schlier sedimentological.
The next method that is used is the Oedometer application which gives important information about the changing of porosity with increase of pressure, the changing of vertical elongation and resistivity with an increase of pressure, the dependency of the elastic parameter or modulus and the changing of resistivity or conductivity when loading with weights.
When loading the sample with weights the depth can be determined due to corresponding to a certain pressure on the sample and the variation of the parameters with depth can be displayed.

4.1 Granulometric Method

4.1.1 Description of sieve analysis

The amount of one sample necessary for sieving is about 150 g. Cohensive samples, due to their clay content, have to be disperged with H_2O_2. That was applied at the samples B2, C1, C2, C3 and Ottnanger Schlier.
The wet sieving starts with a wire size of 1000 µm, followed by 500 µm, 250 µm, 125 µm and 63 µm and grain sizes smaller than 63 µm are collected in a bucket.
The sieving takes as long as the water is clean. The different grain sizes are desiccated in a drying oven and have to be weighed afterwards and evaluated.

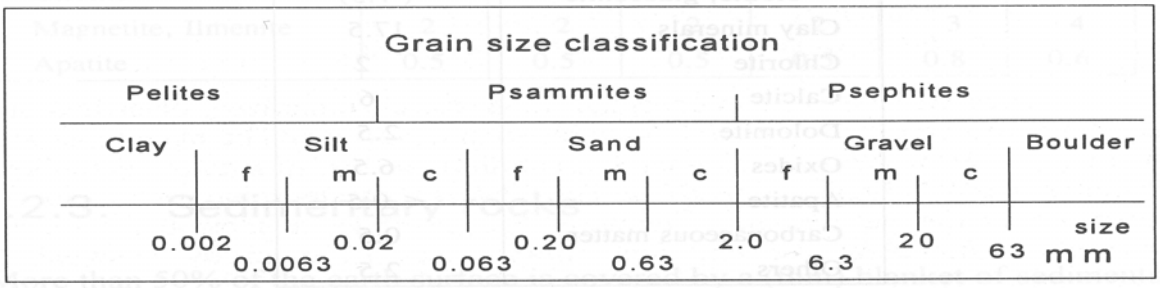

Figure 4.1: Grain size classification

4.1.2 Evaluation

4.1.2.1 Histogram

Sample A1 represents the top lithofacies of the Atzbacher Sands and demonstrates the salient to the Ottnanger Schlier. Due to that position the clay content is relatively high showing a value of more than 11%. The range of 250-125 µm displays with more than 56% the highest fraction in the sample (see Figure 4.2).

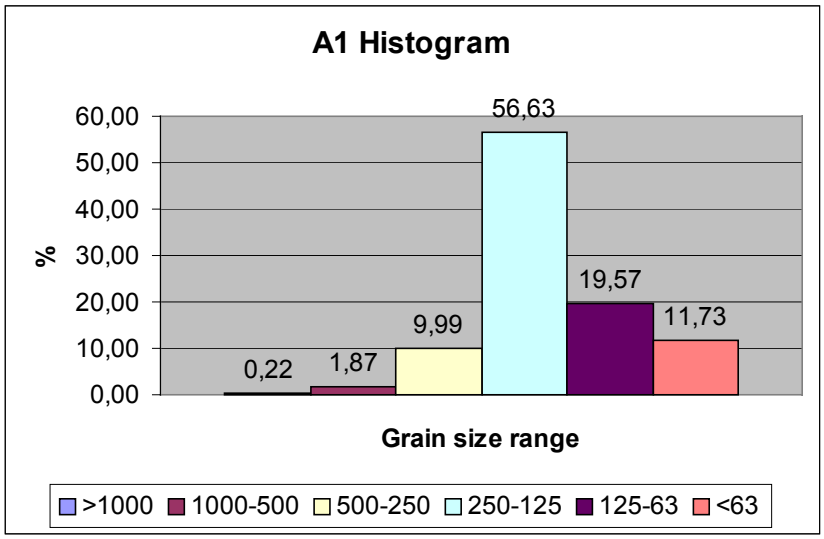

Figure 4.2: Grain size histogram of facies A1; grain size in µm

Beneath the lithofacies A1 lies the facies A2 and representing a cleaner sand with only about 4 % clay content. Again, the grain sizes of 250-125 µm takes the main position (see Figure 4.3).

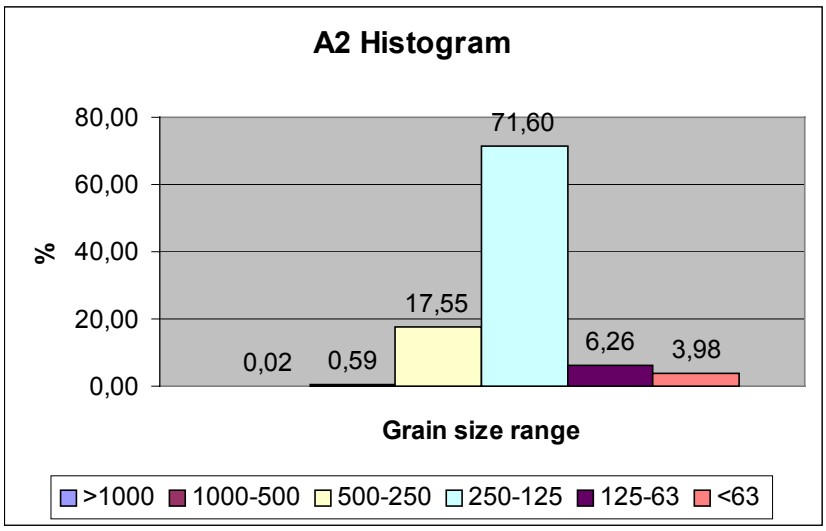

Figure 4.3: Grain size histogram of facies A2; grain size in µm

Lithofacies A3 contains much higher values of clay about 18% and more than 50% received of grain size 250-125 µm (see Figure 4.4).

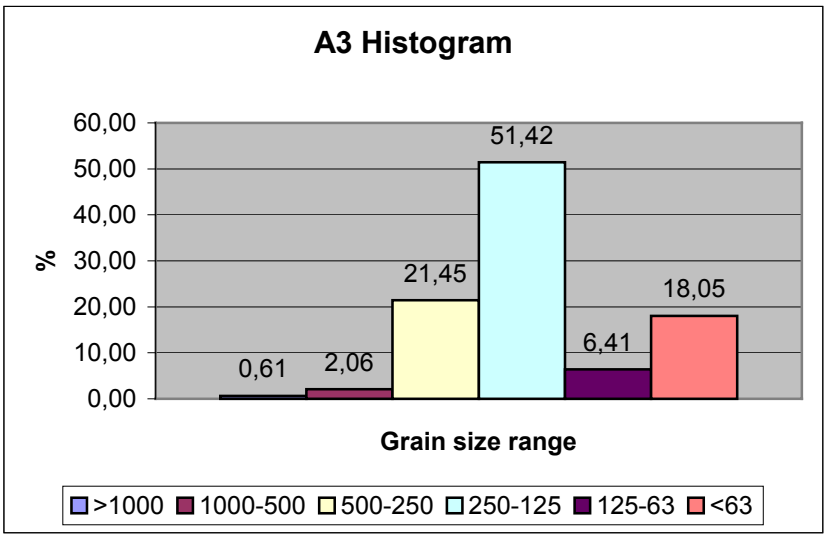

Figure 4.4: Grain size histogram of facies A3; grain size in µm

Facies A4 is a good demonstration for a nearly clean sand without much influence of clay in the sample. Less than 4% grain size of <63 µm represents high quality for a groundwater horizon. More than 50% of the whole composition is represented by the grain sizes between 500 and 250 µm. Compared to the other A-facies of the Atzbacher Sand, the sample contains a coarser sand composition (see Figure 4.5).

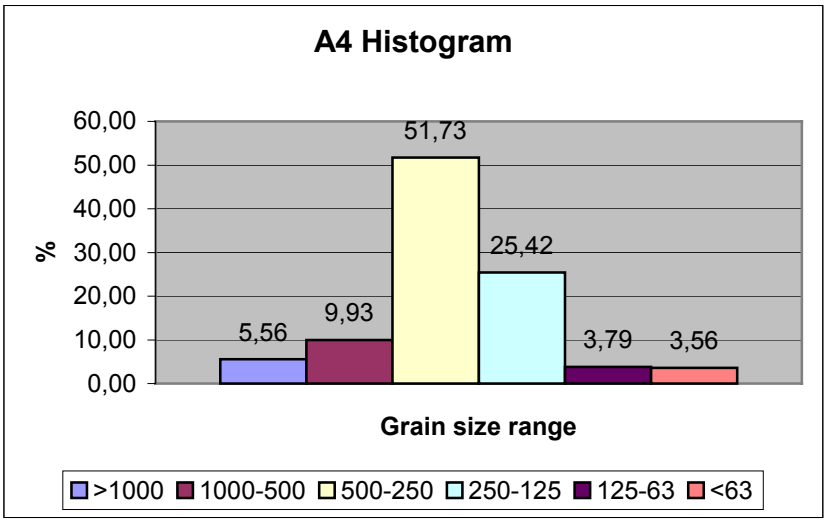

Figure 4.5: Grain size histogram of facies A4; grain size in µm

B1 shows a very similar composition of grain sizes as sample A2 does. The difference is that in this facies no grain sizes above 500 µm occur, but the sand contain more than 76% of grain sizes between 250 and 125 µm (see Figure 4.6).

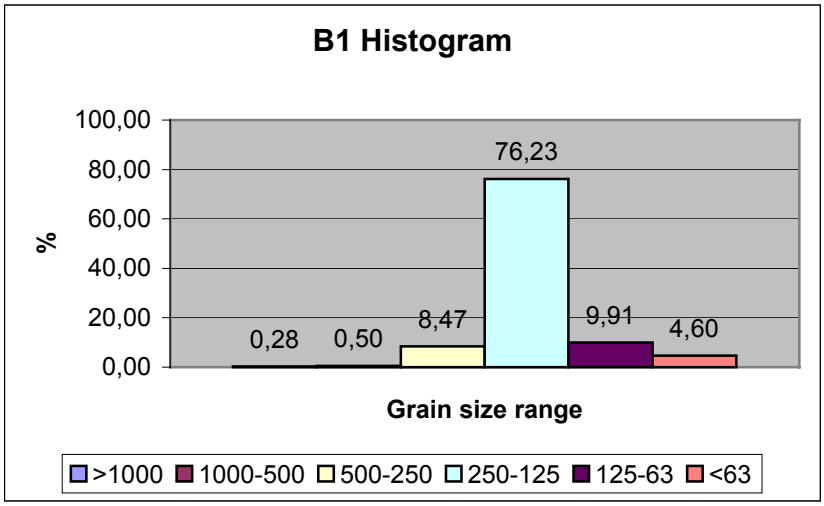

Figure 4.6: Grain size histogram of facies B1; grain size in µm

B2 contains very little parts of grain sizes above 500 µm and the main composition is represented by grains ranging between 250 and 125 µm. The fraction of clay increases slightly and shows an amount of more than 6% (see Figure 4.7).

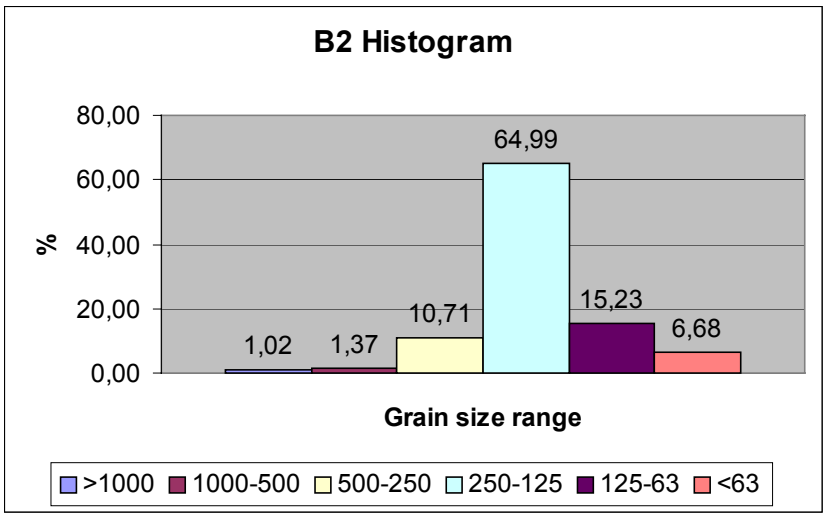

Figure 4.7: Grain size histogram of facies B2; grain size in µm

About the same clay-fraction as sample B2 shows this facies. But the amount of fraction between 500 and 250 µm is with more than 35% very high. The fraction of 500 µm and above is still low (see Figure 4.8).

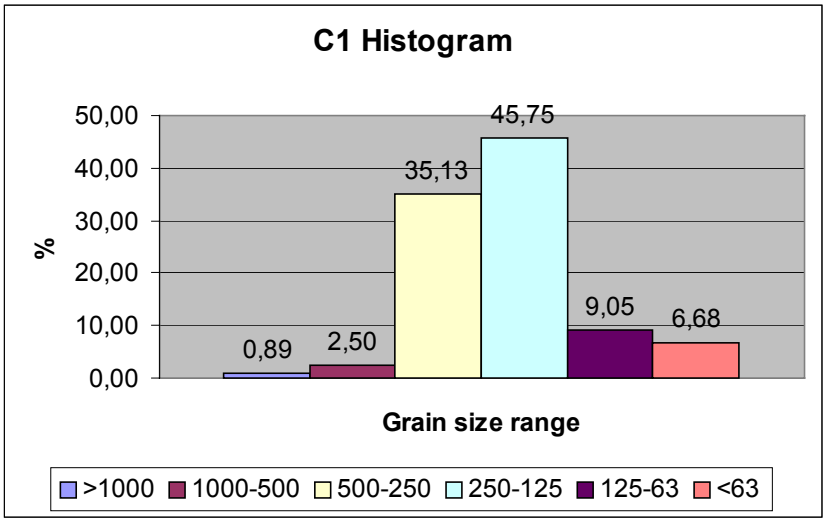

Figure 4.8: Grain size histogram of facies C1; grain size in µm

The main fraction of facies C2 is represented by the grain sizes ranging between 250 and 125 µm. The clay content shows a value of more than 8% (see Figure 4.9).

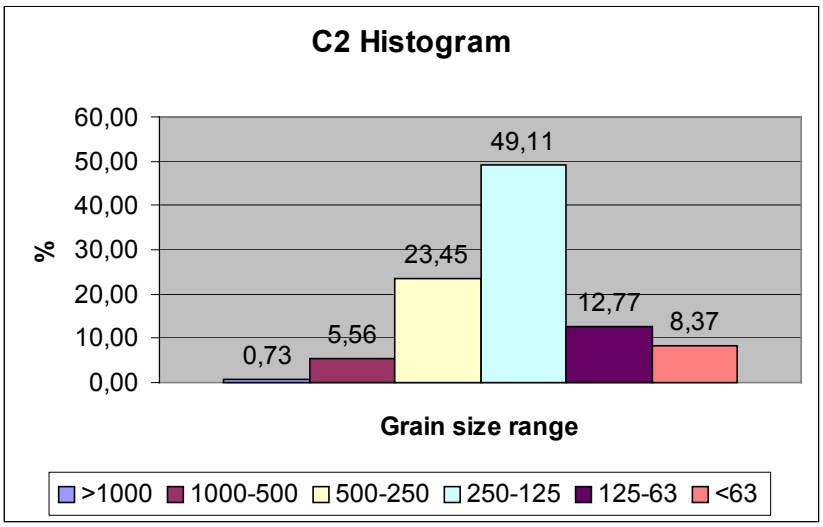

Figure 4.9: Grain size histogram of facies C2; grain size in µm

The main composition, with about 72%, lies in a range between 500 and 125 µm. The clay content shows with 14,5 % a high fraction part. Grain sizes above 500 µm show a small part in that facies (see Figure 4.10).

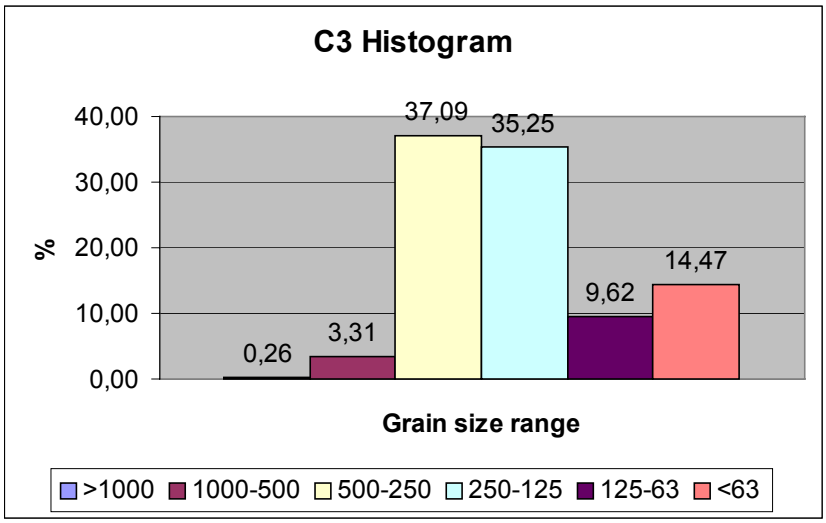

Figure 4.10: Grain size histogram of facies C3; grain size in µm

A very interesting composition displays the histogram of the Ottnanger Schlier facies. The smaller the grain sizes the higher the fraction part in the sample. The clay content reaches a value of more than 38%, which represents the highest part compared to all other facies (see Figure 4.11).

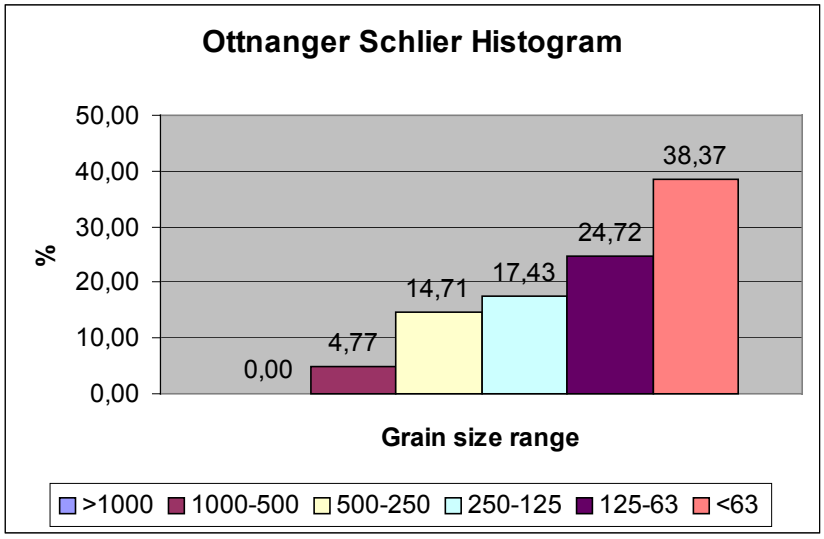

Figure 4.11: Grain size histogram of facies Ottnanger Schlier; grain size in µm

The facies A1 of the Atzbacher Sands represents the salient to the Ottnanger Schlier and the whole C facies the salient to the Vöckla-layers. That is an explanation for high clay contents in the samples, due to the fact that the Ottnanger Schlier as well as the Vöckla layers consist of high clay contents and are representing the sealing to the Atzbacher formation. The transition to the Ottnanger Schlier and the Vöckla layers is gradually and not of tectonic influence. The highest clay contents of the Atzbacher Sand facies appear in the samples A1,

A3 and C3. All the others show a clay content lower than 8,4%. The whole B-facies appears to have the smallest clay content in the samples.
By normalizing the clay part of 100%, Figure 4.12 shows the distribution of the clay part for each facies.

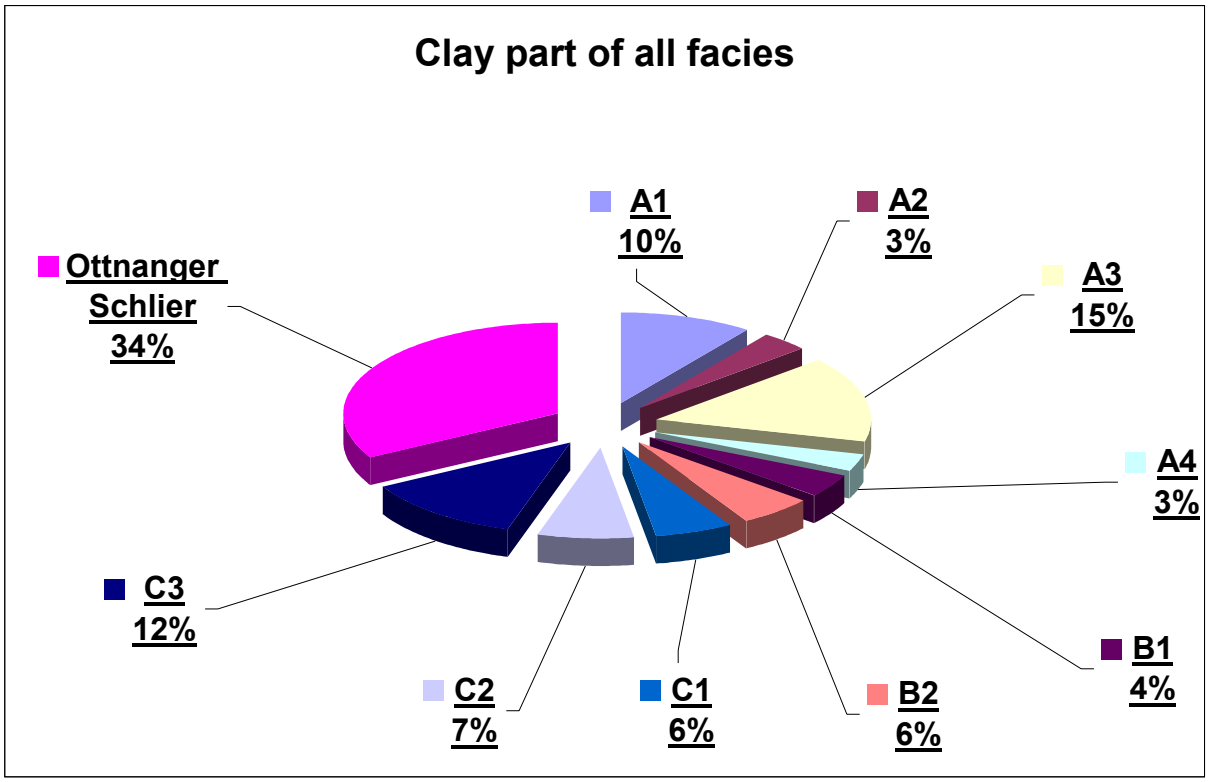

Figure 4.12: Relationship between the clay part of all facies

4.1.2.2 Cumulative Curve

Looking at the cumulative curve all lines lie very close together with two exceptions, the line representing the Ottnanger Schlier and the Atzbacher facies A4. The Ottnanger Schlier curve shows very high values < 63 µm and the curve is much flatter compared to the others. That means that the influence of the grain sizes larger than 63 µm is not very high. The curve representing facies A4 shows trends the other way around. Very low values at small grain sizes and high values at big grain sizes. All the other lines, representing the other facies, show more or less the same ascending slope (see Figure 4.13).

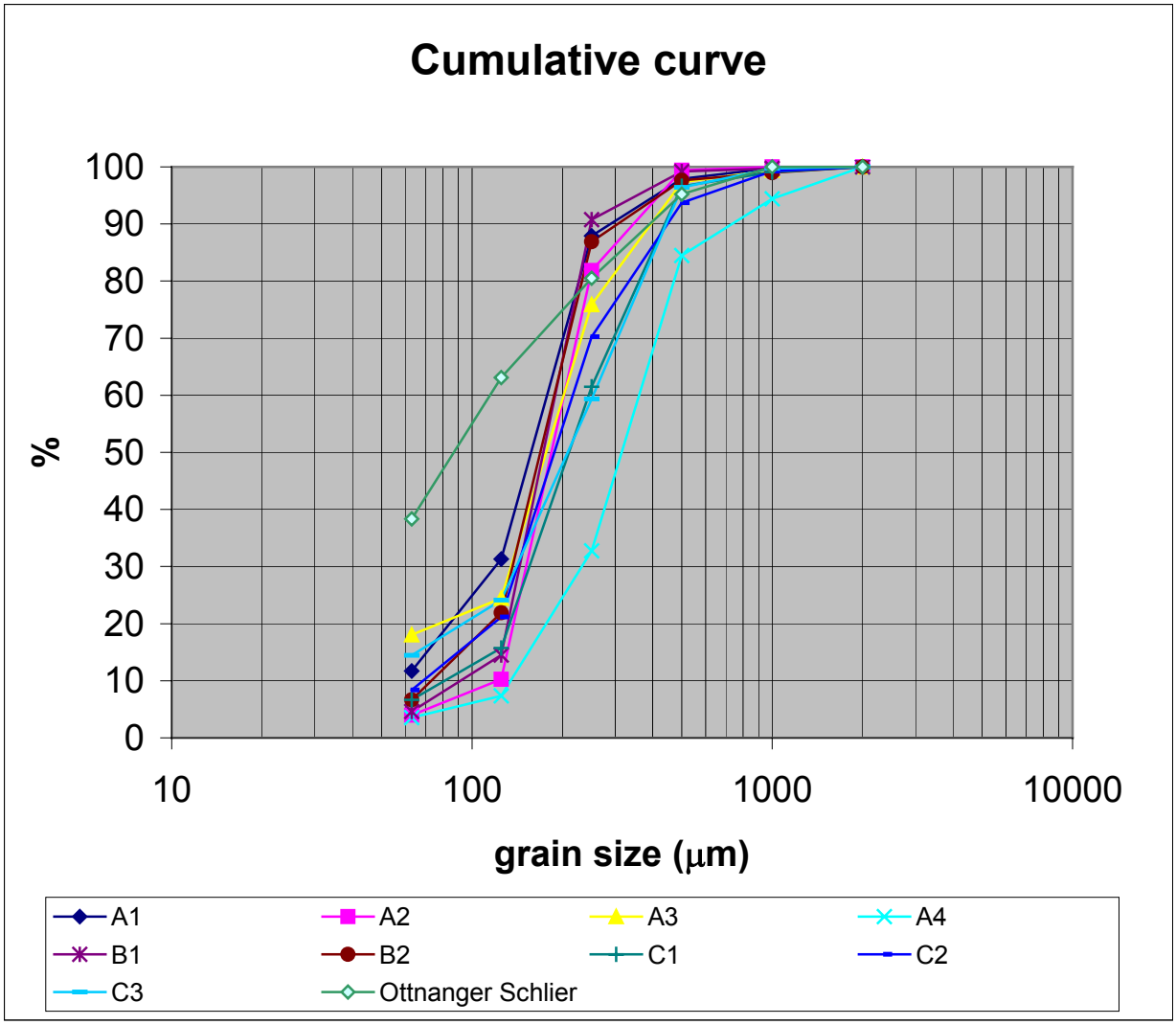

Figure 4.13: Cumulative curves of all facies types

4.2 Gamma-ray method

4.2.1 Description

The gamma-ray experiment was made with the nanoSPEC Version 5.1 equipment of Target Systemelectronic GmbH (see Figure 4.15).
The single lithofacies of the Atzbacher Sands were measured for further classification.
The program for evaluation is called winTMCA (see Figure 4.17).
The measurement took place in a lead shielding for better results without radioactive background radiation.

The nanoSPEC apparatus is a MCA (Multi Channel Analyzer) combined to a PMT-unit (Photo Multiplier Tube) for Szintillation-Detectors.

The energy of the particles are transmitted to the crystal detector (NaJ) and emanated as light-flashes. The light gets collected in the PMT and the energy spectrum can be seen on the computer (see Figure 4.16). Due to the high density and the high atomic mass NaJ-crystals are the best for such measurements (see Figure 4.14).

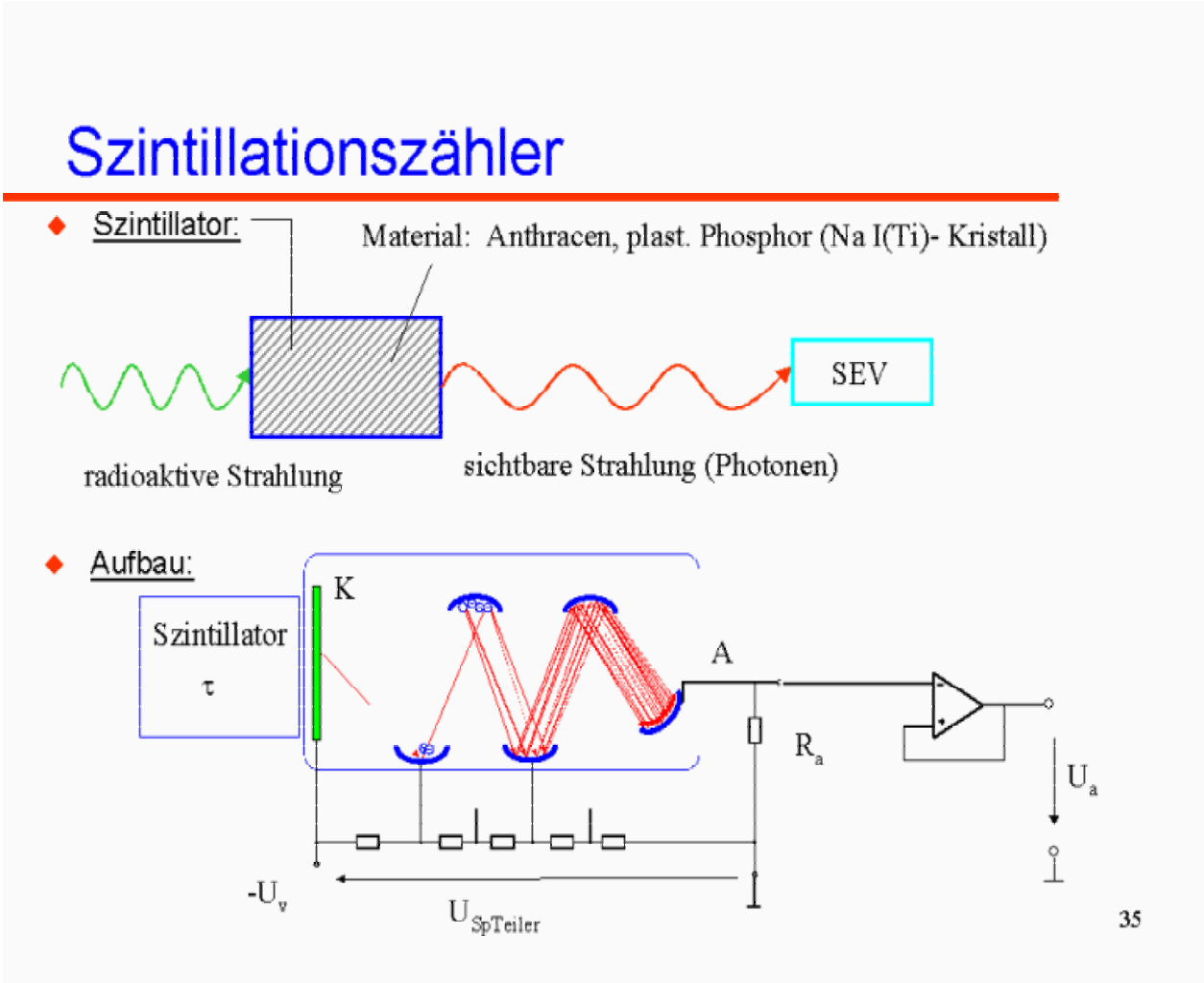

Figure 4.14: Functionality of the Szintillations-Detector

Figure 4.15: Gamma ray equipment; the detectortube (black) is connected with the sample holder (red) and the measurement takes place inside the Pb- shield (white).

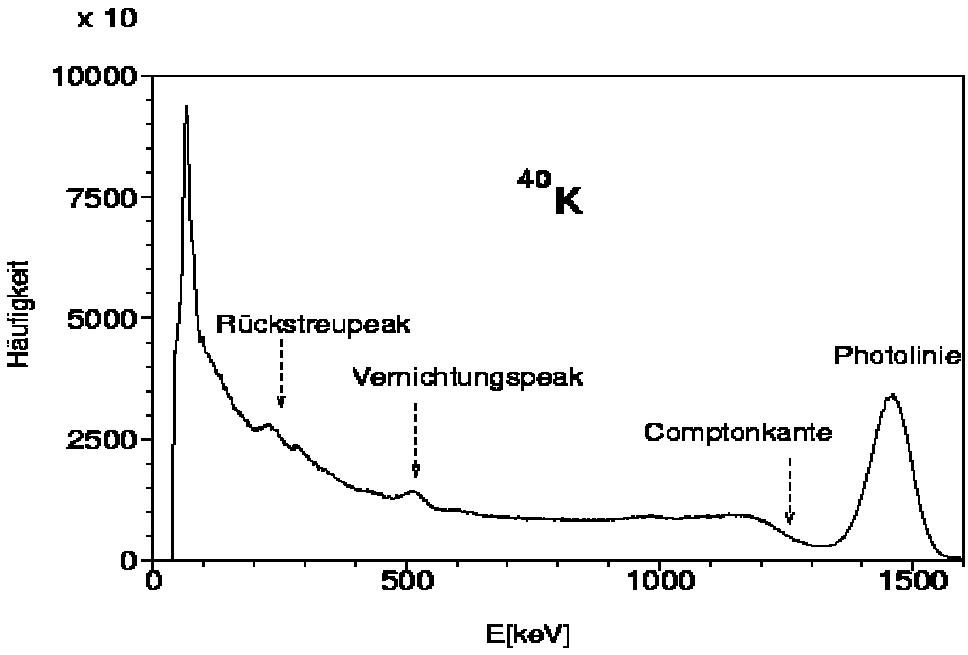

Figure 4.16: Typical spectrum of K^{40} measured with NaJ Detector

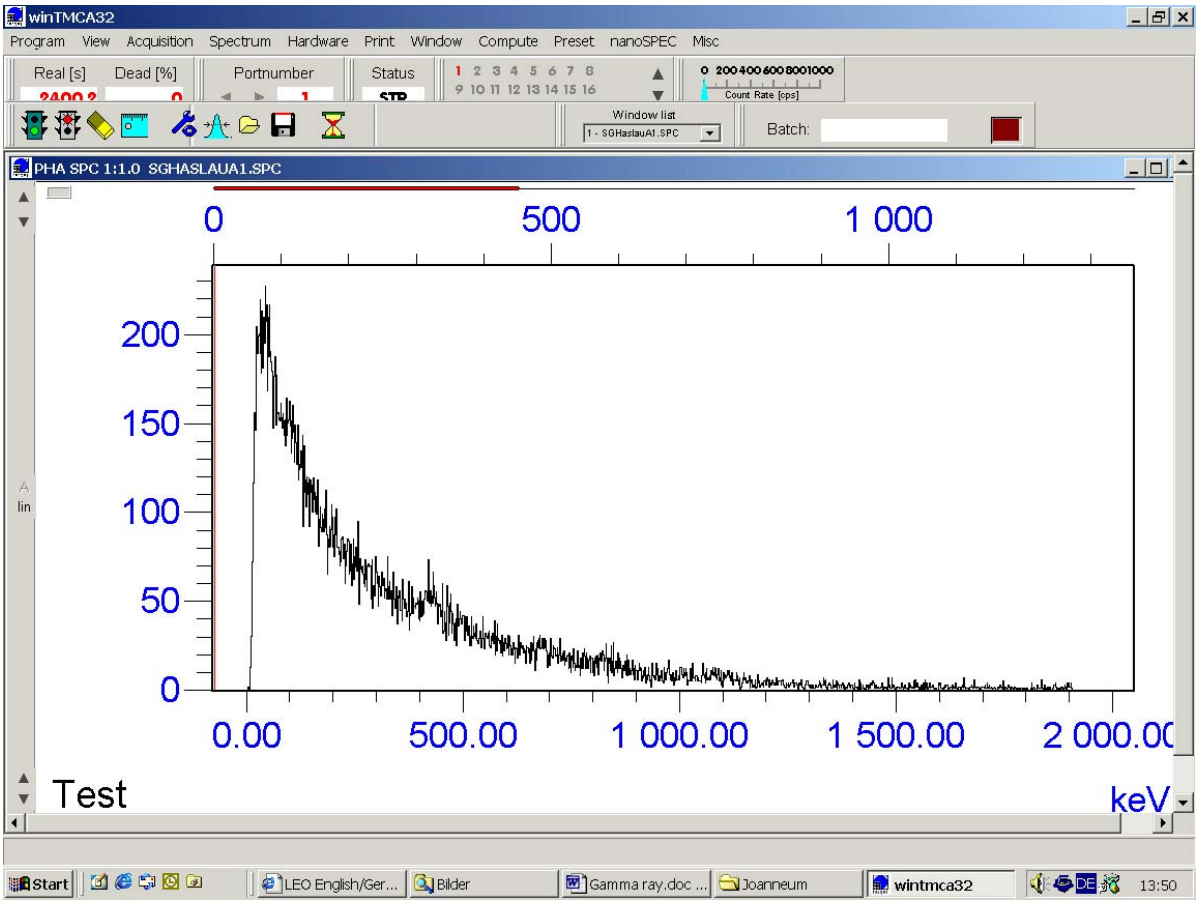

Figure 4.17: winTMCA – program

Each measurement took 2400 s or 40 min and the x-axis gives information about the energy in keV and the y-axis represents the counts per channel.
For analysis the area beneath the curve had to be integrated and is specific for each lithofacies of the Atzbacher Sands as well as for the Ottnanger Schlier facies.

4.2.2 Theoretical background

Gamma as X-rays are highly penetrating electromagnetic radiations characterized by wave lengths in the range of 10^{-7} – 10^{-11} cm, consequently, by frequencies ranging from 10^{17} to 10^{21} 1/sec. Figure 4.18 and Figure 4.20 show the wave length, frequency ranges and energy in electron volts of the electromagnetic spectrum.
Formula by Planck :

$$E = h\nu = \frac{hc}{\lambda}$$

E = *photon energy*
H = *Planck constant*
c = *velocity of light*
ν = *frequency*
λ = *wave length of the radiation*

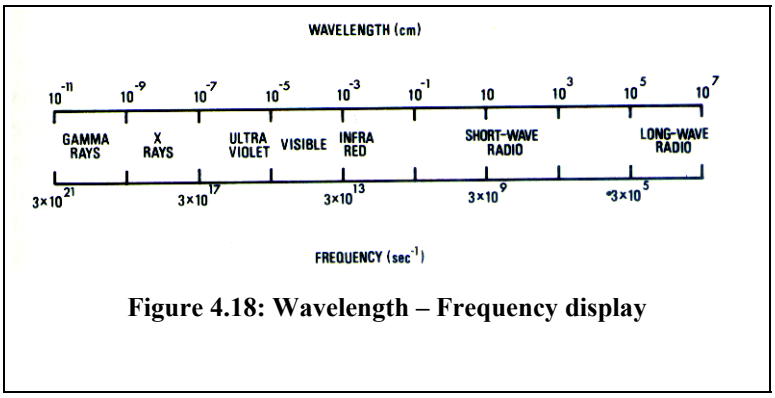

Figure 4.18: Wavelength – Frequency display

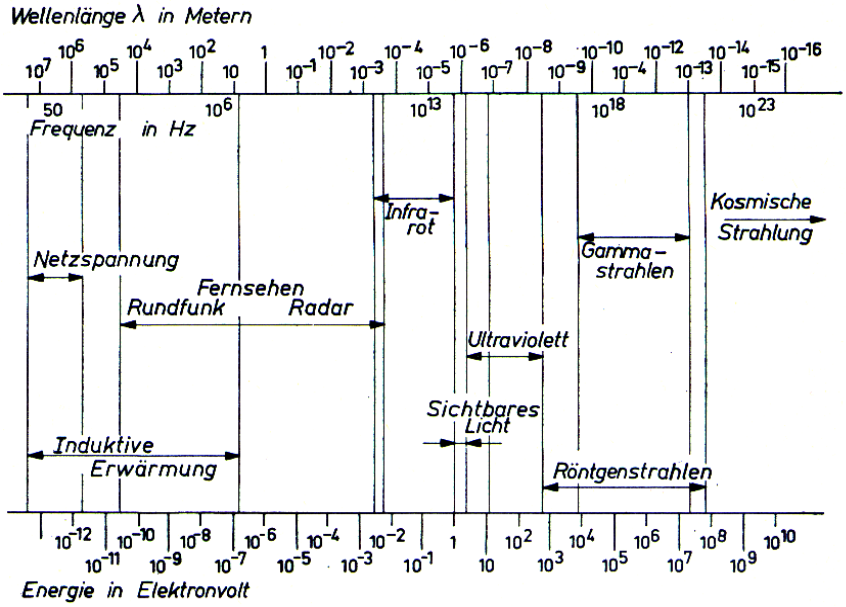

Figure 4.19: Wavelength – Energy (eV) display

Gamma and X-ray energies are usually expressed in electron volts (eV). One electron volt is the energy acquired by a charged particle carrying unit electronic charge when it is accelerated through a potential difference of one volt.

4.2.3 Evaluation

The measurement of the single lithofacies ranges from 0 to about 2000 keV on the energy-axis and shows values from 0 to about 250 counts at the channel-axis.
The area beneath the curve has been integrated and the integrated values are marked as IV, the Integration-value, and represents the sum of the single counts measured from all channels.
The channels are displayed at the top of the diagram as the second x-axis. Due to the clay content this method is ideal for classifying and distinguish between the single facies (see Figures 4.20, 4.21, 4.22, 4.23, 4.24, 4.25, 4.26, 4.27, 4.28, 4.29).

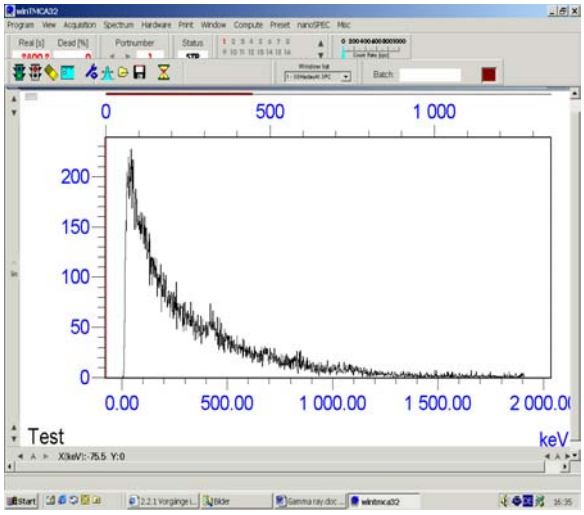

Figure 4.20: shows the result of A1-lithofacies, IV=35448 counts/40 min

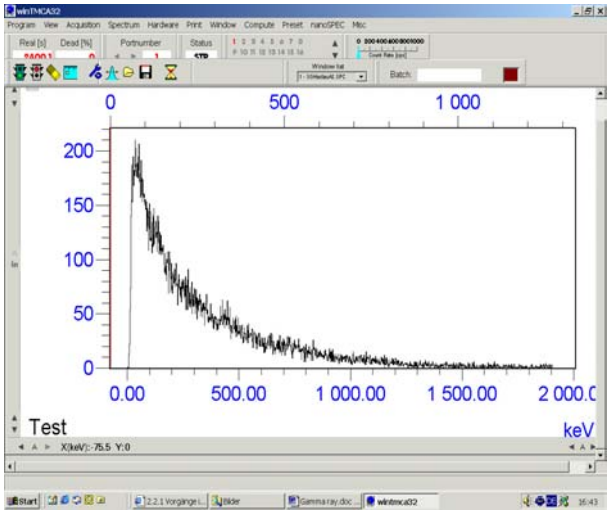

Figure 4.21: shows the result of A2 – lithofacies, IV = 34650 counts/40 min

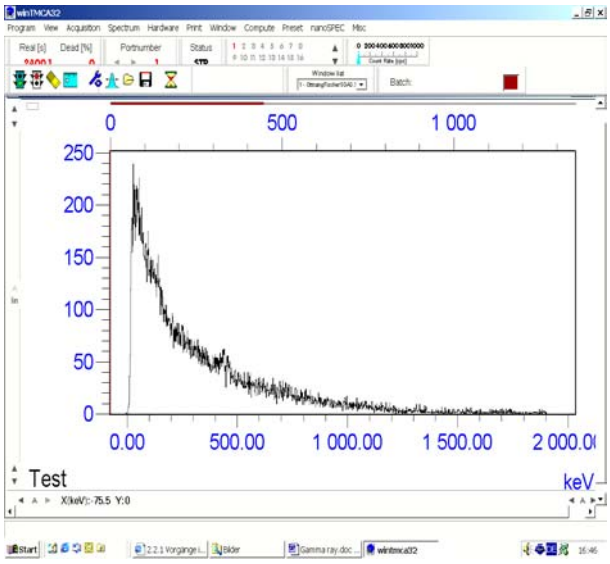

Figure 4.22: shows the A3-lthofacies, IV = 35769 counts/40 min

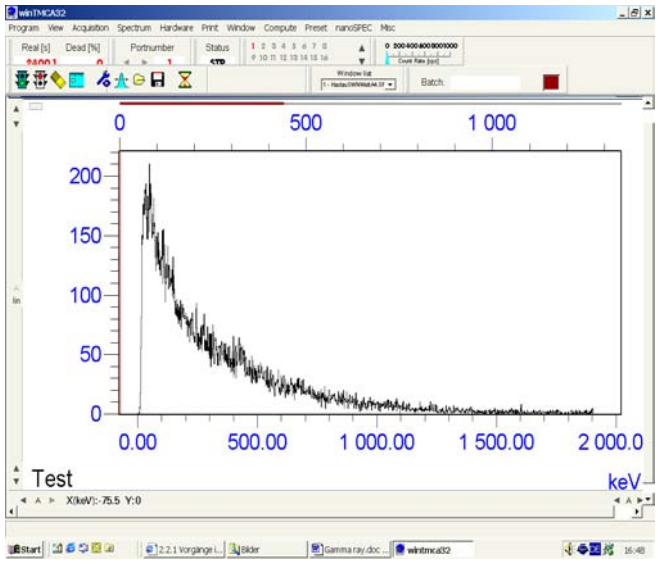

Figure 4.23: shows the A4-lithofacies, IV = 32749 counts/40 min

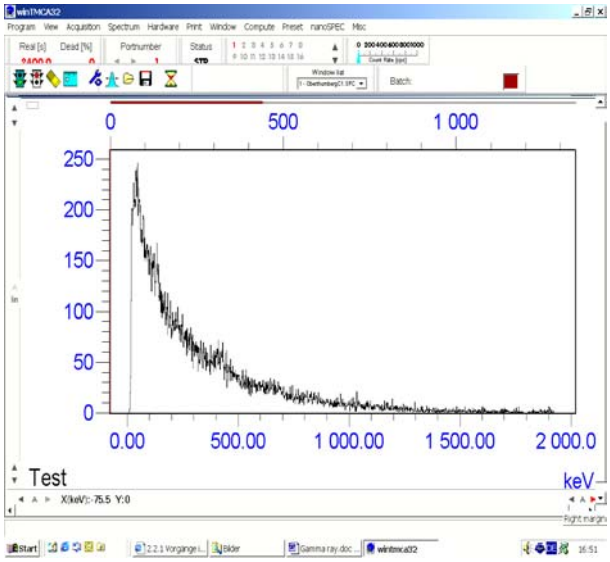

Figure 4.24: shows the C1-lithofacies, IV = <u>36741</u> counts/40 min

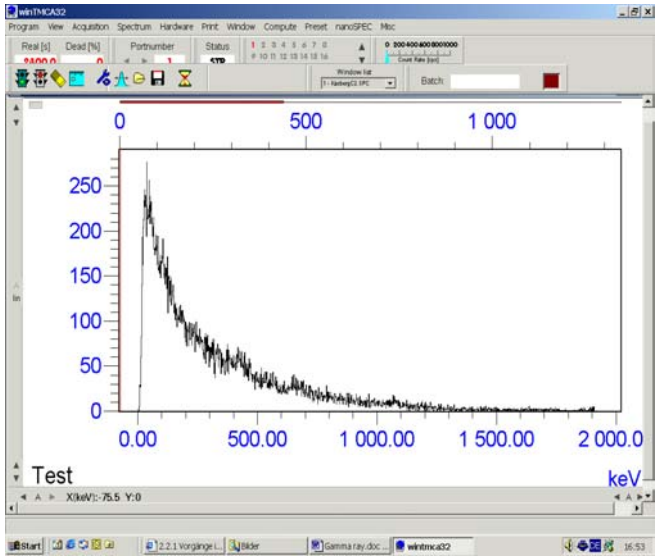

Figure 4.25: shows the C2-lithofacies, IV = <u>39126</u> counts/40 min

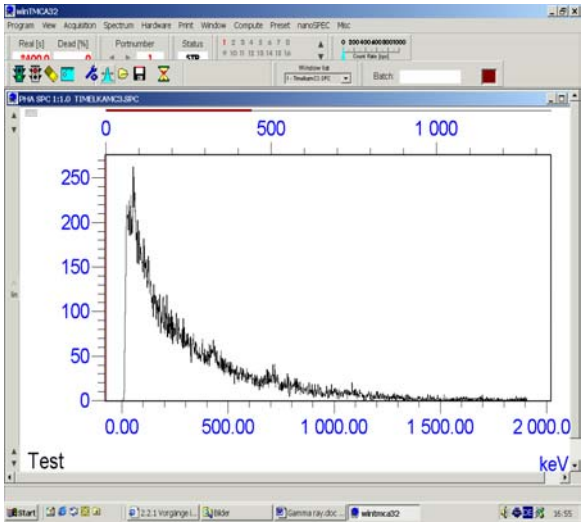

Figure 4.26: shows the C3-lithofacies, IV = <u>38008</u> counts/40 min

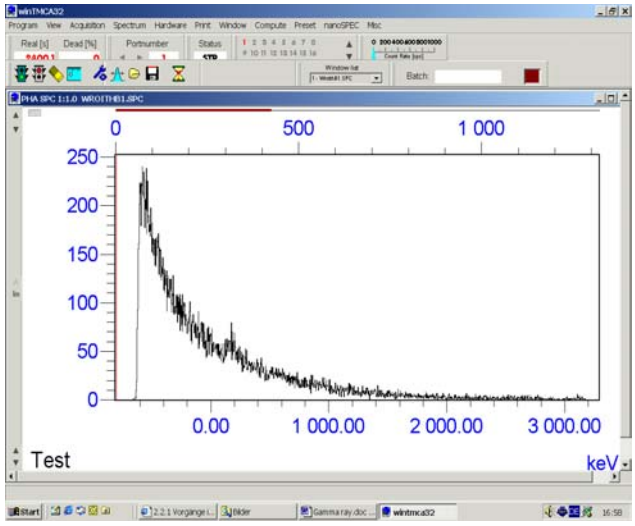

Figure 4.27: shows the B1-lithofacies, IV = <u>36171</u> counts/40 min

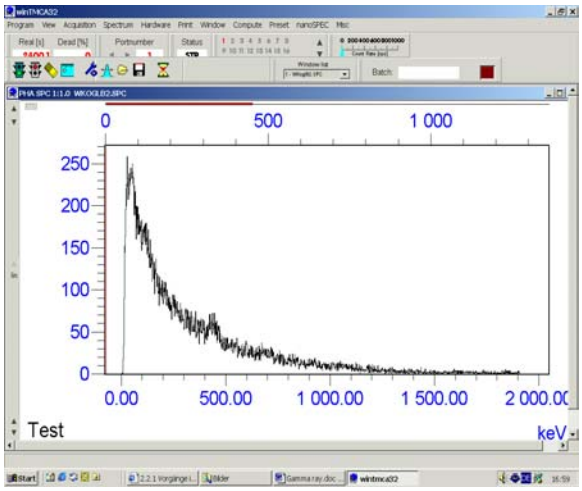

Figure 4.29: shows the B2-lithofacies, IV = 37373 counts/40 min

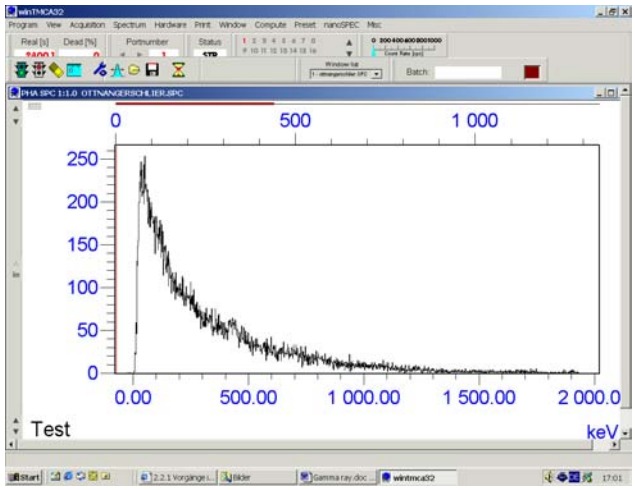

Figure 4.28: shows the Ottnanger Schlier facies, IV=38988 counts/40 min

Notation	Lithofacies	Integrationvalue Counts/40 min
SP Haslau	A1	35448
SP Haslau	A2	34650
SP Ottnang Fischer	A3	35769
SP Haslau SW Neue Welt	A4	32749
SP W Roith	B1	36171
SP W Kogl	B2	37373
SP Oberthumberg	C1	36741
SP Kasberg	C2	39126
SP Timelkam	C3	38008
Ottnanger Schlier	Ottnanger Schlier	38988

Table 4.1: Gamma-ray Intergrationvalues for each lithofacies

The highest Integrationvalues, see Table 4.1, show the samples C3 from Timelkam, C2 from Kasberg and the Ottnanger Schlier. The sample Ottnanger Schlier consists of about 38% clay as well as the sample C3. The C3 facies represents the salient from the Vöckla-formation to the Atzbacher formation and consists mainly of clay and marl minerals.
The facies A4 from location Haslau SW Neue Welt shows the lowest Integrationvalue and this is an indices for very low clay contents and therefore this sample nearly represents a clean sand.
The other facies A1, A2, A3, B1, B2, C1, C2 have medium Integrationvalues and the contents of clay lay between those of Ottnanger Schlier, C2 and C3, representing the maximum, and A4 which shows the lowest value.

4.3 Resistivity method

4.3.1 Description

The single Atzbacher Sand samples were filled into a glas-zylinder and water was added until the sample was 100% water-saturated for the resistivity measurement (see Figure 4.30). Using different saltwater concentrations, the conductivity C_0 of the total water-saturated sample was plotted against the conductivity C_w of the pore water. First normal water without salt was used and then 0.33g salt/l, 1.66 g salt/l, 3.33 g salt/l, 5 g salt/l and finally 6.66g salt/l. The higher the salt concentration the lower the resistivity of the whole measured sample. So it was possible to get a relationship between C_0 and C_w.

Figure 4.30: Resistivity apparatus

For determining the porosity ϕ and the influence of the clay in the sample X_T, the resistivity R_0 of the whole sample, the resistivity R_w of the formation water and the mass of the whole water-saturated sample had to be measured.

4.3.2 Theoretical background

The model to explain the structure of the sample, that means the arrangement of sand and clay, is a laminar one and related to that the following formulas have been used to determine the Formation factor F and the porosity ϕ of the samples.

$$R = \frac{\rho L}{A}$$

$$\rho = R\frac{A}{L}$$

R = measured resistivity (Ω)
ρ = specific resistivity (Ωm)
A = area (m^2)
L = length (m)

The specific resistivity of the water (R_w) depends on the concentration and type of salt in the pore water and the temperature. So the higher the concentration the higher the amount of ions which leads to a higher conductivity and obviously to a lower resistivity.

Determining the Formation-factor:

ARCHIE:

$$R_0 = F * R_W$$

$$F = \frac{R_0}{R_W}$$

$$F = a * \phi^{-m}$$

m= cementation factor

The Formation-factor F depends on the porosity ϕ.

Determining the Porosity:

$$m_{ges} = \rho_{fl}\phi V + \rho_m(1-\phi)V$$

$$\phi = \frac{\left[\left(\frac{m_{ges}}{V}\right) - \rho_m\right]}{\rho_m - \rho_{fl}}$$

m_{ges}= whole mass of the water-saturated sample
V = volume of the sample
ρ_{fl} = density of the fluid
ρ_m = density of the matrix

All samples consist of more or less shaly sands and due to that fact the Archie-formula does not work anymore. The sample consists of two conductivity components instead of one, the electrolytic and the clay component (see Figure 4.31 and Figure 4.32). These two facts have a combined influence on the resistivity or conductivity and a simple parallel conductor model has been used. The result of the parallel conductor model is a higher conductivity compared to the result of the Archie model. This excess conductivity X_T describes the contribution of clay to the total conductivity. Winsauer & McCardell, 1953, introduced the term 'excess conductivity'.

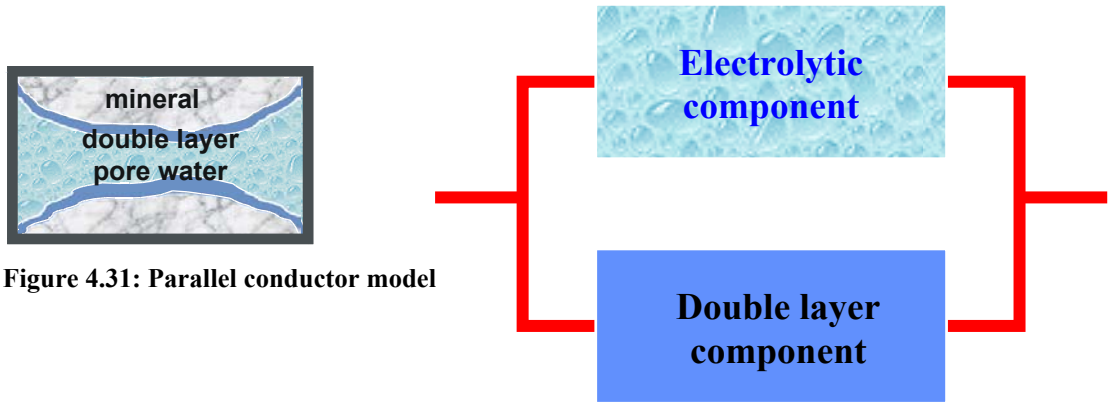

Figure 4.31: Parallel conductor model

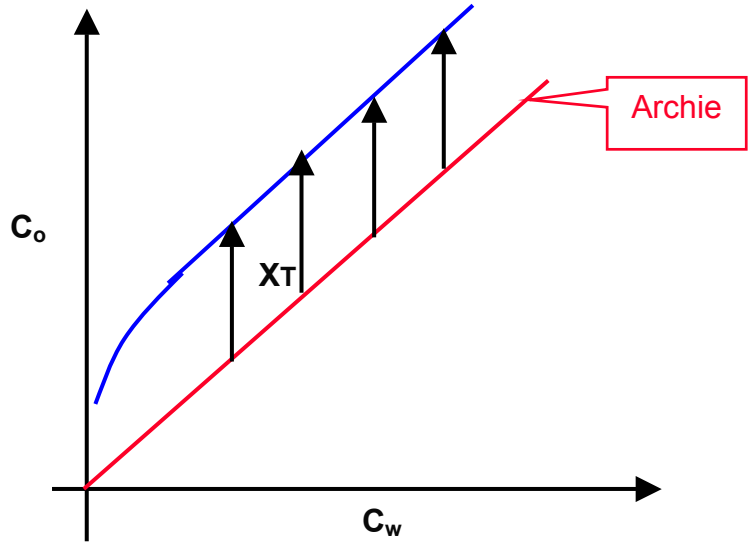

Figure 4.32: Archie diagram and excess conductivity

$$C_0 = C_w/F + X_T$$

↓

Archie

C_0 = Conductivity of the water-saturated sample
C_w = Conductivity of the formation-water
X_T = Influence of the clay in the sample; excess conductivity
F = Formation factor

4.3.3 Evaluation

Each Atzbacher facies sample was analyzed and X_T was calculated to distinguish between three groups (See Table 4.2).

Group	Sample	XT
1	A1, A4, B1	< 0,005
2	A2, A3, B2, C2, C1	0,02-0,005
3	Ottnanger Schlier, C3	>0,02

Table 4.2: XT-range for each group

The measurements of the samples show a linear relationship between C_0 and C_w.

$$y = k * x + d$$

k… gives the mean of the Vs/F
d… gives the mean of X_T
R^2… shows the variance of the measurements

The samples A1, A4 and B1 of the Atzbacher formation show very little influence on the clay content, because the value d is about zero (see Figures 4.33, 4.34, 4.35)
The R^2 value indicates that the statistic of the measurement is very high.

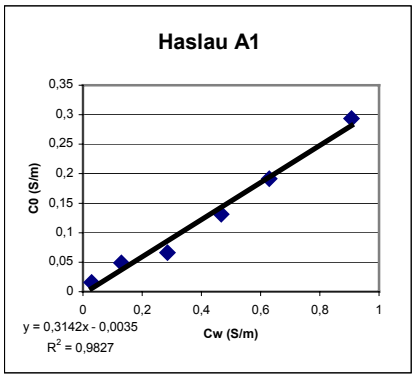

Figure 4.33: C_0 versus C_w diagram of facies A1

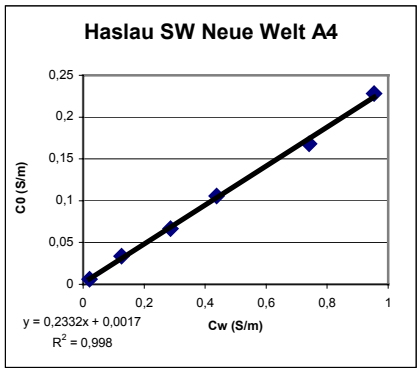

Figure 4.34: C_0 versus C_w diagram of facies A4

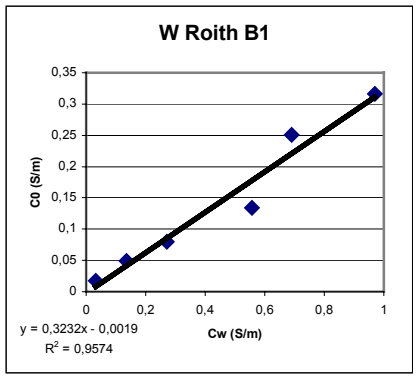

Figure 4.35: C_0 versus C_w diagram of facies B1

The next group able to be distinguished are the facies A2, A3, B2, C1, C2 (see Figures 4.36, 4.37, 4.38, 4.39, 4.40). They show similar d values ranging between 0.0082 and 0.0188. The influence of the clay content is a bit higher compared to the first group. The values of the variance of the samples are as good as the values of the first group.

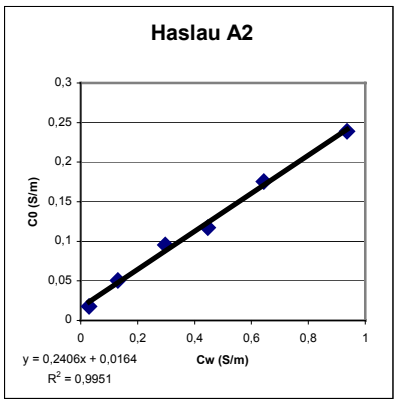

Figure 4.36: C_0 versus C_w diagram of facies A2

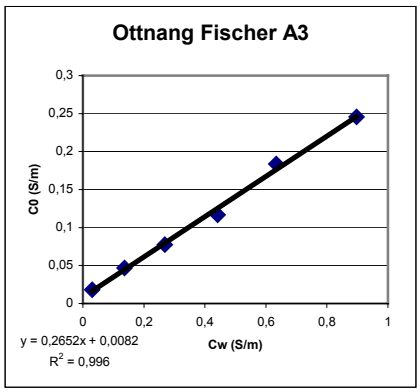

Figure 4.37: C_0 versus C_w diagram of facies A3

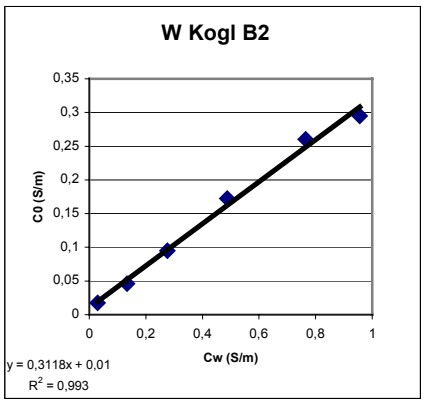

Figure 4.38: C_0 versus C_w diagram of facies B2

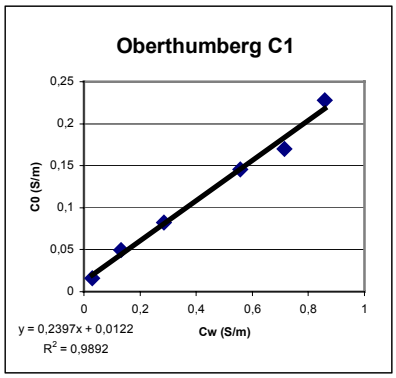

Figure 4.39: C0 versus Cw diagram of facies C1

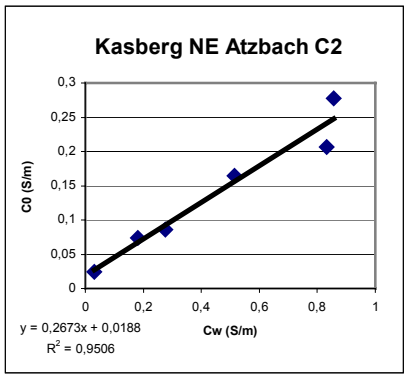

Figure 4.40: C0 versus Cw diagram of facies C2

The third group consists of facies C3 and Ottnanger Schlier. The difference compared to the other groups is enormous. The influence the clay content is much higher and very significant at the Ottnanger Schlier. The variance R^2 of the sample Ottnanger Schlier is too low and so there is too little probability to give a reliable statement about the resistivity of that sample. The resistivity shows no trend and it seams like the distribution of the measured values is randomly. Due to the fact that the sample Ottnanger Schlier shows the highest clay content it is obvious that the amount of clay is the reason for such results. The d values ranges between 0.08 and 0.2511 (See Figures 4.41 and 4.42)

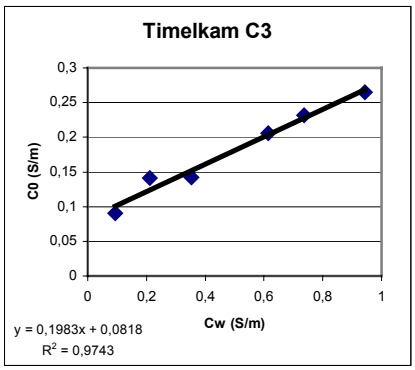

Figure 4.41: C0 versus Cw diagram of facies C3

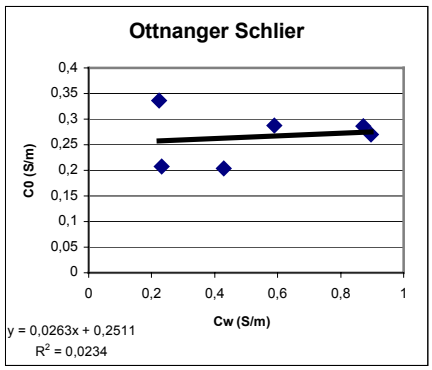

Figure 4.42: C0 versus Cw diagram of the Ottnanger Schlier facies

The k values have no influence on the interpretation. The k value depends on the porosity and normally means that high k values show a high porosity, but the measurement was not standardized on porosity and so no deposition is able to make.

4.4 Evaluation of Gamma ray, Resistivity and Granulometric analysis using crossplots

In Table 4.3 we compare individual values like the percentage of grain sizes <63 μm, the gamma-ray Integrationvalues as well as the resistivity of the water saturated sample R_0.

Lithology	% < 63 μm	GR	R_0
A1	11,7	35448	63,62
A2	3,98	34650	55,7
A3	18,05	35769	54,85
A4	3,56	32749	168,23
B1	4,60	36171	58,39
B2	6,68	37373	57,4
C1	6,68	36741	61,64
C2	8,37	39126	41,28
C3	14,47	38008	11,08
Ottnanger Schlier	38,37	38988	4,82

Table 4.3: Display of clay fraction (<63μm), gamma-ray, IV and resistivity values R_0 for each sample

Figure 4.43 shows the Intergrationvalues versus the clay fraction for each facies. Three trends can be recognized, which show a non linear relationship and this is confessed by the work of Clavier et al.(1971). In general, it is true that with increasing clay content the Integrationvalue increases as well, but this also depends on the composition of the clay minerals. Clay which consists of an high amount of Kaolinite show lower Gamma-ray API values compared to clays with high amounts of Montmorillonite, Chlorite or Illite (see Table 4.4). This is the reason why facies C2 shows with a relatively low amount of clay an high amount of Gamma-ray Integrationvalues. The same effect but the other way around show the facies A1 and A3. The amount of clay is relatively high but the gamma-ray values are much lower compared to facies C2.

Clay minerals	Gamma-ray; API values
Kaolinite	80…130
Montmorillonite	150…200
Chlorite	180…150
Illite	250…300

Table 4.4: Clay minerals and their Gamma-ray API values

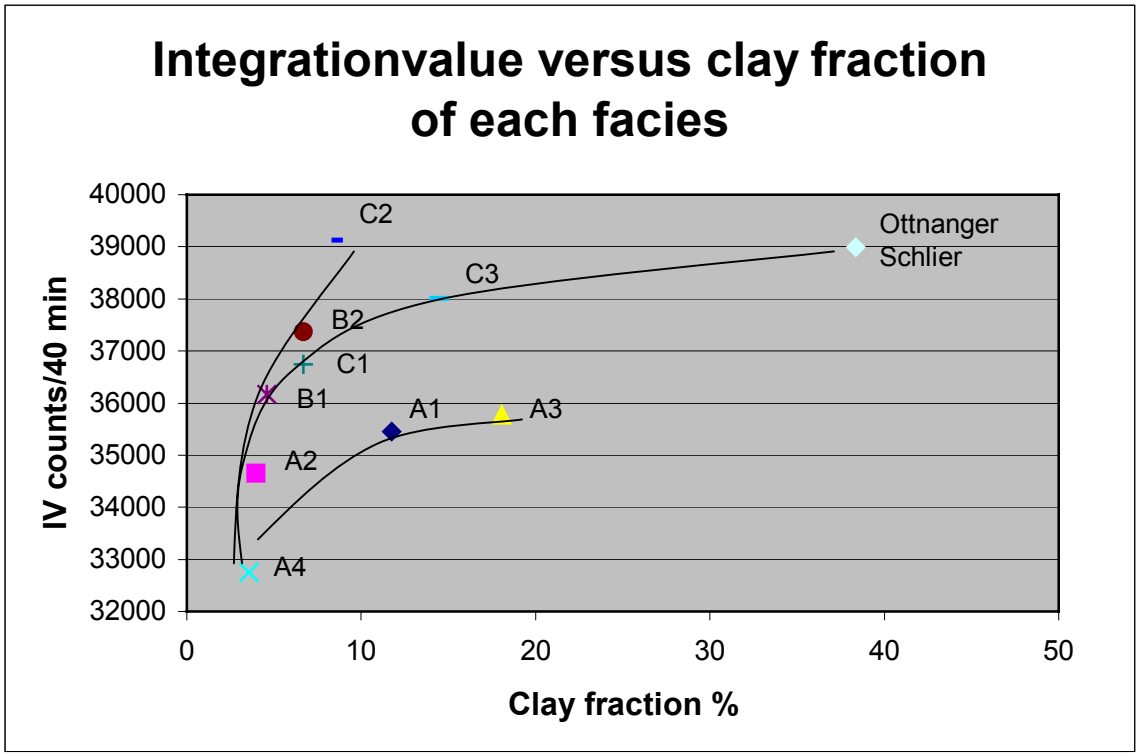

Figure 4.43: Integrationvalue versus clay fraction of all facies samples

The resistivity versus clay fraction (<63µm) shows a cluster distribution of most of the samples with low resistivity and low clay fractions, but two samples represent very different values and that leads to the classification of three groups (see Figure 4.44). The first group consists of the sample A4, which shows high resistivity values, over 150 Ωm, and a low part of clay with about 3,6%. The second group consists of the facies types A1, A2, A3, B1, B2, C1, C2, C3 and shows lower resistivity values, ranging from 11-64 Ωm and the clay values are ranging from 4-18%. The third group consists as well as the first group of only one sample the Ottnanger Schlier. The resistivity value shows a minimum of 4,8 Ωm and the clay fraction represents with more than 38% the highest value.

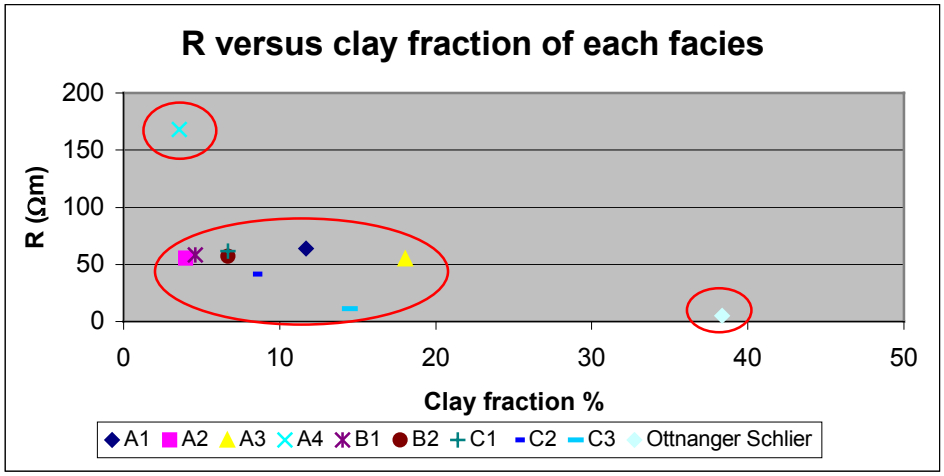

Figure 4.44: Resistivity R0 versus clay fraction % (<63 µm)

The GR-R plot distinguishes between three kinds of clusters (see Figure 4.45).

- The first cluster consists of the samples Ottnanger Schlier and Timelkam C3. They show high GR-values and low R-values because of a high clay content (15 to 40%).
- The second cluster is built by the main part of the Atzbacher Sands and show medium GR- and R-values and also have a medium clay part from 4 to 18% of the whole samples.
- The third cluster only consists of one sample. SP Haslau SW Neue Welt is nearly a shear sand of the Atzbacher lithologies and has low GR and the highest R values. The clay content is about 4% of the whole composition.

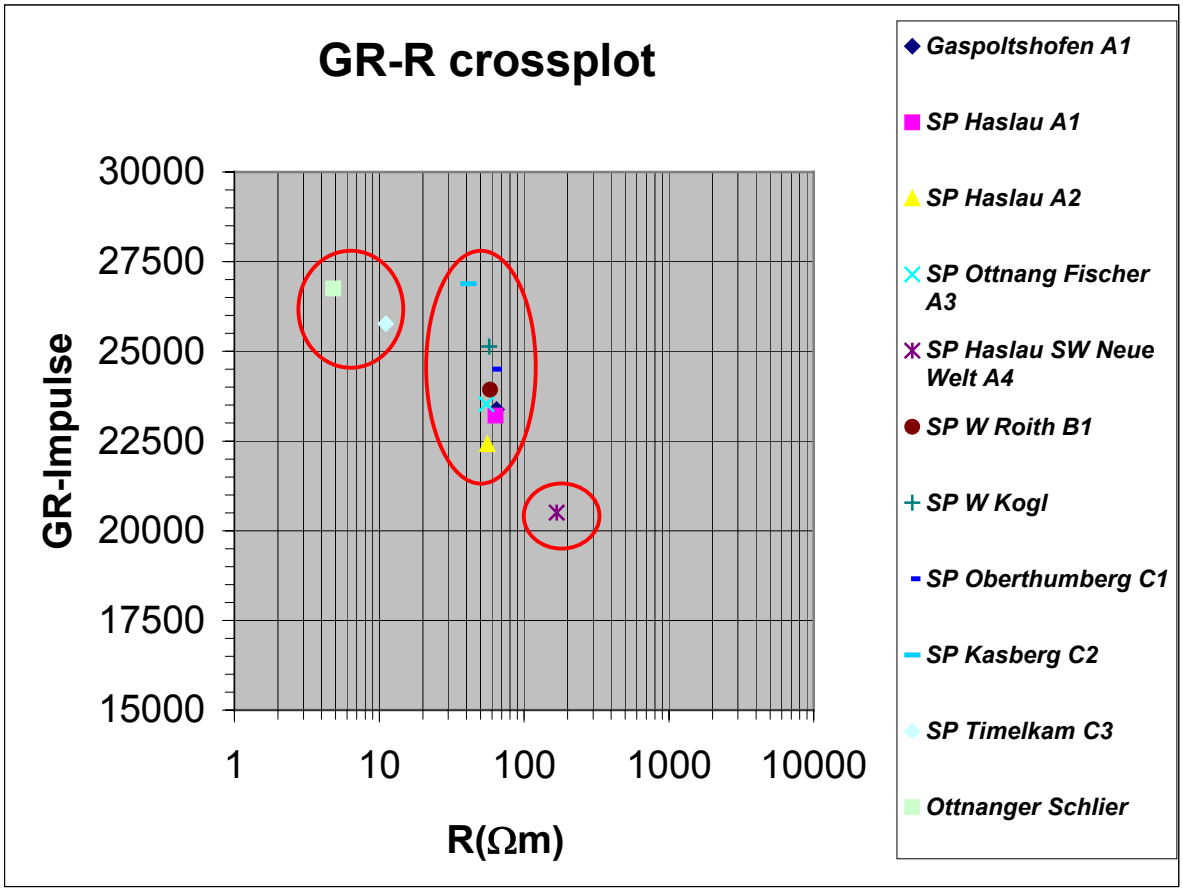

Figure 4.45: GR-R crossplot, GR logging time = 40min

The investigations show tendency of **:**

- Increase of gamma-radiation
- Decrease of resistivity/ Increase of conductivity

with growing clay content in the samples.

4.4.1 Summary

Due to the evaluation of the gamma-ray, resistivity and granulometric measurements the different facies samples can be distinguished between three groups.

- Group1: consisting of facies Ottnanger Schlier and C3
- Group2: consisting of facies A1, A2, A3, B1, B2, C1, C2
- Group3: consisting of facies A4

These evaluated clusters/groups from the GR-Resistivity cross plot were confirmed by the granulometric evaluation. The samples Ottnanger Schlier and Timelkam C3 have a medium clay content of about 26,4% (see Figure 4.46), the resistivities are very low, ranging from 4-11 Ωm and the gamma ray values are relatively high (see Table 4.3).

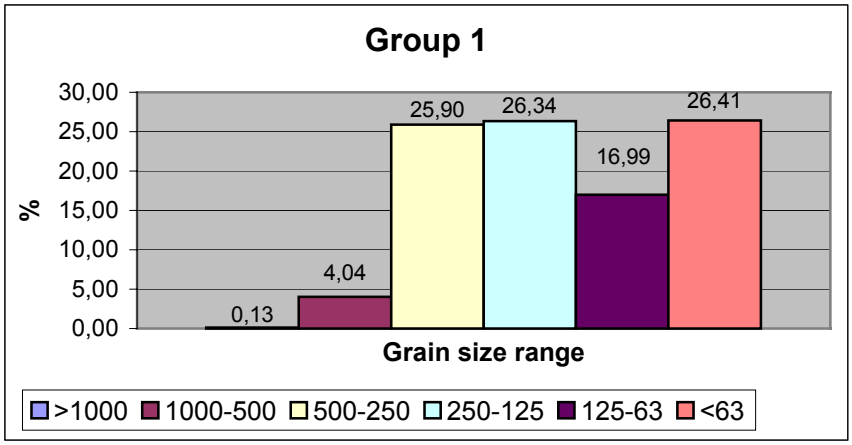

Figure 4.46 Grain size distribution of group 1 (µm)

The second group of Atzbacher facies shows an average clay content of about 8,6% and therefore is much lower compared to the first group (see Figure 4.47). The whole % distribution of the single grain size ranges are very different compared to group1, due that the grain sizes ranging from 250-125 µm is dominating. The whole diagram shows a more or less symmetric distribution.

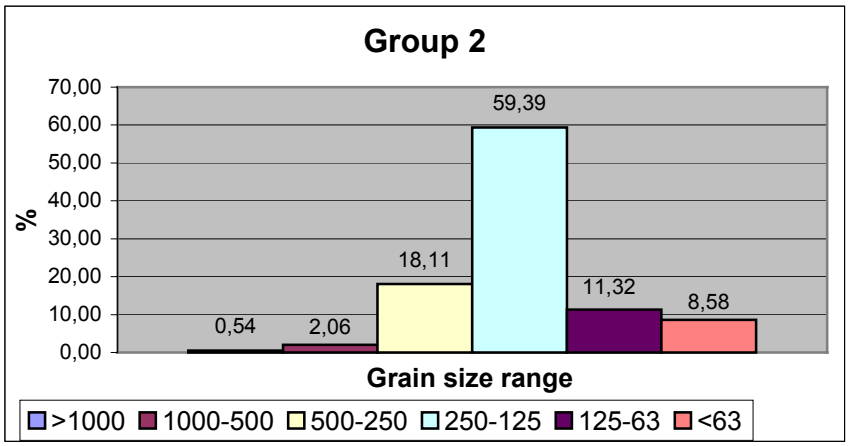

Figure 4.47: Grain size distribution of group 2 (µm)

The third group only consists of one sample A4, Haslau SW Neue Welt (see Figure 4.48). Due to the low clay content of about 4% and the high resistivity value, 168 Ωm, as well as the low GR value I decided to represent this sample as a single group.
This sample of the Atzbacher facies represents a nearly shear sand and looking at all the different crossplots like the gamma-ray versus clay fraction (see Figure 4.43), the resistivity versus clay fraction distribution (see Figure 4.44), the gamma-ray versus resistivity (see Figure 4.45), facies A4 always differs from the other facies samples.
The grain size ranging between 500-250 μm is dominating and therefore the whole facies consists of coarser grain sizes as the other two groups.

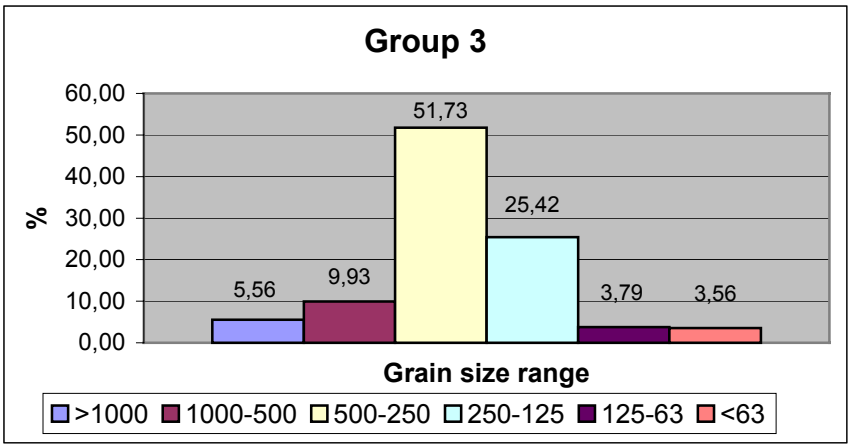

Figure 4.48: Grain size distribution of group 3 (μm)

4.5 Oedometer method

4.5.1 Description

This lever type Oedometer is based upon an original design by Professor A.W.Bishop late of Imperial College, London for determining the consolidation characteristics of soils using specimens confined laterally, but which are allowed to drain vertically in both directions. The cell with its locating ring is manufactured from brass and is finished in dull chrome plating (see Figure 4.49).

Figure 4.49: Oedometer

The cell is supplied with two porous ceramics, the upper ceramic is screwed to the underside of the loading cap and is placed upon the sample, whilst the lower stone rests underneath the lower surface of the sample.
A filter paper is placed between each ceramic interface, to ensure that they do not become impregnated with soil particles.
The apparatus for loading the different weights is joint with a lever to the loading cap and a linear strain transducer is fixed for measure the strain directly.
For not only measuring the strain but also the resistivity of the sample an insulating plastic cap is necessary and placed at the bottom of the cell, because otherwise the electric current does not flow through the sample and maybe a short-circuit is produced. I didn't use the ring of brass, but of plastic to prevent a short-circuit (see Figure 4.50).

Figure 4.50: The oedometer with the sample in the ring of plastic

After filling the cell with the sample, the sample and also the space outside the plastic ring has to be saturated with water or different concentrations of saltwater to guarantee that the sample is still totally filled with water or saltwater during the whole experiment (See Figure 4.51). During putting one weight of the other onto the apparatus the strain is measured with a linear strain transducer. More and more weight is put on as long as there is enough weight on the apparatus and afterwards the weights were taken down step by step whilst reading the changing values of the strain again.
The weight put on the apparatus were 0.5 kg, 1.5 kg, 3.5 kg, 7.5 kg, 15.5 kg, 23.5 kg and the last measurement was made with 31.5 kg and the whole measurements again with putting the weights down step by step.
The cross section area of the sample is 19.95 cm^2. Thus the load can be converted into pressure (see Table 4.6). Assuming a mean density of 2.4 g/cm^3 for the sediment the pressure corresponds to a depth z (see Figure 4.55).

Figure 4.51: Measuring the resistivity during loading

Due to the high clay content in the Atzbacher samples saltwater had to be taken with different concentrations of salt.
For the sample A4 no saltwater was needed, because of the low clay content, but for the other experiments different salt-water concentrations were used.
6.66g salt/l, 13.33g salt/l and 20g salt/l were the concentrations of the fluid.
A well known problem is the fact that clay influences the resistivity of the sample very much, and explanations for this behavior and the consequences for the measurements with clay in the sample, like the reduction of the resistivity with an increase of clay content, is described in the next chapter.

4.5.2 Theoretical background

4.5.2.1 The chemical behavior of clays

Replacement of the primary rock-forming minerals by clay minerals generally involves both physical and chemical processes (Gillot, 1968).
Physical processes:
Physical processes cause the mechanical break-up of the parent material. This is of the fold-importance to clay-mineral formation. In the first place water and active solutions gain access to the rock and in the second place the disintegration leads to an increase in specific surface. Surfaces are chemical active and an increase in specific surface leads to an increase in rate of chemical reaction. Mechanical damage results from five major physical processes. These are unloading, thermal expansion and contraction, crystal growth including frost action, colloid plucking, organic activity. Under hydrothermal conditions steam and other gases and vapors exert pressure, which may be relieved explosively with accompanying mechanical damage. Transportation of all kinds also causes mechanical damage.
Chemical processes:
The tendency for a chemical reaction to take place is determined by the potential or gradient. This is estimated in terms of characteristic thermodynamic functions. A major class of chemical reactions in which one solid is converted into another involves an intermediate stage in which the reactants are in true or colloidal solution. There are three major types of such reaction. These are: interaction between acids and bases; electron transfer and free radial interaction.
Another important class of reactions involves no intermediate solution stage and reorganization of the atoms or ions take place in the solid state. The crystal structure of the parent material often exerts some control over the orientation of the crystal structure of the product. If the control is in three dimensions the term epitactic is used.

Principal of consolidation theory:
The theory is based on a consideration of the mechanics of void ratio reduction a loading. The cylinder of the odometer is filled with a sample and is 100% water saturated. When a load is applied to the piston it is at first carried by the pore water. The water is able to escape until the load is gradually transferred and the pressure is carried by the mineral particles.
Pore volume is a function of particle-size distribution, grain shape, and packing geometry. Particle size is also important since it determines the relative importance of surface, physical-chemical, or gravitational forces.

The unit particles by which the crystal is composed may be molecules, atoms or ions. The forces between the units are electrical in nature. Attractive forces are of longer range than repulsive forces but this increases more rapidly as particles come close together. There are

two chief types of attractive forces: Coulomb forces which exist between oppositely charged particles and exchange forces which result from electron sharing between neighboring atoms. When exchange forces dominate the bonding it is described as covalent. In addition to ionic and covalent bonds there are weaker forces such as the hydrogen bonds and the even weaker Van der Waal bonds. The water molecule also plays an important structural role as it is a permanent dipole. It may be become orientated in the structure and sometimes is strongly attached particularly to small high charged cations. Cations being generally smaller than the anions.

4.5.2.2 Hydraulic conductivity

The soil is strongly influenced by the repulsive force between the clay particles.
The reason for the repulsive force between clay particles is their net negative charge, which is caused by irregularities in the clay crystal. The negative charge is balanced by cations outside the clay particle (Madsen & Mitchell, 1989).
The distributions of ions adjacent to a clay surface for a clay particle in an electrolyte can be described according to the diffuse double layer theory as developed by Gouy (1910), and Verwey and Overbeek (1948). The diffuse double layer consists of the negative charge clay particle surface and the ions surrounding it as shown in Figure 4.52. According to the theory the overlap of the double layers of individual clay particles is the source of the interparticle repulsion which controls the flocculation-deflocculation behavior of clay suspensions and the swelling-shrinking behavior of soils.

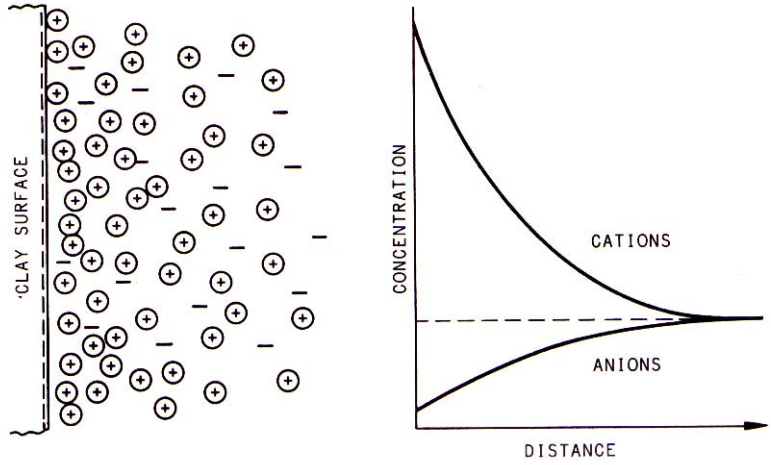

Figure 4.52: Distribution of ions adjacent to a negative charged surface according to the double layer theory

The double layer is sensitive to the variation of the dielectric constant (ε) of the fluid, the temperature (T), the electrolyte concentration (n) in the pore water, and the cation valence (ν). An approximate quantitative indication of the "thickness" of the double layer as given by the formula

$$\frac{1}{\kappa} = \sqrt{\frac{\varepsilon kT}{8\pi n e^2 \nu^2}}$$

where k is the Boltzmann constant and e is the electronic charge.

From this relationship it may be noted that the thickness of the double layer, and thus also the magnitude of the repulsive force between the clay particles, varies directly with the square root of the dielectric constant and temperature, and inversely as the valence and the square root of the electrolyte concentration.
The influence of the temperature is very small because a change in temperature will cause a change of the dielectric constant in a way that the product εT remains nearly constant.
Beside the above-mentioned variables some other factors as the size of the cations in the double layer, pH of the fluid, and anion absorption on the clay particles may also influence the clay behavior and thus the soil fabric.
The pH influences the dissociation of the hydroxyl groups (OH^-) exposed on the clay crystal surfaces and edges; the higher the pH, the greater the tendency for the H^+ to go into solution, and the greater the negative charge of the clay particles.
The effect of the various parameters influencing the double layer thickness, and thus the soil fabric and the hydraulic conductivity, are summarized in Table 4.5.

Pore Fluid Parameter	Change in Parameter	Change in Double Layer Thickness	Fabric Change Tendency	Usual Effect on Hydraulic Conductivity
Diectric Constant	increase	increase	dispersed	decrease
	decrease	decrease	flocculated	increase
Electrolyte Concentration	increase	decrease	flocculated	increase
	decrease	increase	dispersed	decrease
Cation Valennce	increase	decrease	flocculated	increase
	decrease	increase	dispersed	decrease
Cation Size	increase	increase	dispersed	decrease
	decrease	decrease	flocculated	increase
pH	increase	increase	dispersed	decrease
	decrease	decrease	flocculated	increase
Anion Adsorption	increase	increase	dispersed	decrease
	decrease	decrease	flocculated	increase

From Evans et al. (1985), modified.

Table 4.5: Effect of changes in pore fluid parameters on double layer thickness, soil fabric, and hydraulic conductivity

The hydraulic conductivity will be almost determined by the flow rates through the largest flow channels. Three levels of fabric will be important when dealing with fine-grained soils as barriers to the flow of chemicals.

1) The micro fabric consists of the regular aggregation of particles and the very small pores between them through which little fluid will flow.

2) The minifabric contains these aggregations and the inter-assemblage pores between them. Flow through these pores will be much greater than through the intra-aggregate pores, since the hydraulic conductivity varies with the square of the pore radius.

3) On a larger scale there may be micro fabric that contains cracks, fissures, root holes, laminations, etc., corresponding to the "trans-assemblage pores", through which the flow rate is so great as to totally obscure that through the other pore space types.

The hydraulic conductivity of the pore water and the conductivity of the clay are connected in parallel and cause a systematic resistivity reduction when the clay content increases. The curve measured of samples with 0% clay content follows the Archie equation and with an amount of clay in the sample the Archie equation is not true anymore. When the clay content increases from 0% to 2.5 % the resistivity changes over more than 50% depending on the water saturation (see Figure 4.53). Because of the 100% water filled sample the specific density decreases and the plasticity increases. To give an explanation for these effects surface- or cation exchange capacity is named.

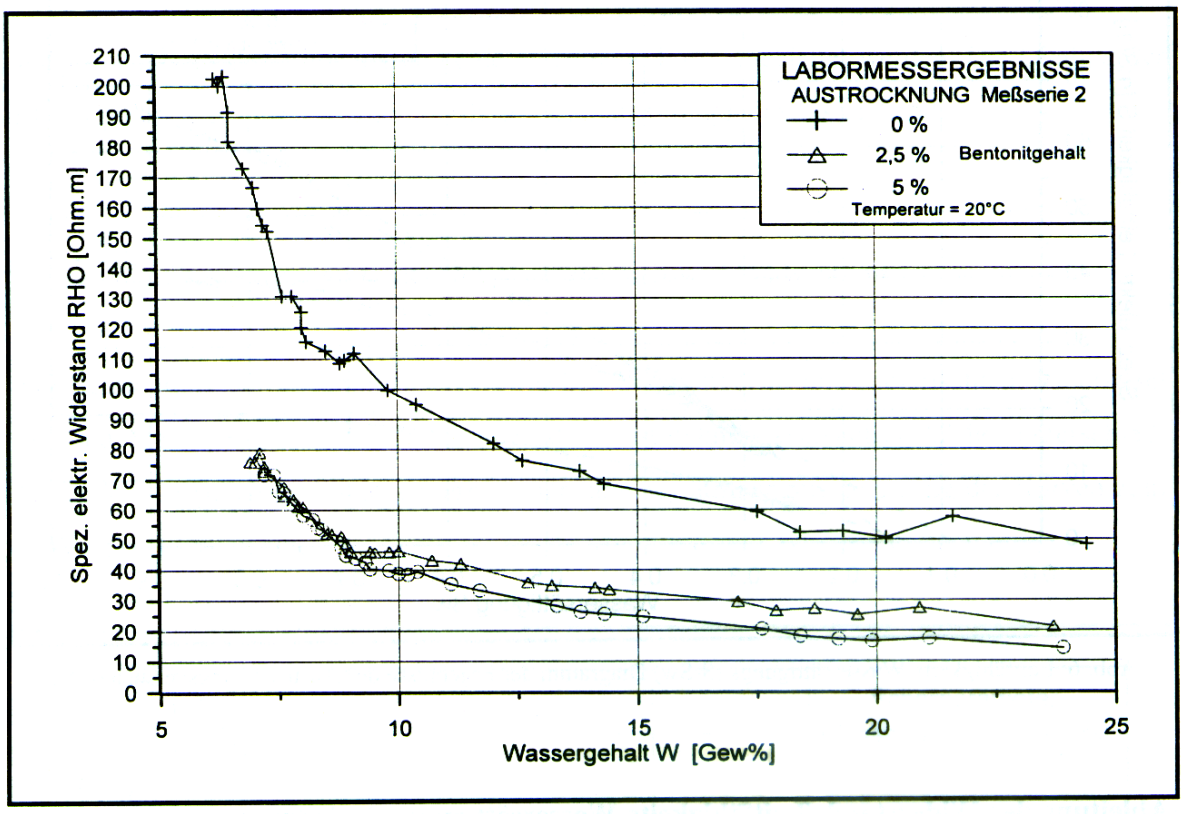

Widerstands-Wassersättigungs (RHO-Sw) Diagramm der Ergebnisse des Austrocknungsversuches A2

Figure 4.53: Resistivity – Water saturation diagram

Three theoretical models :

1) The DeWitte model (DeWitte, 1955)

The conductivity of the fine disperse distributed clays in the rock depend on pore water. The water saturation does not only effect the specific electric conductivity of the pore electrolyte but also the clay part of the sample

$$\sigma_G = \frac{\sigma_W S_W^{\ 2}}{F} + \sigma_t S_W V_t$$

σ_W = *Electrolytic conductivity*
σ_t = *Conductivity of the clay*
F = *Formation factor*
V_t = *Part of clay in the sample*
S_w = *Water saturation*

2) Waxman and Smith model (Waxman & Smits, 1967)
This model assumes the cation exchange capacity CEC. The concentration of the cations depends on the water saturation and the volume of the water fixed to the clay. More cations can be released when the water saturation and the clay content increases.

$$\sigma_G = \frac{S_W^{\ n}}{F}\left[\sigma_W + K\left(\frac{Q_v}{S_W}\right)\right]$$

K = *Mobility of the cat ions depending on temperature*
Q_v = *Concentration of the cat ions*

3) Dual Water model (Clavier et. al., 1984)
This model assumes two kinds of water, the free water in the sample and the bounded water.

$$\sigma_G = \frac{S_W^{\ n}}{F}\left[\sigma_W + \left(\frac{\phi_B}{\phi_T S_W}\right)(\sigma_t - \sigma_W)\right]$$

Φ_T = *Porosity of the whole sample*
Φ_B = *Volume of water bonded to the clay*

The cation exchange capacity of clays takes a main part of the dual water model. The thickness of the bonded water of clay increases with the decrease of salinity of the formation water. The CEC is proportional to the specific surface of clay and also proportional to the volume of bonded water. The conductivity of clays results from the surface of the bonded water. Clay therefore exists of clay minerals and the bonded water (see Figure 4.54).

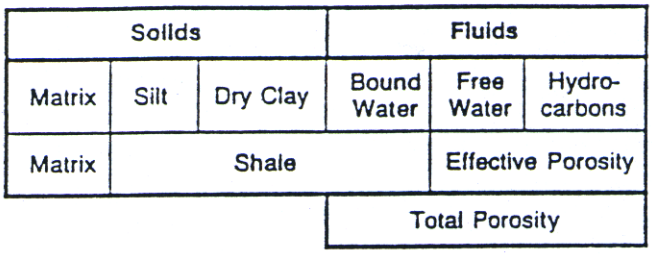

Figure 4.54: Clay composition

The minerals of the clay are not conductive but only water. The part of the bonded water varies with the species of clay and increases with the fine-grained of the particles.

$$Q_v = CEC \frac{1-\phi_T}{100\phi_T} \rho_{ma}$$

$\phi_T = \phi + \phi_B$ ... *Whole porosity*
ϕ_B= *Volume of the bonded water*
Q_V = *Concentration of the cat ions*
ρ_{ma} = *Density of the dry rock inclusive clay*

The higher the resistivity of the formation water the lower the concentration of the cations. The dual water model only exists for rocks that are not conductive, for example, no pyrite is accepted.

4.5.3 Evaluation

With this experiment I simply wanted to demonstrate the change of resistivity during different pressures when loading with weights. It's obvious that the resistivity of the water filled sample increases with pressure because the pores of the sample are getting smaller and the resistivity increases of the effect that water has a lower resistivity in contrast to the matrix particles.
But I did not bargain for the effect of the clays influenced my measurement. So I have tried to give an explanation for these results of my samples.

With the modified Oedometer experiment it was possible to receive information about the pressure on the sample when loading with weights for calculating the depth z (see Figure 4.55/Table 4.6) with the following formula

$$z = \frac{p}{\rho * g}$$

p...pressure
ρ*...assumed mean density (2.4 g/cm*^{3}*)*
g...acceleration due to gravity

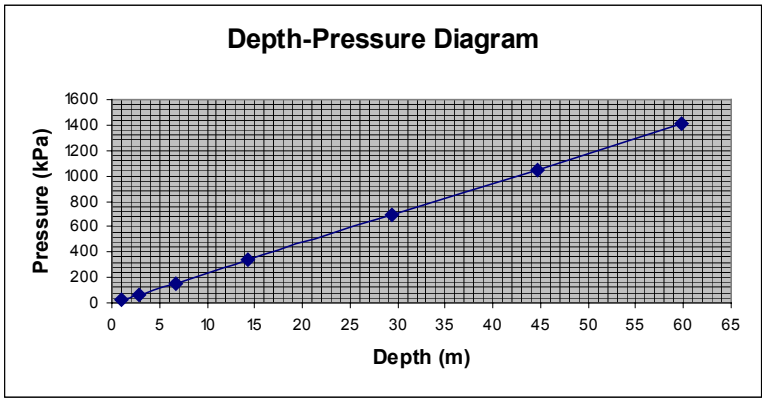

Figure 4.55: Depth-Pressure diagram

Load (kg)	Pressure (kPa)	Depth (m)
0.5	22.351	0.949
1.5	65.054	2.848
3.5	156.459	6.645
7.5	335.270	14.240
15.5	692.891	29.430
23.5	1050.513	44.619
31.5	1408.134	59.809

Table 4.6: Load, depth and pressure values

For determining the porosity of the sample changing with pressure it was necessary to measure the volume of the cylinder within the sample, the weight of the sample and to give the density for the grains and for the liquid (water). This leads to the formula

$$\Phi = \frac{\frac{m_{ges}}{V} - \rho_m}{\rho_m - \rho_{li}}$$

ϕ...porosity
m_{ges}...weight of the sample
ρ_m...density of the grains (2.65 g/cm^3)
ρ_{li}...density of the liquid (1.0 g/cm^3)

The deformation behavior of a material we can describe by the Young's modulus and this is the modulus of elasticity E. It is defined by the Hook's law as the ratio of the stress (pressure) p and the corresponding strain (deformation) ε.
The pressure p is given as follows:

$$p = \frac{F}{A}$$

F... force
A... cross section area

The determination of the strain ε is given by the formula:

$$\varepsilon = \frac{\Delta H}{H}$$

ΔH… change of height
H… initial height

For the nonlinear deformation characteristics the Young's modulus is defined as

$$E = \frac{\partial p}{\partial \varepsilon}$$

Assuming a power law for the nonlinearity (Kezdi, 1969) we set

$$E = E_0 * p^m = \frac{\partial p}{\partial \varepsilon}$$

E_0 …initial elasticity
m…exponent depending on the rock types

The deformation-pressure function is given by the differential equation

$$\partial \varepsilon = \frac{1}{E_0} * p^{-m} * \partial p$$

which leads to the solution

$$\varepsilon = \frac{1}{E_0(1-m)} * p^{1-m}$$

The logarithmic notation results in

$$\log \varepsilon = \log \frac{1}{E_0(1-m)} + (1-m) \log p$$

From a log(ε) versus log(p) plot of experimental data we can determine:

- The value (1-m) and m from the slope
- The value $1/E_0(1\text{-}m)$ and E_0 from the intercept at p=1

Now we can write the nonlinear Young's modulus expression

$$E = E_0 * p^m$$

for each sample.

The relationship between the specific resistivity R and the pressure p is described by the formula:

$$R = R_0 * p^n$$

R_0... initial specific resistivity
n... pressure exponent

From a log(R) versus log(p) plot of the experimental data we can determine

- The value n from the slope
- The value R_0 from the intercept at p=1

For representing the relationship between the porosity ϕ and the pressure p, the E-modulus and the pressure p, the logarithmic illustration of the E-modulus and the pressure p as well as the relationship between the specific electrical resistivity and the pressure, the logarithimic illustration of the specific electrical resistivity and the pressure for different salt concentrations the sample A1 has been used (see Figures 4.56, 4.57, 4.58, 4.59, 4.60, 4.61). The illustrations for all the other facies samples is shown in Appendix.

Sample A1 measured with 6.66 gS/l:

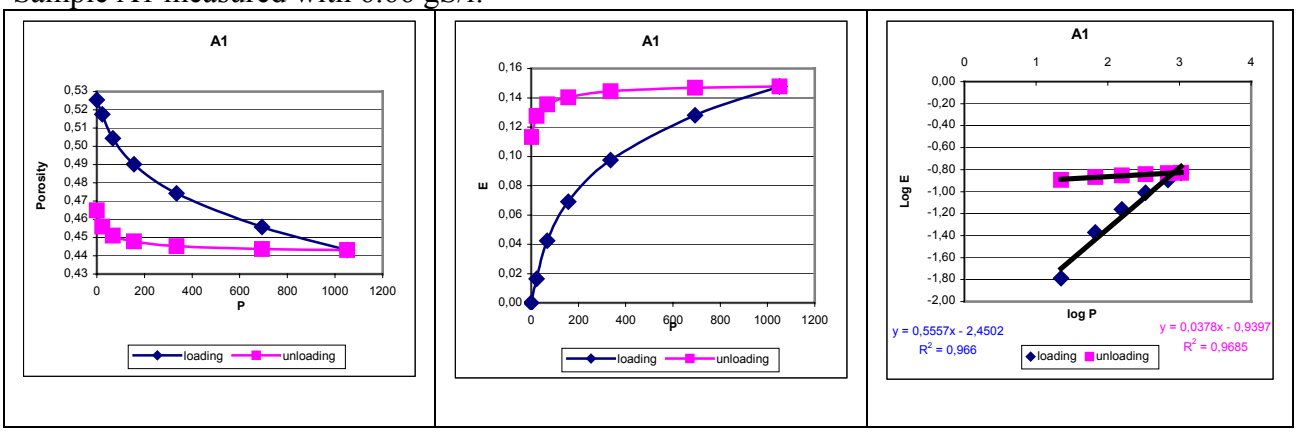

Figure 4.56: Porosity vs pressure, elasticity modulus vs pressure, log of elasticity modulus vs log of pressure for facies A1 measured with 6.66 gS/l

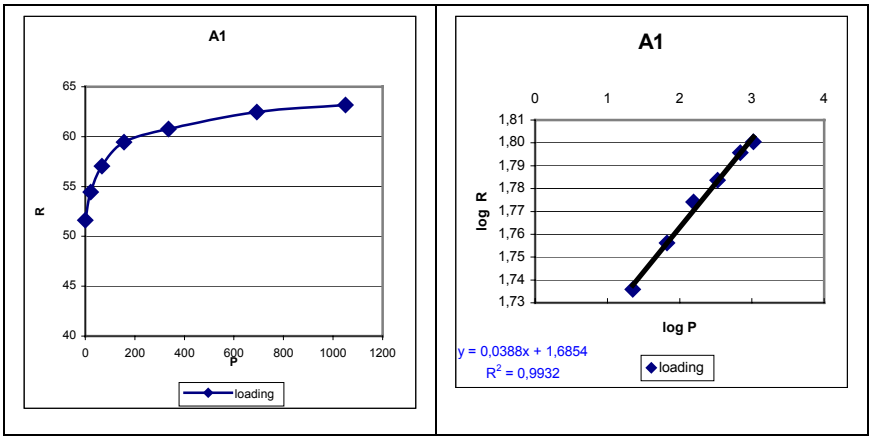

Figure 4.57: Specific electrical resistivity vs pressure, log of specific electrical resistivity vs log pressure for facies A1 measured with 6.66 gS/3l

Sample A1 measured with 13.33 gS/l:

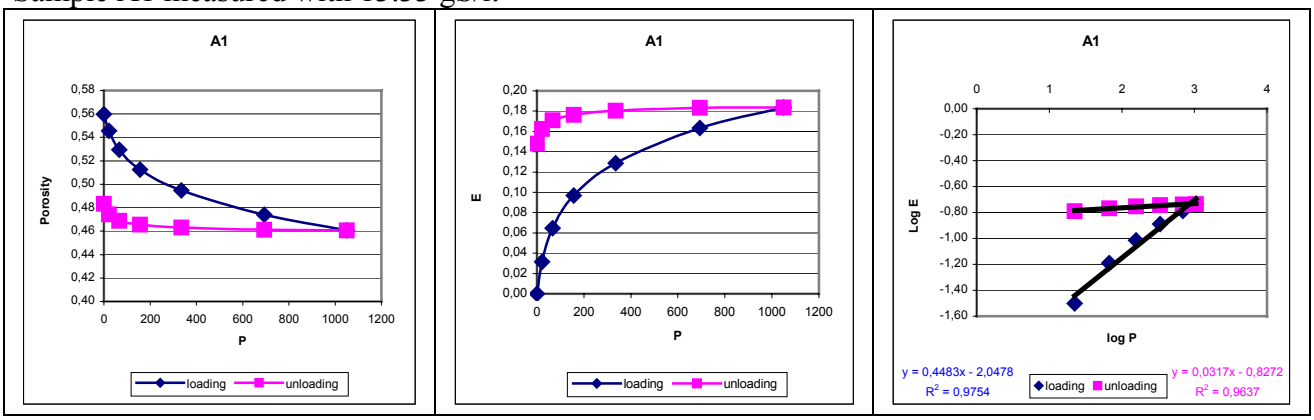

Figure 4.58: Porosity vs pressure, elasticity modulus vs pressure, log of elasticity modulus vs log of pressure for facies A1 measured with 13.33 gS/l

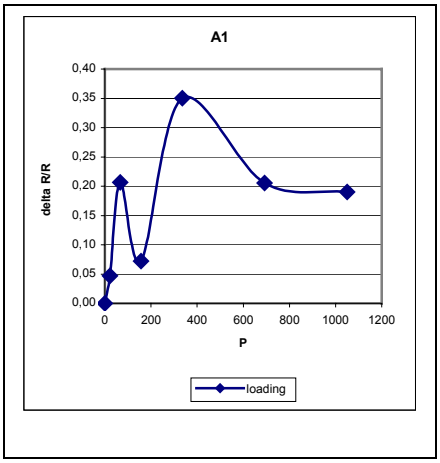

Figure 4.59: Specific electrical resistivity vs pressure for facies A1 measure with 13.33 gS/l

Sample A1 measured with 20 gS/l:

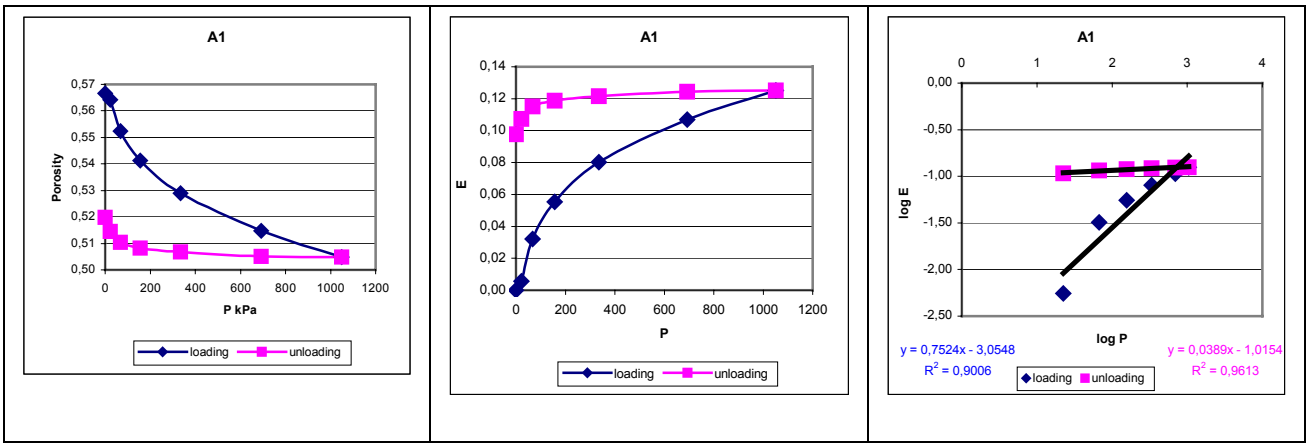

Figure 4.60: Porosity vs pressure, elasticity modulus vs pressure, log of elasticity modulus vs log of pressure for facies A1 measured with 20 gS/l

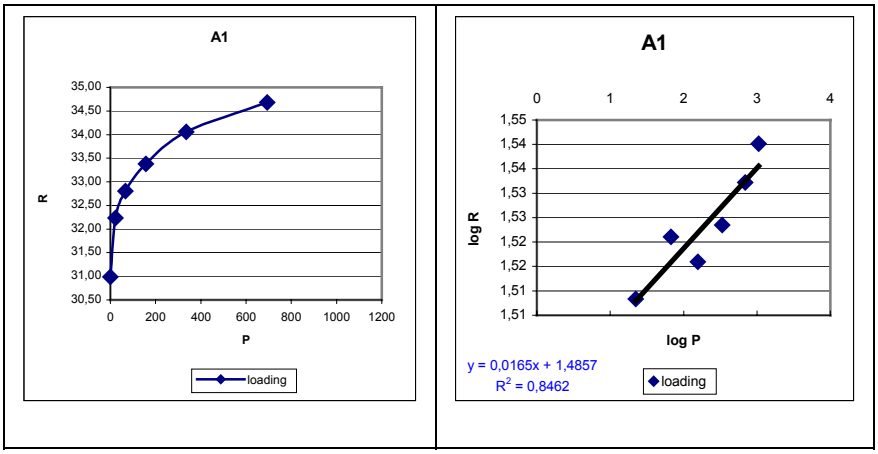

Figure 4.61: Specific electrical resistivity vs pressure, log of specific electrical resistivity vs log pressure for facies A1 measured with 20gS/l

Table 4.7 shows the relationship between the E-modulus E and the pressure p as well as the relationship between the specific electrical resistivity R and the pressure p. The E_0 versus p relationship has been calculated for all facies types measured with 6.66 gS/l, 13.33 gS/l and 20 gS/l and for facies A4 with 0.33 gS/l during loading and unloading conditions. The

resistivity versus pressure relationship has only been calculated for the samples when reasonable resistivity versus pressure trends occur without too much oscillation effects.

Sample	Type (g Salt/l)	Loading/Unloading	E-modulus	Resistivity
A1	6.66	loading	$E = 0{,}0064 * p^{0{,}4443}$	$R = 48{,}46 * p^{0{,}039}$
A1	6.66	unloading	$E = 3{,}0395 * p^{0{,}9622}$	
A1	13.33	loading	$E = 0{,}01998 * p^{0{,}5517}$	
A1	13.33	unloading	$E = 4{,}696 * p^{0{,}9683}$	
A1	20.00	loading	$E = 0{,}0012 * p^{0{,}2476}$	$R = 30{,}6 * p^{0{,}017}$
A1	20.00	unloading	$E = 2{,}481 * p^{0{,}9611}$	
A2	6.66	loading	$E = 0{,}005 * p^{0{,}4651}$	$R = 42{,}8 * p^{0{,}019}$
A2	6.66	unloading	$E = 2{,}0999 * p^{0{,}9639}$	
A2	13.33	loading	$E = 0{,}0026 * p^{0{,}3857}$	
A2	13.33	unloading	$E = 1{,}5069 * p^{0{,}9523}$	
A2	20.00	loading	$E = 0{,}0008 * p^{0{,}2864}$	
A2	20.00	unloading	$E = 0{,}6109 * p^{0{,}9342}$	
A3	6.66	loading	$E = 0{,}0012 * p^{0{,}3163}$	
A3	6.66	unloading	$E = 0{,}7237 * p^{0{,}9272}$	
A3	13.33	loading	$E = 0{,}0018 * p^{0{,}3263}$	
A3	13.33	unloading	$E = 2{,}8955 * p^{0{,}9701}$	
A3	20.00	loading	$E = 0{,}0001 * p^{-0{,}1711}$	
A3	20.00	unloading	$E = 1{,}2397 * p^{0{,}9509}$	
A4	0.33	loading	$E = 0{,}0082 * p^{0{,}5164}$	$R = 268{,}6 * p^{0{,}052}$
A4	0.33	unloading	$E = 3{,}5188 * p^{0{,}9748}$	
B1	6.66	loading	$E = 0{,}0145 * p^{0{,}5371}$	
B1	6.66	unloading	$E = 5{,}2633 * p^{0{,}9744}$	
B1	13.33	loading	$E = 0{,}0141 * p^{0{,}5274}$	
B1	13.33	unloading	$E = 4{,}8772 * p^{0{,}9725}$	
B1	20.00	loading	$E = 0{,}0162 * p^{0{,}5622}$	
B1	20.00	unloading	$E = 4{,}0078 * p^{0{,}9711}$	
B2	6.66	loading	$E = 0{,}0088 * p^{0{,}5017}$	
B2	6.66	unloading	$E = 3{,}6536 * p^{0{,}9713}$	
B2	13.33	loading	$E = 0{,}0077 * p^{0{,}5781}$	
B2	13.33	unloading	$E = 0{,}4875 * p^{0{,}9318}$	
B2	20.00	loading	$E = 0{,}0017 * p^{0{,}2698}$	
B2	20.00	unloading	$E = 3{,}4409 * p^{0{,}9653}$	
C1	6.66	loading	$E = 0{,}0014 * p^{0{,}2722}$	$R = 31{,}05 * p^{0{,}077}$
C1	6.66	unloading	$E = 2{,}2456 * p^{0{,}9576}$	

C1	13.33	loading	$E = 0{,}0074 * p^{0{,}4728}$	
C1	13.33	unloading	$E = 3{,}448 * p^{0{,}9653}$	
C1	20.00	loading	$E = 0{,}0061 * p^{0{,}4533}$	$R = 31{,}71 * p^{0{,}037}$
C1	20.00	unloading	$E = 3{,}8242 * p^{0{,}9683}$	
C2	6.66	loading	$E = 0{,}0067 * p^{0{,}4728}$	
C2	6.66	unloading	$E = 1{,}9039 * p^{0{,}9532}$	
C2	13.33	loading	$E = 0{,}0083 * p^{0{,}4876}$	$R = 32{,}31 * p^{0{,}037}$
C2	13.33	unloading	$E = 2{,}757 * p^{0{,}9618}$	
C2	20.00	loading	$E = 0{,}0089 * p^{0{,}4917}$	$R = 28{,}87 * p^{0{,}041}$
C2	20.00	unloading	$E = 2{,}7492 * p^{0{,}9614}$	
C3	6.66	loading	$E = 0{,}0056 * p^{0{,}425}$	$R = 32{,}2 * p^{0{,}039}$
C3	6.66	unloading	$E = 3{,}6214 * p^{0{,}9669}$	
C3	13.33	loading	$E = 0{,}0096 * p^{0{,}4809}$	
C3	13.33	unloading	$E = 3{,}874 * p^{0{,}9667}$	
C3	20.00	loading	$E = 0{,}0079 * p^{0{,}4663}$	
C3	20.00	unloading	$E = 3{,}7199 * p^{0{,}9672}$	
Ottnanger Schlier	6.66	loading	$E = 0{,}0465 * p^{0{,}6155}$	
Ottnanger Schlier	6.66	unloading	$E = 7{,}2906 * p^{0{,}9732}$	
Ottnanger Schlier	13.33	loading	$E = 0{,}0384 * p^{0{,}5993}$	
Ottnanger Schlier	13.33	unloading	$E = 7{,}2950 * p^{0{,}974}$	
Ottnanger Schlier	20.00	loading	$E = 0{,}0302 * p^{0{,}574}$	$R = 30{,}38 * p^{0{,}054}$
Ottnanger Schlier	20.00	unloading	$E = 6{,}7053 * p^{0{,}9723}$	

Table 4.7: Relationship between the elasticity modulus E and the pressure as well as the relationship between the specific electrical resistivity and the pressure for the facies types measured with different salt concentrations and loading/unloading conditions

Table 4.8 shows the calculated initial elasticity modulus E_0 and the exponent m, calculated for all facies types with different salt concentrations and loading/unloading conditions.

Sample	Type (g Salt/l)	Loading/Unloading	E_0	m

A1	6.66	loading	0,0064	0,4443
A1	6.66	unloading	3,0395	0,9622
A1	13.33	loading	0,02	0,5517
A1	13.33	unloading	4,6961	0,9683
A1	20.00	loading	0,0012	0,2476
A1	20.00	unloading	2,4811	0,9611
A2	6.66	loading	0,005	0,4651
A2	6.66	unloading	2,0999	0,9639
A2	13.33	loading	0,0026	0,3857
A2	13.33	unloading	1,5069	0,9523
A2	20.00	loading	0,0008	0,2864
A2	20.00	unloading	0,6109	0,9342
A3	6.66	loading	0,0012	0,3163
A3	6.66	unloading	0,7237	0,9272
A3	13.33	loading	0,0018	0,3263
A3	13.33	unloading	2,8955	0,9701
A3	20.00	loading	0,0001	-0,1711
A3	20.00	unloading	1,2397	0,9509
A4	0.33	loading	0,0082	0,5164
A4	0.33	unloading	3,5188	0,9748
B1	6.66	loading	0,0145	0,5371
B1	6.66	unloading	5,2633	0,9744
B1	13.33	loading	0,0141	0,5274
B1	13.33	unloading	4,8772	0,9725
B1	20.00	loading	0,0162	0,5622
B1	20.00	unloading	4,0078	0,9711
B2	6.66	loading	0,0088	0,5017
B2	6.66	unloading	3,6536	0,9713
B2	13.33	loading	0,0077	0,5781
B2	13.33	unloading	0,4875	0,9318
B2	20.00	loading	0,0017	0,2698
B2	20.00	unloading	3,4409	0,9653
C1	6.66	loading	0,0014	0,2722
C1	6.66	unloading	2,2456	0,9576
C1	13.33	loading	0,0074	0,4728
C1	13.33	unloading	3,448	0,9653
C1	20.00	loading	0,0061	0,4533
C1	20.00	unloading	3,8242	0,9683
C2	6.66	loading	0,0067	0,4728
C2	6.66	unloading	1,9039	0,9532
C2	13.33	loading	0,0083	0,4876
C2	13.33	unloading	2,757	0,9618

C2	20.00	loading	0,0089	0,4917
C2	20.00	unloading	2,7492	0,9614
C3	6.66	loading	0,0056	0,425
C3	6.66	unloading	3,6214	0,9669
C3	13.33	loading	0,0096	0,4809
C3	13.33	unloading	3,874	0,9667
C3	20.00	loading	0,0079	0,4663
C3	20.00	unloading	3,7199	0,9672
Ottnanger Schlier	6.66	loading	0,0465	0,6155
Ottnanger Schlier	6.66	unloading	7,2906	0,9732
Ottnanger Schlier	13.33	loading	0,0384	0,5993
Ottnanger Schlier	13.33	unloading	7,295	0,974
Ottnanger Schlier	20.00	loading	0,0302	0,574
Ottnanger Schlier	20.00	unloading	6,7053	0,9723

Table 4.8: Calculated initial elasticity modulus E_0 and the exponent m for all facies types measured with different salt concentrations and loading/unloading conditions

Figures 4.62, 4.63 and 4.64 show the initial E-modulus E_0 versus the facies types and the exponent m versus the facies types measured with different salt concentrations during loading. The E_0 ranges between 0.001 to 0.05 for all samples but only the Ottnanger Schlier sample can be distinguished from the others. For the measurements with different salt concentrations during the loading process the Ottnanger Schlier figures out to reach the maximum E_0 values. All the other facies types show very similar E_0 values and no differentiation is possible. For the m versus facies types values no differentiation between the single facies types is possible due to the fact that they vary irregularily depending on the salt concentration. The negative m value for facies A3 in Figure 4.64 can be traced back to an error during the measurement process. The m values are ranging between 0.2 and 0.6.

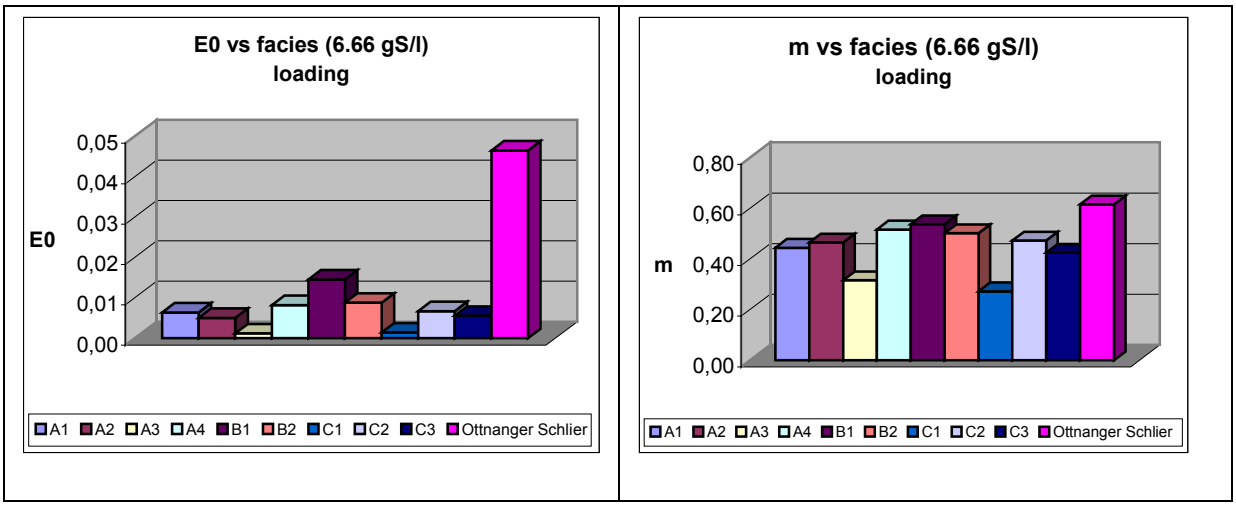

Figure 4.62: E_0 versus facies types, m versus facies types measured with 6.66 gS/l during loading

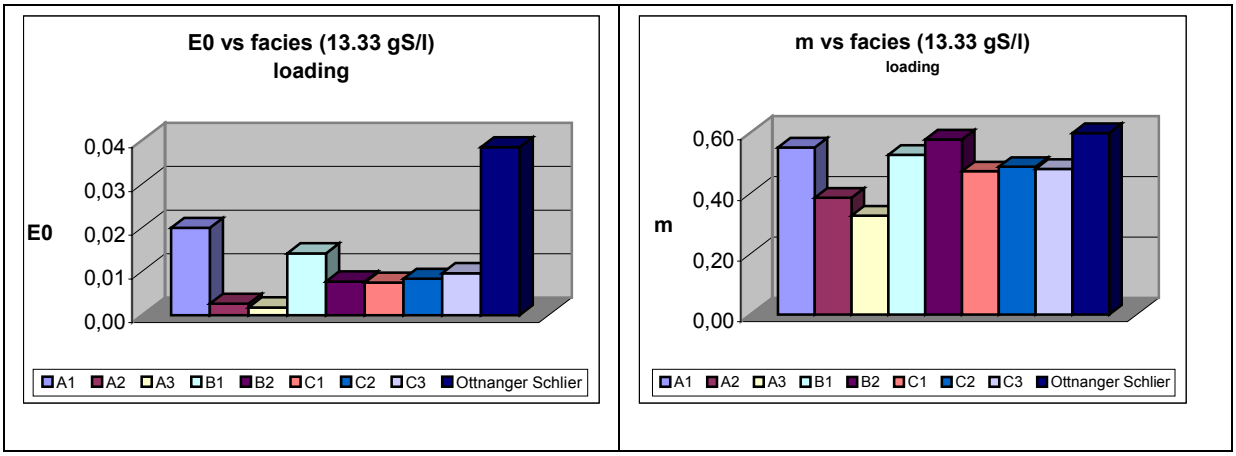

Figure 4.63: E_0 versus facies types, m versus facies types measured with 13.33 gS/l during loading

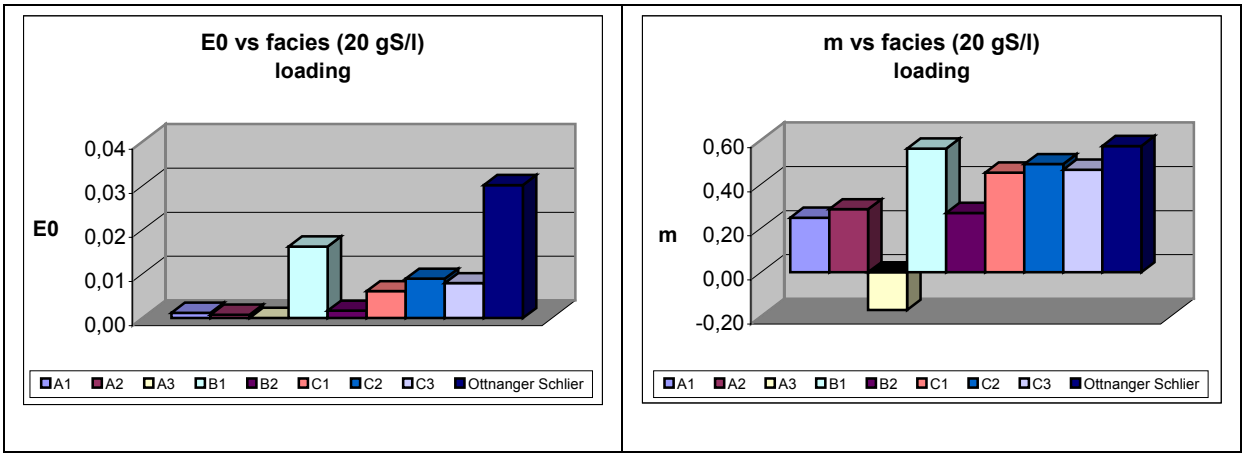

Figure 4.64: E_0 versus facies types, m versus facies types measured with 20gS/l during loading

Figure 4.65, 4.66, 4.67 show the initial E-modulus values E_0 versus the facies types and the m values versus the facies types during the unloading process. The result for the E_0 values is the same as for the loading process except the values are now ranging between 0.05 and 8.0 and are much higher compared to those of the loading process. One facies sample can be distinguished again from all the others and that is the sample Ottnanger Schlier, reaching the highest E_0 values. The m evaluation for the unloading process has as well the same characteristic as in the loading process and no differentiation between the single facies types is possible. The m values are ranging between 0.92 and 0.98 and are higher compared to the m values of the loading process.

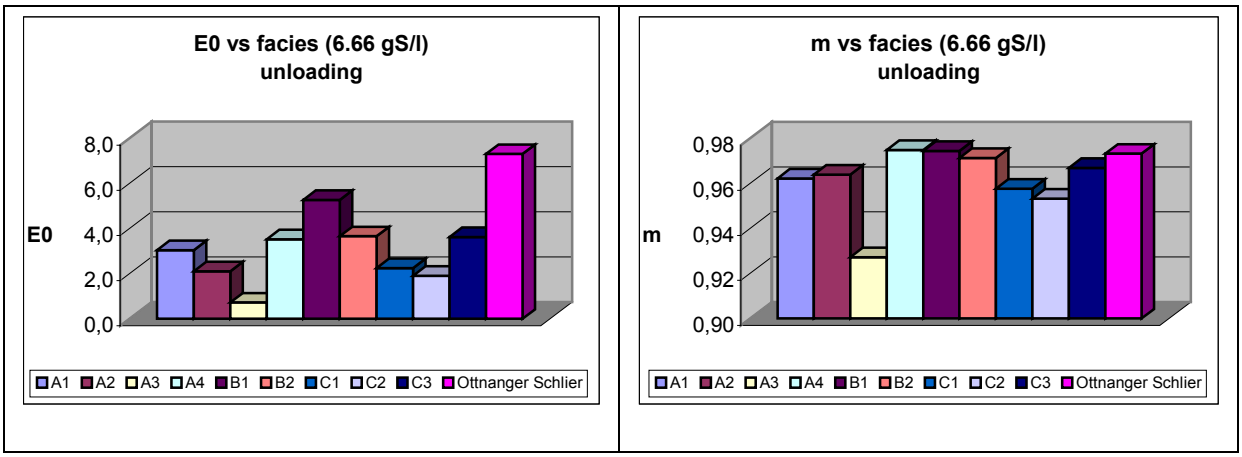

Figure 4.65: E_0 versus facies types, m versus facies types measured with 6.66 gS/l during unloading

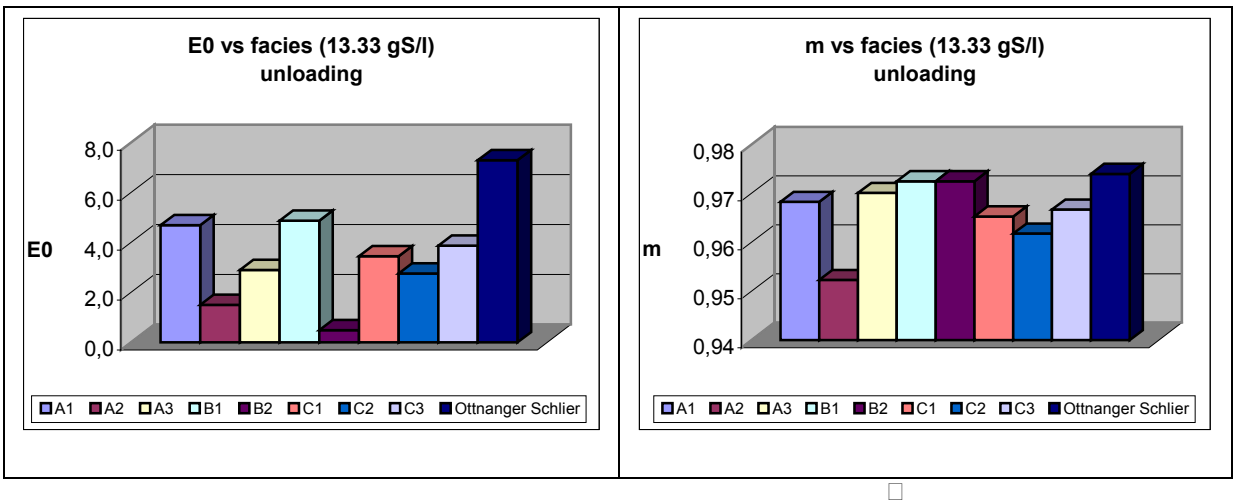

Figure 4.66: E_0 versus facies types, m versus facies types measured with 13.33 gS/l during unloading

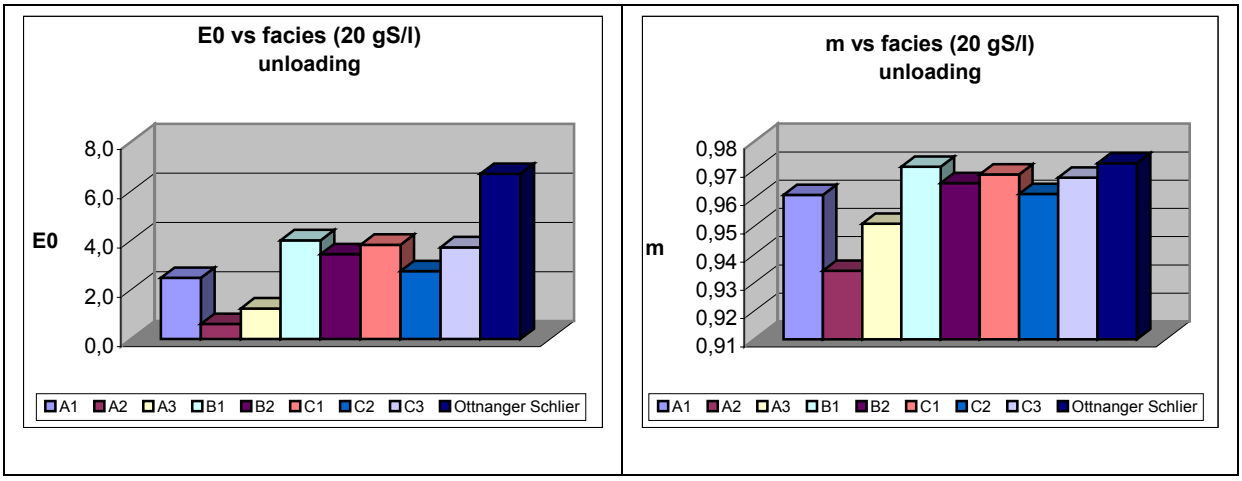

Figure 4.67: E_0 versus facies types, m versus facies types measured with 20 gS/l during unloading

Table 4.9 represents the initial experimental specific resistivity values as well as the calculated once and the exponent n, depending on the slope of the straight line.
The experimental initial resistivity values are slightly higher than the calculated resistivity values due to mistakes of embedding the samples into the Oedometer equipment.

The initial specific resistivity has only been calculated for the samples when reasonable resistivity versus pressure trends occur without too much oscillation effects.

Sample	Type (g Salt/l)	R_0 exp.	R_0 calc.	n
A1	6.66	51,62	48,46	0,039
A1	20.00	30,99	30,6	0,017
A2	6.66	45,48	42,8	0,019
A4	20.00	308,45	268,6	0,052
C1	6.66	45,7	31,05	0,077
C1	20.00	35,13	31,71	0,037
C2	13.33	36,55	32,31	0,037
C2	20.00	32,27	28,87	0,041
C3	6.66	36,34	32,2	0,039
Ottnanger Schlier	20.00	34,2	30,38	0,054

Table 4.9:Experimental and calculated initial specific electrical resistivity values and the exponent n

4.5.3.1 Evaluation errors

Most of the samples were measured with a pore fluid of 6.66 gSalt/l, 13.33 gSalt/l and 20 gSalt/l and the sample A4 was measured with 0.33 gSalt/l . The sense of this was to eliminate or diminish the influence of the clay, due to the fact that all samples contain a more or less amount of clay. Therefore the problem appears that the porous stones at the top and the bottom of the sample, which makes sure that the water can escape during loading the sample with weights, are saturated with the pore water of different salt concentrations. But the salt in the porous stones does not escape anymore and therefore giving different and fluctuating conductivity results.
This leads to the fact that the measurement of the resistivity of the sample is influenced by that effect and leading as well to those fluctuating results when looking at the R versus P diagrams of the different samples.
The data show no evidence that the clay influence becomes lower when using higher salt concentrations for the pore liquid.
The reason why I have not displayed the R versus P results for the unloading state is, when putting off the weights the water does not flow back into the sample and therefore the pores are not filled properly with the fluid again. That means that air is filling most of the pores and the measured resisitivity leads to wrong results.
Another explanation for those strange results is the conductivity of the clay. The current should only be conducted by the porewater, but the clay contains a lot of bounded water with

a high negative charged surface and the current flows through this layers. The higher the pressure on the sample the higher is the conductivity of the clay particles in the sample, due to the high contact with each other, which could lead to those irregularities of the resistivity measurements.
Not only the amount of clay in the sample is responsible for those irregulations but also the distribution and arrangement of those particles. If there is a lot of clay in the sample and the distribution is homogenous so that the particles do not touch each other, then it only has a little effect on the resistivity measurements. But of course the relationship is a linear one. The higher the relationship between the clay and sand particles the higher is the probability that the particles get in contact with each other and lead the current through the sample.

For the calculation of the E-modulus an other problem rises that has to be discussed. Normally the relationship between the E-modulus and the pressure should be the same for one sample, not depending on the different salt concentrations that have been used. But for each measurement the sample had to be changed due to filling the pores with different pore fluid and therefore this leads to different initial situations concerning the beginning- porosity which as well affects the elongation values.
The relationship between the E-modulus and the pressure has been calculated for each the loading and the unloading process.

4.5.4 Summary

With the Oedometer experiment no differentiation between the Atzbacher Sand facies is possible, but a differentiation is possible when comparing the initial E-modulus E_0 of the Atzbacher Sands and the Ottnanger Schlier facies. The Ottnanger Schlier facies shows much higher E_0 values for the loading as well as the unloading process compared to the whole Atzbacher Sand facies. The evaluation of the exponent m is not useful for a differentiation between the single facies types.

5 Boreholecorrelation

5.1 Introduction

For determining the top of the Atzbacher Sands and therefore the transition to the Ottnanger Schlier as well as the top of the Ottnanger clay a borehole correlation with resistivity and GR measurements was made with the wells shown in Table 5.1.

Wells	Measurement
W03	GR, R16
W14	GR, R-IND
W06	GR, R16
W10	GR, R16
W12	GR, R16
W05	GR, R16
W01	GR, R16
W07	GR, R16
W20	GR, R-IND

Table 5.1: Wells used for the borehole correlation

5.2 Theoretical background

5.2.1 GR evaluation

The gamma-ray log has traditionally been used for correlating zones from well to well, for crude identification of lithology, and for rough estimation of the volume of shale present in the formation. Continuous shale beds can be readily identified in wells separated by large distances from their characteristic gamma-ray "signature" (Ellis, 1987).
For estimating the volume fraction of shale in a formation V_{sh}, the traditional approach is to scan the log for minimum and maximum gamma-ray readings, γ_{min} and γ_{max}. The minimum reading is then assumed to be the *clean point* (0% shale), and the maximum reading is taken as the *shale point* (100% shale). Then the gamma-ray reading in API units at any other point in the well (γ_{log}) may be converted to the gamma-ray index I_{GR} by linear scaling:

$$I_{GR} = \frac{\gamma_{\log} - \gamma_{\min}}{\gamma_{\max} - \gamma_{\min}}.$$

The use of spectral gamma-ray devices can point out anomalies with some unusual excess of U, K, or Th. They permit recording the individual mass concentration of the three radioactive components of the total gamma-ray signal. For one type of tool, the relationship between the concentration of the three radioactive components and the gamma-ray signal in API units is given approximately by:

$$\gamma_{API} = 4Th + 8U + 16K,$$

when thorium and uranium are measured in ppm and potassium in percent by weight.

5.2.2 R16 evaluation

For measuring the apparent resistivity R_a three electrodes are positioned in the borehole and one outside on the surface. Two electrodes named A and B are the current-electrodes and the two others M and N are the measurement electrodes. The R16 measurement is a normal one.

$$R_a = \Delta V \big/ I \, 4\pi \overline{AM}$$

The depth of investigation is about two times spacing.

5.2.3 R-Ind Evaluation

The principle of the Induction Log based on electromagnetic coupling between the probe and the formation. An alternating current of about 20 kHz flows through a coil and produces an electromagnetic field and a current arises in the formation, produces a secondary magnetic field and induces a voltage in the receiver coil. This signal is a measure for the conductivity or resistivity of the formation.

5.3 Evaluation

Figure 5.2 and Figure 5.3 show the correlation of the Ottnanger clay and the Atzbacher Sand determined from GR, R16 and R-IND measurements and all the elevations are related on the

well Hiptmair (422.4m). The location of the wells can be seen in Figure 5.1 and the data for each well are shown in Table 6.1.
When measuring the resistivity with the R16 and the R-IND tool different GR tools have been used. The two GR tools use different units, the CPS and the API units, but for the correlation and for creating the crossplots the difference is not important and does not effect the general statement.
The correlation is important for generating the structuremap with the RC^2 program, because markers, for example the top of the Atzbacher Sand, could easily be defined then.
The crossplots of R16 or R-IND versus GR give an evidence for the different composition between the Ottnanger clay and the Atzbacher Sand horizon.
Crossplots show on the x-axis the R16 in a logarithmic scale and on the y-axis the GR value. The values representing the Atzbacher Sand are shown in dark-blue and for the Ottnanger clay in yellow. The resistivity values for the Ottnanger clay are lower than those for the Atzbacher Sand and the GR values are slightly higher comparing to those of the Atzbacher Sand. The cloud for the Ottnanger clay does not scatter where the Atzbacher Sand generally shows a broad spectrum on the resistivity as well as on the gamma-ray axis.
Due to the fact that for the gamma-ray measurement different tools were used, no absolute comparison is possible. The resistivity values for the Ottnanger clay lie in a range between 10 and 30 Ωm and the values for the Atzbacher Sand vary in a range of 15 and 50 Ωm.
Clay has a lower resistivity compared to sand and therefore the two different lithologies, the Ottnanger clay and the Atzbacher Sand, can be distinguished. But the Atzbacher Sand shows as well high parts of clays in the horizon and that is the reason why the plots show an overlay. But looking at the focal point of each cloud, the Ottnanger clay and the Atzbacher Sand show a large difference for the gamma-ray as well as for the resistivity values.

Figure 5.1 shows the position of the wells and the two profiles for the Log-correlation. The black profile displays the position for the Log-correlation shown in Figure 5.2 and the blue profile the log correlation shown in Figure 5.3.

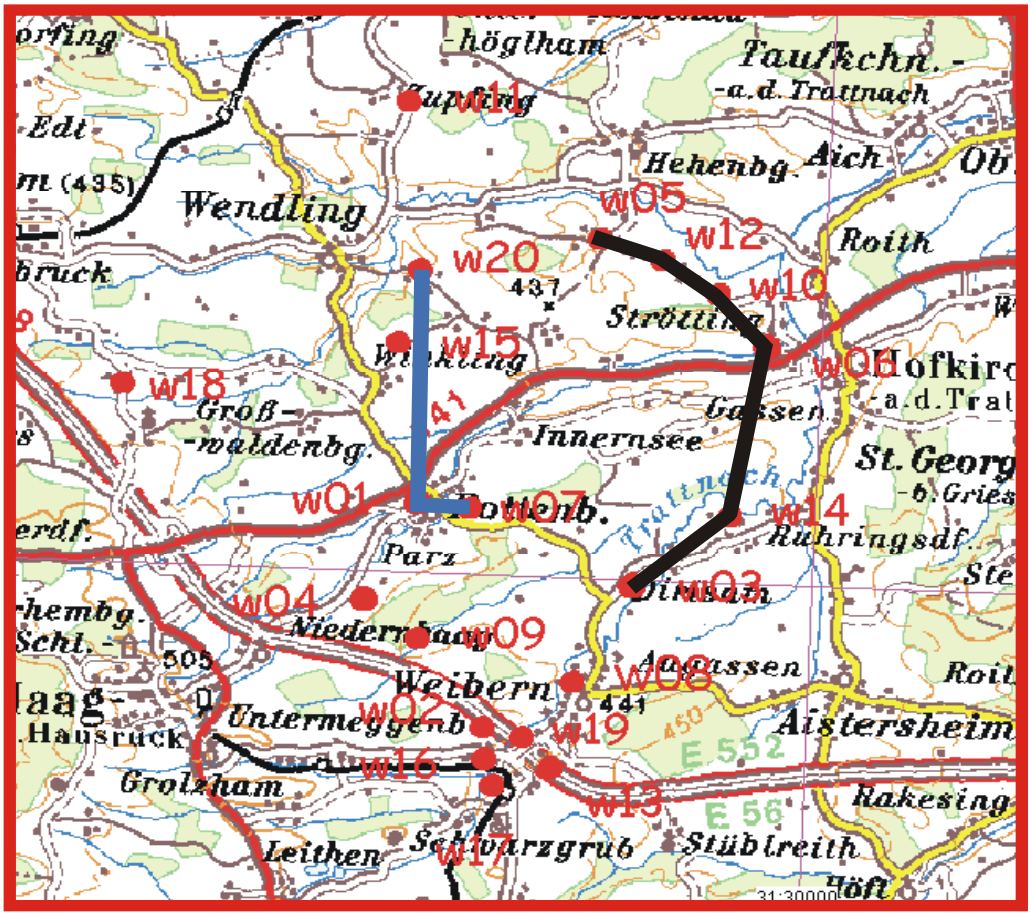

Figure 5.1: Position of the wells and two profiles

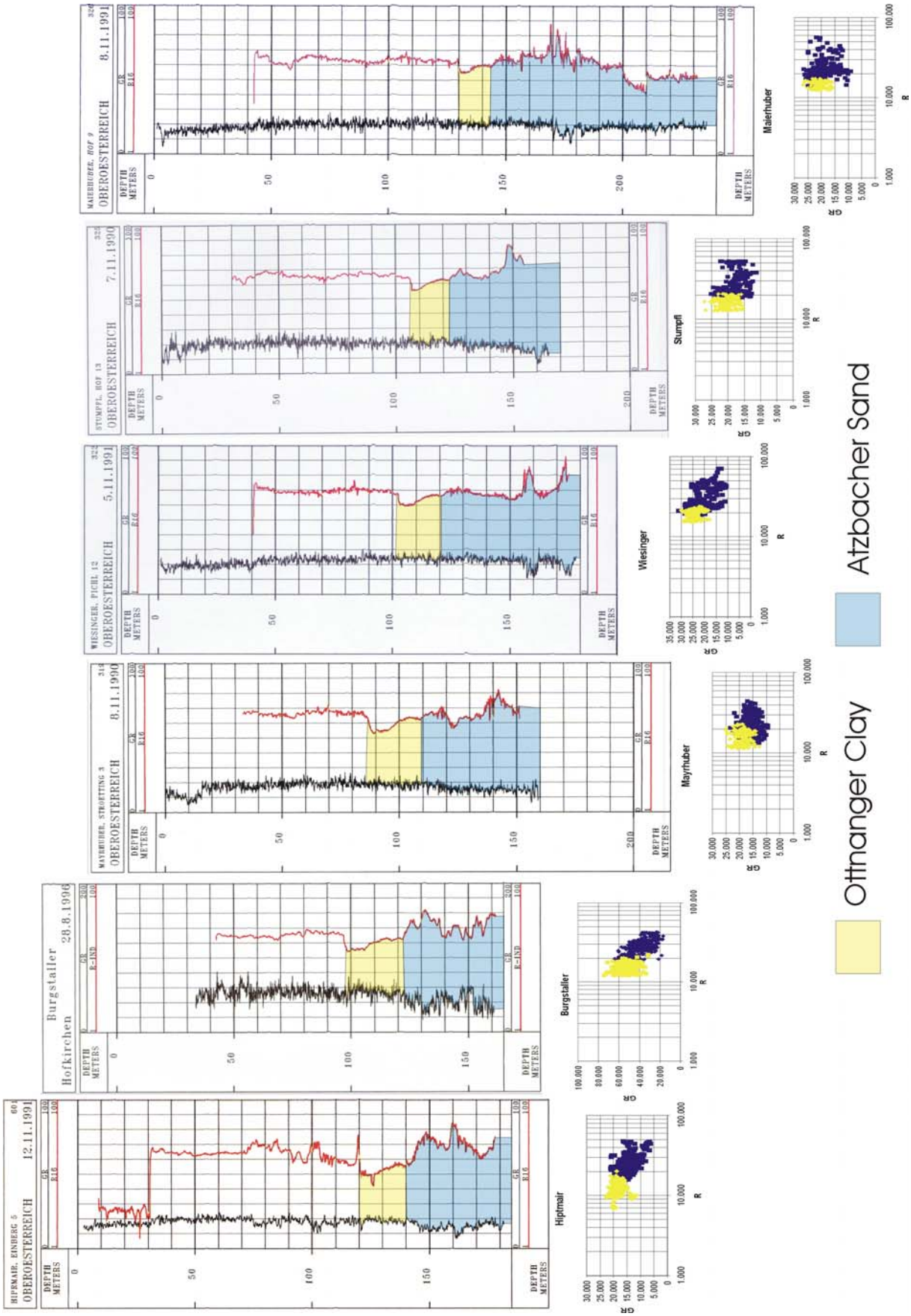

Figure 5.2: Log-correlation with its GR versus R plots

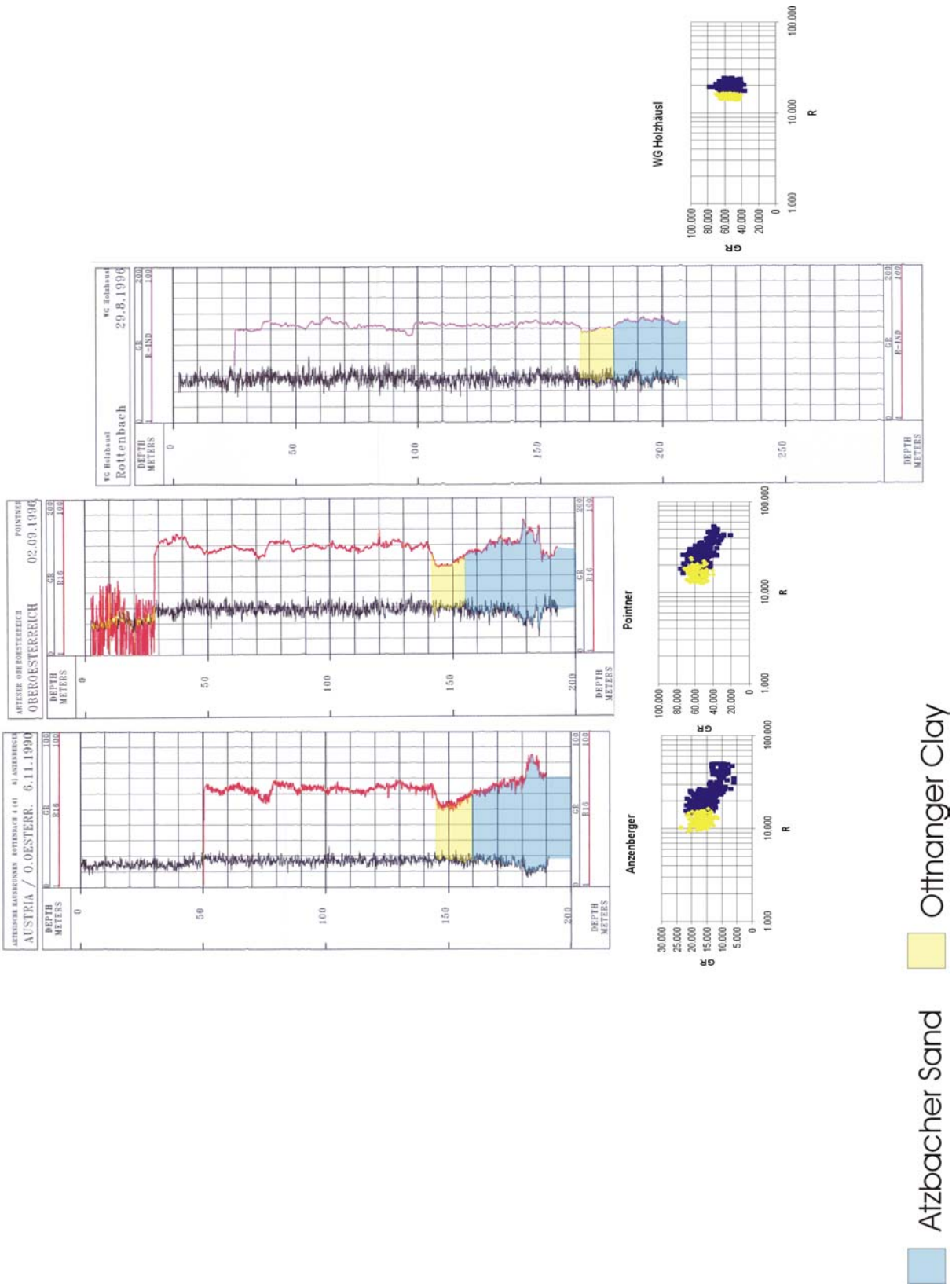

Figure 5.3: Log-correlation with its GR versus R plots

6 Structuremap and Variograms

6.1 Description

Veritas DGC Inc. company developed a program for reservoir characterization named RC$^{2®}$. The company is located in Houston and deals among other things with marine and land-seismic, data processing, geology and petrophysic studies, reservoir-technology and characterization. For developing a structuremap of the top edge of the Atzbacher Sands I needed the RC$^{2®}$ software and its subprograms called RESPREP®, RESGRAM® and RESMOD®.

RESPREP®: Data of wells with location coordinates and elevation, seismic markers and seismic-lines have to be loaded into the program and converted into HDF format. For presentation of the data the Viewsuf window opens. A marker describes a limit between two different lithologies and a marker has to be defined for the limit of Ottnanger Sand and Ottnanger clay, Ottnanger clay and Atzbacher Sand. Markers were defined with the help of the borehole correlation.
After loading data, a suitable grid has to be defined and the grid should not be too large because the program interpolates between the spaces with no information.

RESGRAM®: Vertical and lateral variograms were generated. Vertical variograms describe the consistency of one determined lithology and lateral variograms show the consistency between the wells of one lithology.
With these program statistical data were produced and the modulation of the curve for the data have to be defined by ones own. When modeling these data with empiric curves I had to be aware of the consequence of creating unrealistic geology circumstances or interpretation due to the fact that these created variograms directly effect the modeling of the strucutremap.

RESMOD®: With that program it is possible to create the structuremap with the generated variograms. With the information on seismic data an isoline-map was generated with seismic times and now it is possible to take this map and match it to the defined marker of the Atzbacher Sand/Ottnanger clay limit. So the stratigraphic map shows real depth values measured from absolute elevation above Adria level and no time values anymore.

6.2 Theoretical Background

6.2.1 Semi-Variograms

The semi-variogram is the basic geostatistical tool for visualizing, modeling and exploiting the spatial autocorrelation of a regionalized variable. As the name implies, a semi-variogram is a measure of variance. Although procedures exist for modeling the semi-variogram through iterative or last-squares methods, practitioners recommend actual inspection of the observed semi-variogram and the fitted model. A properly fitted model allows the computer program to calculate linear estimates that reflect the spatial extend and orientation of autocorrelation in the variable to be mapped.
The process of fitting a theoretical semi-variogram model to an observed semi-variogram is called “structural analysis”. The model chosen for a given set of data depends upon both practical and theoretical considerations. Most experimental semi-variograms can be described by a very few theoretical models (Hohn, 1988).
The semi-variogram is used for computing parameters necessary for kriging.

Three models which occur most often are the spherical, the exponential and the gaussian (see Figure 6.1).

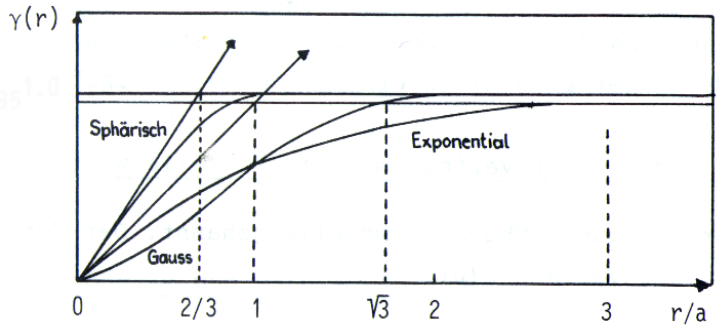

Figure 6.1: Typical models

Geological features represent the similarity or rather the dissimilarity which exists between the grade at one point and the grade some distance away. The error of estimation is thus a function of the similarity which can be expected between samples and a block.

We measure the variability of a regionalized variable z (x) by computing the dissimilarity between pairs of data values, z_α and z_β, located at the points x_α and x_β, in a spatial domain D. The measure for the dissimilarity of two values, labeled γ^*, is given by the formula

$$\gamma_{\alpha\beta}^{*} = \frac{(z_\alpha - z_\beta)^2}{2}$$

i.e. half of the square of the difference between two values (Wackernagel, 1995).
The two points x_α and x_β in geographical space can be linked by a vector

$$h_{\alpha\beta} = x_\beta - x_\alpha$$

as shown in Figure 6.2.

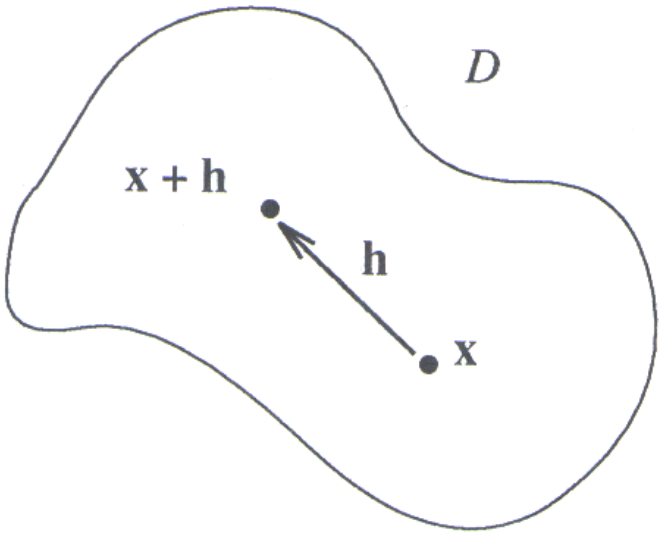

Figure 6.2: **A vector h linking x_α to $x_\beta = x_\alpha + \mathbf{h}$**

The dissimilation depends on the spacing and on the orientation of the point pair.
On graphical representations the dissimilarities will be plotted against absolute values of the vector h. Using all sample pairs in the dataset, a plot of dissimilarities against the spatial separation h is produced which is called the variogram cloud. The h value, so called lag, can be subdivided into a sequence of classes, computing an average for each class.
Usually we can observe that the average dissimilarity between values increases when the spacing between the pairs of sample points increases.
For large spacing the experimental variogram sometimes reaches a sill which can be equal to the variance of the data and the range can be determined on the x-axis. At that point where the curve reaches the sill, a value can be determined at the x-axis and this value is called range. Reaching a certain kind of sill means that there is no similarity any more.
The continuity is reflected by the rate of growth of γ (h) for small values of h. In a sedimentary deposit, changes usually occur very slowly.

A semi-variogram across structural highs and lows displays a so called hole effect. It represents fairly continuous processes. The tangent at the origin is horizontal and it shows a periodic behavior which is often encountered when there exists a succession of similar or non-similar layers, for instance.

The most natural way to compare two values is to consider their difference. We want to consider the squared differences and select the dissimilarity. As a simple case, take samples regularly distributed along a line as in Figure 6.3. We have **n** samples at an interval of **d** feet, thus we will have (n-1) pairs to compute γ(d), (n-2) pairs to compute γ (2d) and so on.

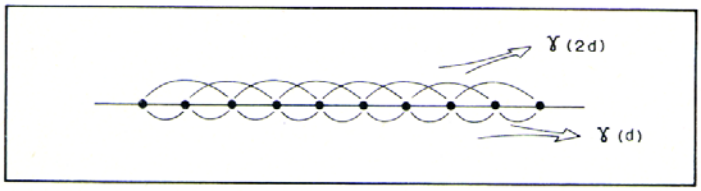

Figure 6.3: Schematic computation of a variogram, using pairs of samples a given distance apart

Many observed variograms do not approach zero with decrease of separation distance. Instead, projecting a straight line fitted to the first few points of the experimental semi-variogram gives a nonzero y-intercept C_0. This observation is known as the nugget effect from characteristic appearance of the semi-variogram for gold deposits.
The nugget effect implies that sampling a given site more than once would yield different measurements because of low precision in the measurement or fine-scale variation in the phenomenon under study.

6.2.2 Kriging

Kriging can be used as an interpolation method to estimate values on a regular grid using irregularly spaced data. Kriging is preceded by analysis of the spatial structured of the data. The representation of the average spatial variability is integrated into the estimation procedure in the form of a variogram model. A regular grid is defined on the computer and so a raster presentation of the kriged grid was chosen. The kriging variance is primarily a measure of the density of information around the estimation point.
A way to represent the results of kriging in a smooth way is to contour them with a different sets of isolines.

Kriging is in fact a word which has been coined to cover both “best linear unbiased estimator” (B.L.U.E.) of a point and the best linear weighted moving average of a block.
The problem of searching a data file for the samples influencing the block is not particular to kriging. It occurs for any weighted average method, but not much literature is available on this subject. Two points are important for us: the searching technique and the stopping criterion.
The stopping criterion can simply be based upon the distance of the sample to the block or point to be estimated.
In most sophisticated weighted average programs, the search around a block is performed by octan in the plane or cones in space, in order to insure a balanced representation of all directions in space rather than taking the first N neighbors. This is to avoid the shadow effect when clusters of samples occur in some directions and not in others.
This is an unnecessary step in kriging since if clusters of samples occur, the introduction of the covariances between samples automatically splits the influence among the constituents of the cluster avoiding its overrepresentation. A good example is given by Delfiner (1973), comparing the weights given by kriging or inverse distance method (see Figure 6.4). It can be seen how to insure a regular density of sampling points (David, 1988).

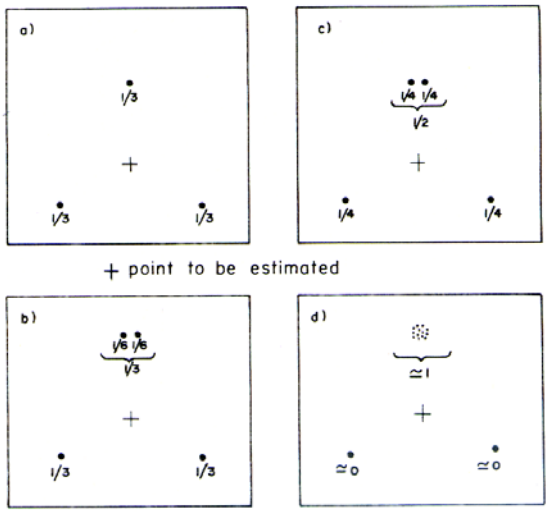

Figure 6.4 Kriging ensures a correct representation of clusters of samples (a and b), while an inverse distance method overestimates their weight (c and d). After Delfiner (1973).

6.3 Evaluation

The positions of the wells used for the structure map is shown in Figure 6.5. Table 6.1 represents all data like the coordinates, the elevation, the depth of the wells and the depth of the measurements available. The wells written in blue show a reasonable depth to reach the Atzbacher Sand horizon.
All the others are too shallow in depth for gaining their water from the Atzbacher aquifer. That gives rise to the assumption that there must be a second aquifer lying on the top of the Atzbacher Sands in the Ottnanger Schlier facies, which as well has the potential for an aquifer.

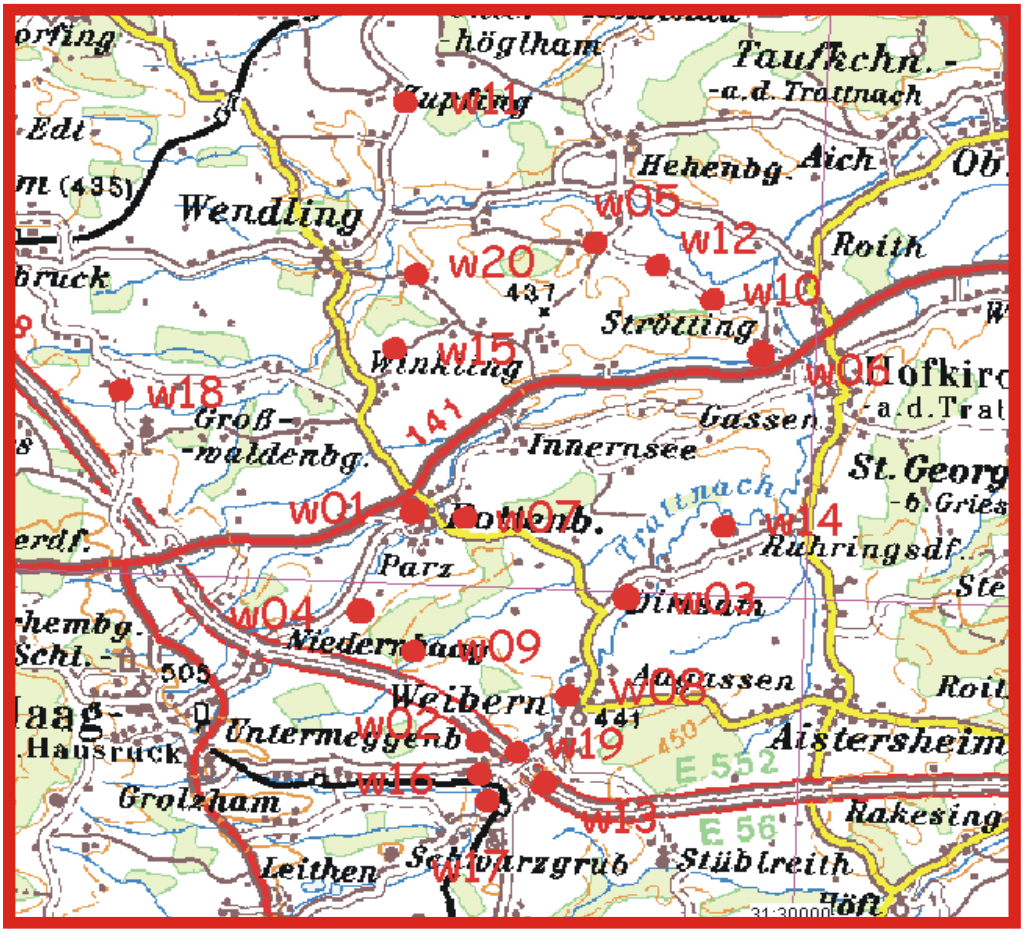

Figure 6.5: Position of the wells

Notation	Wellname	Measurement	Coordinate X	Coordinate Y	Elevation m	Welldepth m	Measurementdepth m
w01	ANZENBERGER	GR,R16	5.340.873	25.782	424.4	200.0	191.0
w02	HANGL	GR,R16	5.338.137	26.722	453.6	110.0	105.4
w03	HIPTMAIR	GR,R16	5.339.754	28.047	422.4	184.0	182.3
w04	JEDINGER	GR,R16	5.339.846	25.358	438.5		84.8
w05	MAIRHUBER	GR,R16	5.344.192	27.728	388.9	240.0	231.7
w06	MAYRHUBER	GR,R16	5.342.923	29.485	385.5		159.2
w07	POINTNER	GR,R16	5.340.990	25.907	419.0	192.0	194.0
w08	SCHROEGENDORFER	GR,R16	5.338.845	27.458	434.4		151.5
w09	THALHAMMER	GR,R16	5.339.157	25.913	447.9	97.0	96.5
w10	WIESINGER	GR,R16	5.343.390	28.923	387.0	186.0	178.5
w11	ZUPFING	GR,R16	5.345.507	25.536	433.1		240.0
w12	STUMPFL	GR,R16	5.343.816	28.160	384.9	165.0	162.0
w13	BRUCKMUELLER	GR,IND	5.337.849	27.326	450.8	170.0	160.0
w14	BURGSTALLER	GR,IND	5.340.842	29.143	405.5	162.0	162.0
w15	DIRISAMER	GR,IND	5.342.655	25.471	422	300.0	199, 178
w16	HOERANDTNER	GR,IND	5.337.888	26.630	449,6	90.0	87.0
w17	KREMPL	GR,IND	5.337.668	26.555	447.9	90.0	75.0
w18	RAAB	GR,IND	5.342.067	22.481	335.3	340.0	172, 141
w19	SCHOENLEITNER	GR,IND	5.337.904	26.921	448.2	90.0	87.0
w20	WG HOLZHÄUSL	GR,IND	5.343.557	25.707	402.6	290.0	284, 210
w21	MITTER	GR,R16	5.340.734	25.835	416,8	185	174,1
w22	ZAUNER	GR,R16	5.338.217	27.254	443,6		85,5
w23	KITZMANTEL	GR,R16	5.338.263	27.455	445,1	160	85
w24	MAIR	GR,R16	5.343.689	28.457	380	170	146,8
w25	SCHWARZGRUBER	GR,R16	5.342.320	30.276	388,8	170	40
w26	VORABERGER	GR,R16	5.342.619	27.695	398,5	192	56
w27	WALDERDORFER	GR,R16	5.343.896	29.826	376,1	70	101,2

Table 6.1: Data for the wells in Upper Austria, the wells shown in blue are reaching the Atzbacher horizon

6.3.1 Gridmap

The Figure 6.6 represents the gridmap generated in Viewsurf. Seismic lines are colored yellow and the wells are shown in red. The grid has to be defined to represent the area of the structuremap. In reality the whole grid area represents a square with the width and the height of 12.000m. The number of sub-classified grids representing the whole area is 120 x 120. Figure 6.7 displays the geographical map of the investigated area.

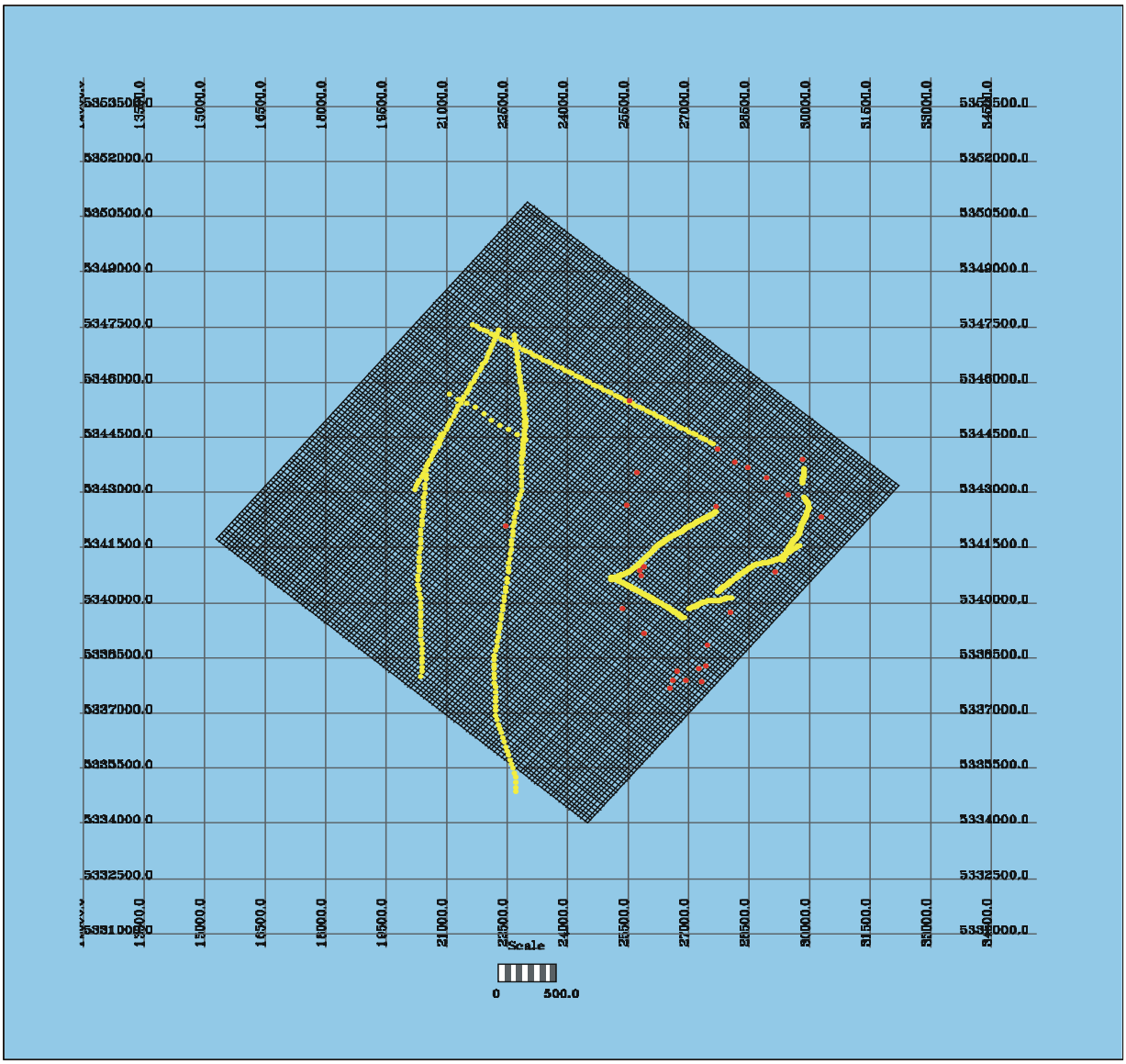

Figure 6.6: Gridmap, M 1:500

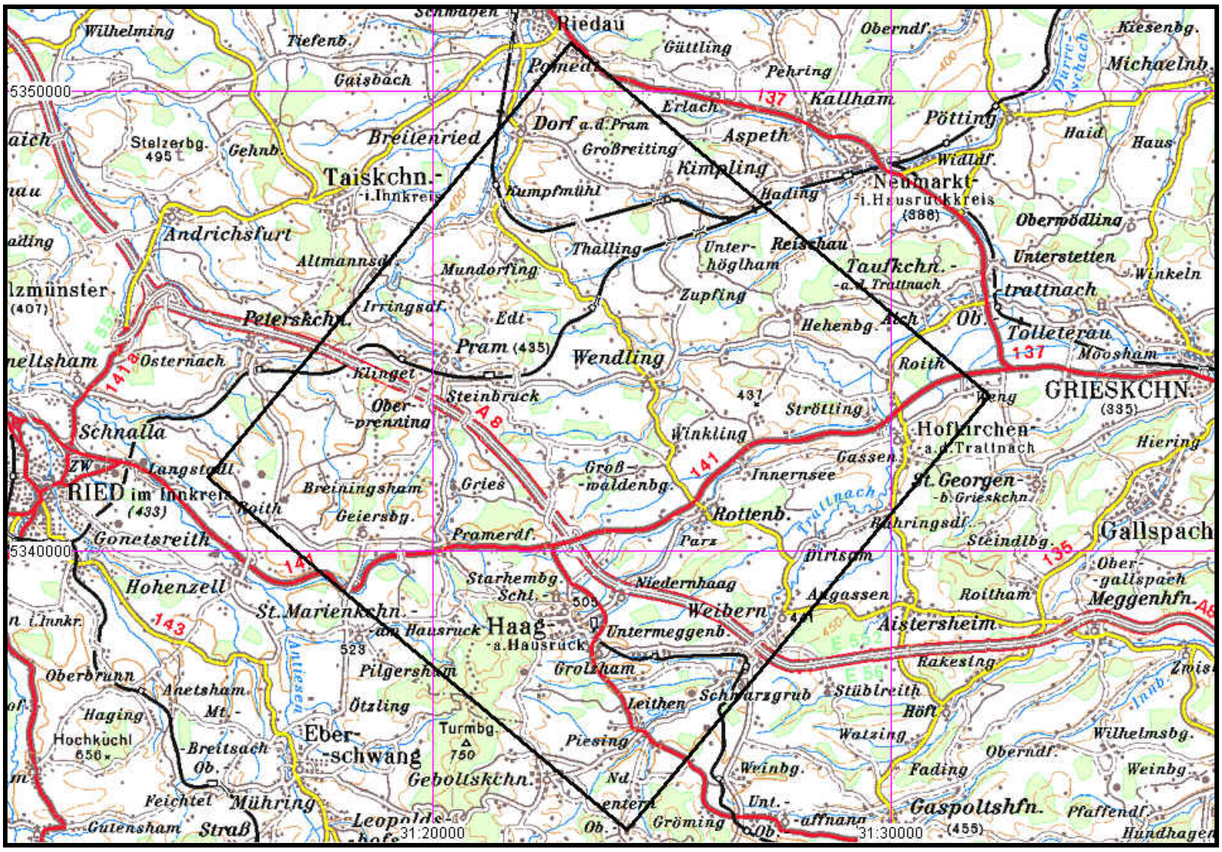

Figure 6.7: Geographical map of the investigated area

6.3.2 Structuremap

The scale in the structuremap tells about the elevation of the horizon and ranges between 170-310 m above Adria level. It is obvious to see that the inclination dip of the Atzbacher horizon is NW and the strike direction is from SW to NE (see Figure 6.8). The red colored syncline has to be discussed because most probably it is an artifact and does not represent the true geological structure. The question how such a mistake could occur can be answered as false picking the Atzbacher horizon on the seismic line.

To avoid a false interpretation of the structure map, I decided to delete the suspicious seismic line supported by the fact that the two other crossing seismic lines show no assumption for such an increase of depth. As a consequence this would lead to a false interpretation and representation of the depth-map of the top of the Atzbacher Sands.
The result of the new created structure map is shown in Figure 6.9.

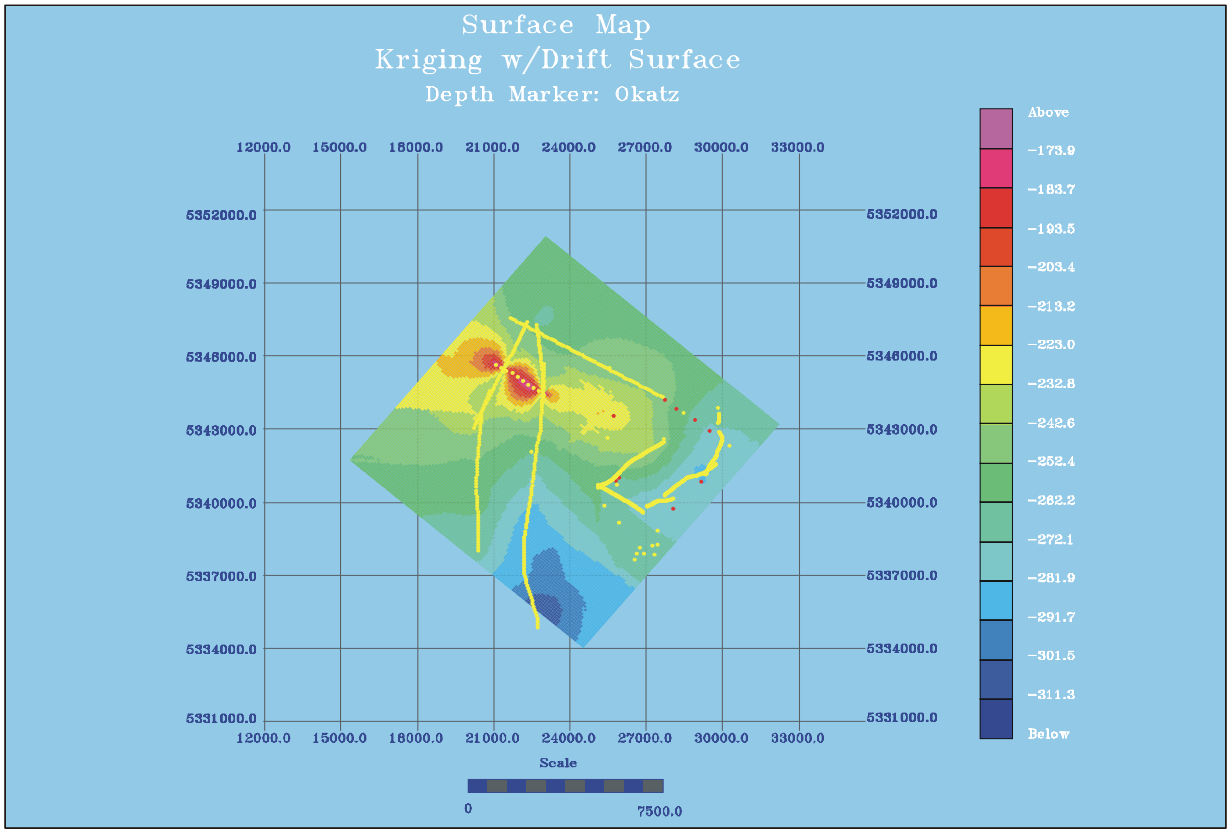

Figure 6.8: Structuremap

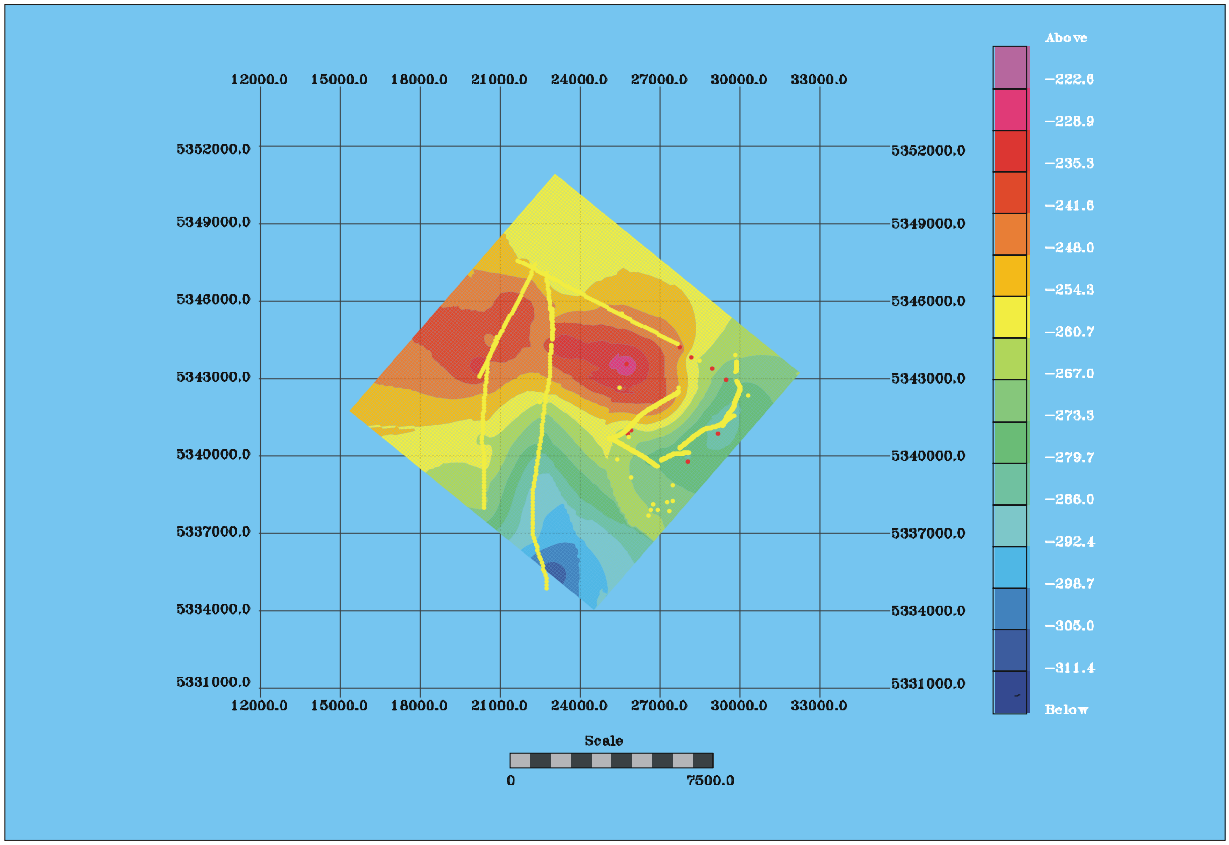

Figure 6.9: New structuremap without the suspicious seismic line

6.3.3 Vertical Variograms

In that case the y axis γ^*(h) equals R16(h) and the x-axis represents the lag-distance in m. The number of lags are 30, and the lag size is 0,1 m and the lag tolerance 0,05 m. The gamma-ray data are not used for displaying the variogram because it shows no typical variation due to the Schlier is relatively monotonic in its gamma log.
The yellow boxes, shown in the variogram, display the number of data available for the statistic evaluation. The data density decreases with increasing of lag distance.
The number of data can be calculated when dividing the thickness of the Ottnanger clay or Atzbacher Sand horizon by the variation of lag distance.

6.3.3.1 Vertical variogram of Ottnanger Schlier facies at well w05

The variogram, displayed in Figure 6.11, shows a range-value of 4,1 meter and the theoretical model that is used for approaching the empirical data, shown in red, is an exponential one. That means in a distance of 4,1 m the values of R16 are still correlating .Upon the distance of 4,1 m the layer shows dissimilarity. The layer-thickness is about 14 m. The increase of dissimilarity with lag distance shows a slow trend and therefore the whole horizon can be interpreted as a more or less homogenous strata. There is no evidence for a strong lithofacies change in that horizon.
The same statement can be made when looking at the resistivity values of the plot in Figure 6.10 and that is supported by the statistical evaluation.

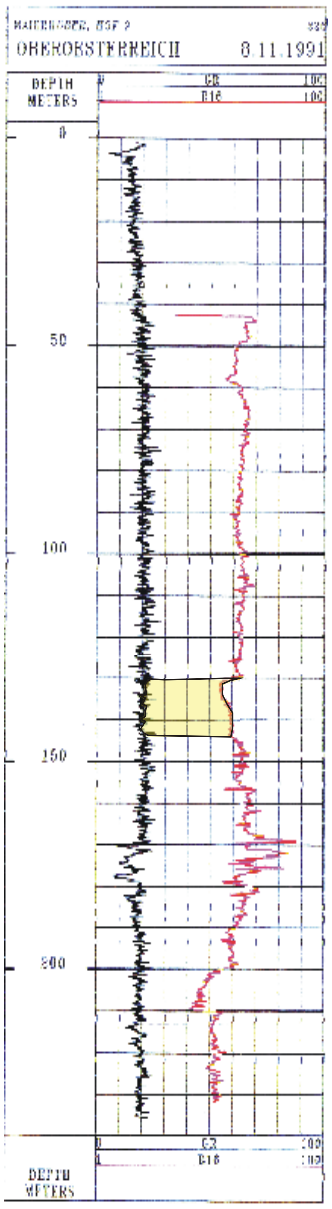

Figure 6.10: Plot of w05

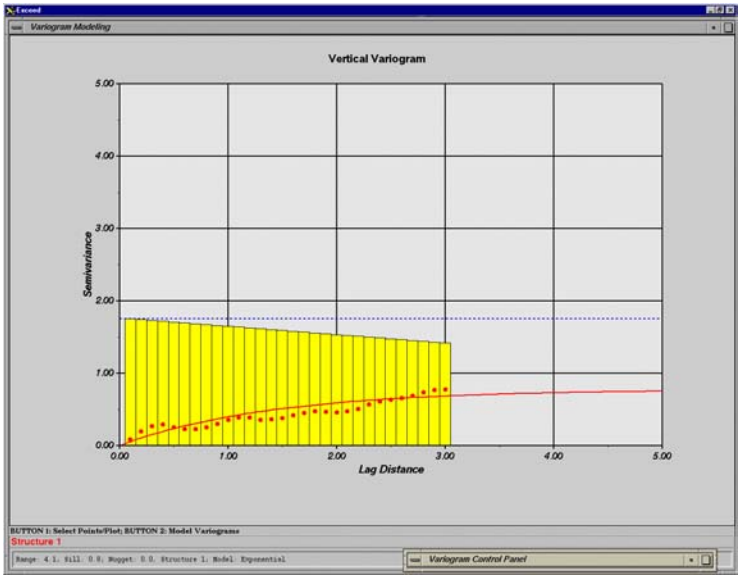

Figure 6.11: Variogram of w05

6.3.3.2 Vertical variogram of Ottnanger Schlier facies at well w07

The empirical data are approached by a gaussian model. After a range of 3 meters the horizon shows dissimilarity. The rise of the curve is relatively high but still there is a correlation in a distance of less than 3 meters when using the gaussian model for approaching the empirical data. Comparing this data with the data from well w05 than the y-values are much higher and therefore implying a worse correlation as it is the case in variogram w05. The layer-thickness with 15 meters, compared to well w05, did not change much. After a lag distance of 3 meters the dissimilarity reaches a value of more than 4 and this is compared to well w05 very high. This is a good example for demonstrating the choice of the model witch is approaching the data (see Figures 6.12 and 6.13).

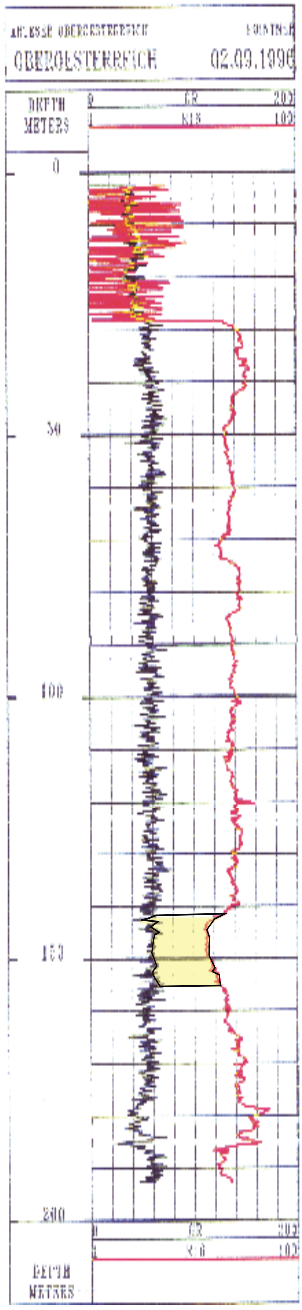

Figure 6.12: Plot of w07

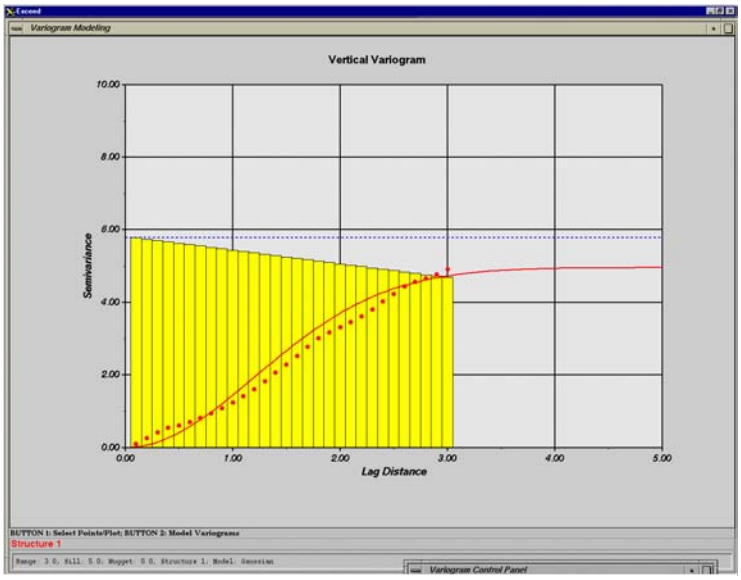

Figure 6.13: Variogram of w07

6.3.3.3 Vertical variogram of Ottnanger Schlier facies at well w14

The thickness of the horizon is about 26 meter and the gaussian model has been used for approaching the data. The sill is reached after 3 meters and at that distance the dissimilarity is very high. A correlation is only possible in between 3 meters. This variogram is very similar to that of well w07 (see Figures 6.14 and 6.15).

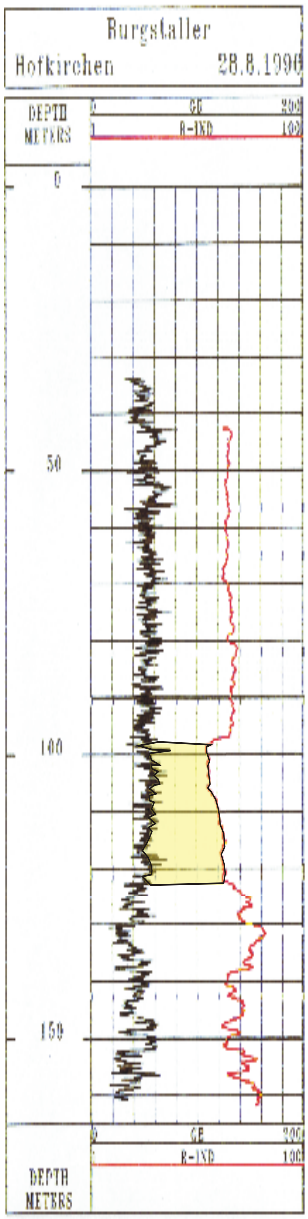

Figure 6.14: Plot of w14

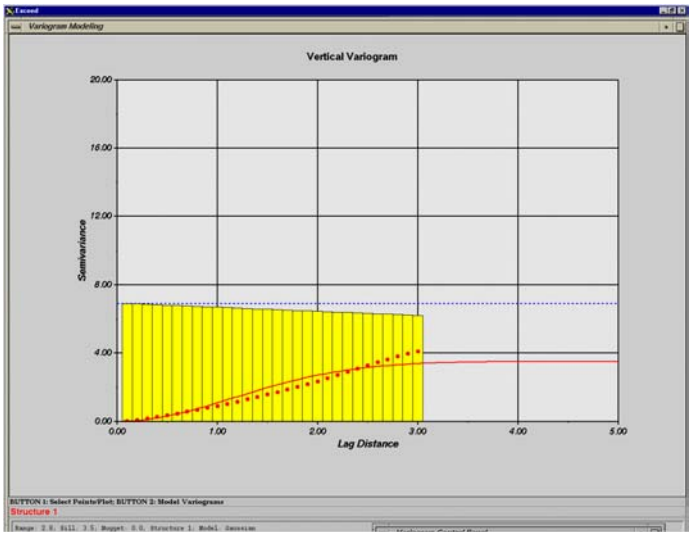

Figure 6.15: Variogram of w14

6.3.3.4 Vertical variogram of Ottnanger Schlier facies at well w01

The curve does not start at 0 point on the y-axis and that effect is called “nugget effect”.

The nugget effect means that the variogram does not approach zero with decreasing separation distance. An exponential model has been used for approaching these data points and the nugget effect is about 0.7. The thickness of the clay horizon is 14 m and as you can see from the up and down trend of the data that the horizon is not very homogenous. After a certain distance the dissimilarity becomes less and then more again and so on. This is an evidence for a slight layering (see Figures 6.16 and 6.17).

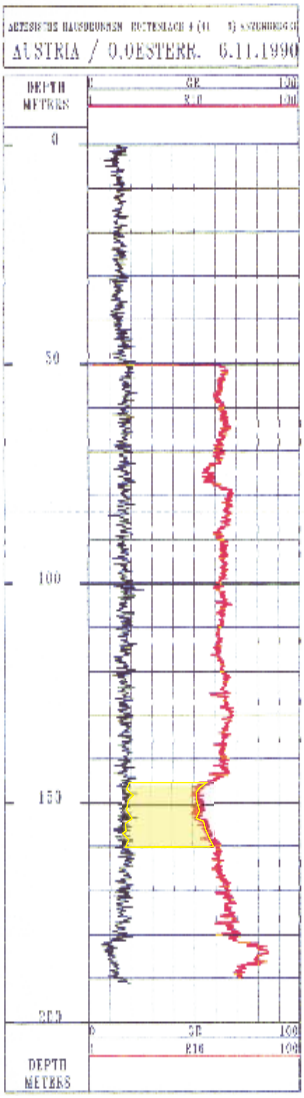

Figure 6.16: Plot of w01

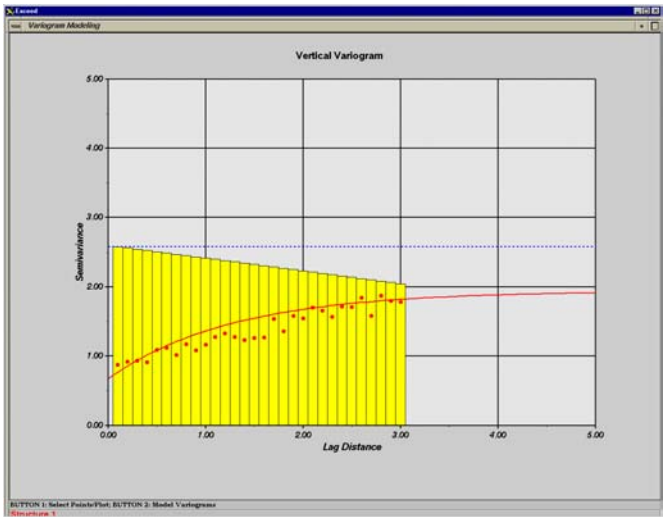

Figure 6.17: Variogram of w01

6.3.3.5 Vertical variogram of Ottnanger Schlier facies at well w20

The linear model has been used to approach the empirical data and the range is about 2,4 m. The thickness riches a value of 13m. Looking at the dissimilarity of 0,2 in a lag distance of 2,4 meter than the correlation between the data is still very high. The data show no oscillation effects at all and that means that there occurs no layering and the horizon can be interpreted as a very homogenous one (see Figures 6.18 and 6.19).

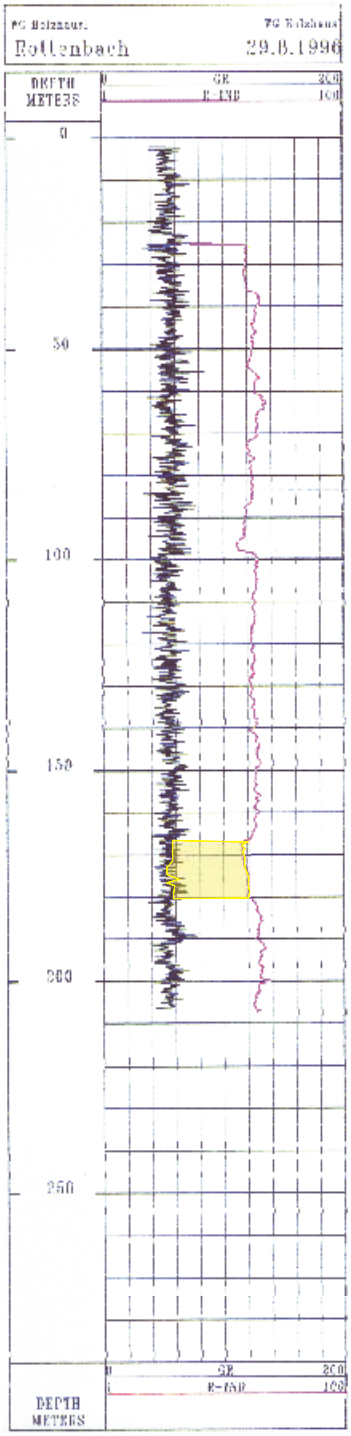

Figure 6.18: Plot of w20

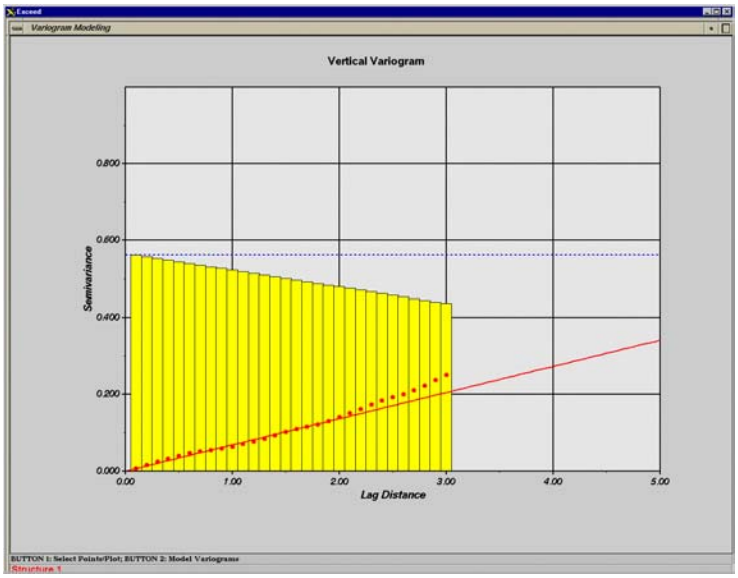

Figure 6.19: Variogram of w20

6.3.3.6 Vertical variogram of Ottnanger Schlier facies at well w03

The exponential model fits the empirical data of the variogram best. A range of 1,8 m has been determined and the thickness of the horizon is about 23 m. But the homogenity of the Ottnanger clay is a more or less good one without oscillation effects and a low value of dissimilarity after a distance of 3 meters (see Figures 6.20 and 6.21).

Figure 6.20: Variogram of w03

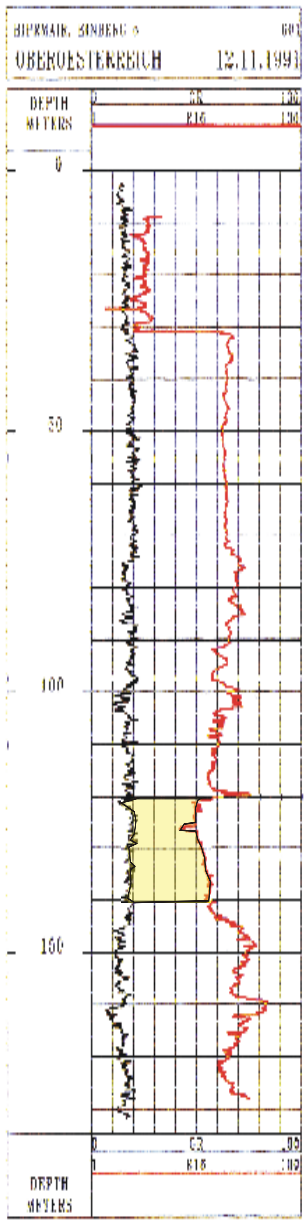

Figure 6.21: Plot of w03

6.3.3.7 Vertical variogram of Ottnanger Schlier facies at well w06

A very nice correlation between the data demonstrates this example. For modeling the data the exponential model has been used. The range of 5 m is very high and the thickness is about 23 m. The homogenity of that horizon is brilliant without hole effects or nugget effects. The similarity of the data is expressed by the linear trend of the curve (see Figures 6.22 and 6.23).

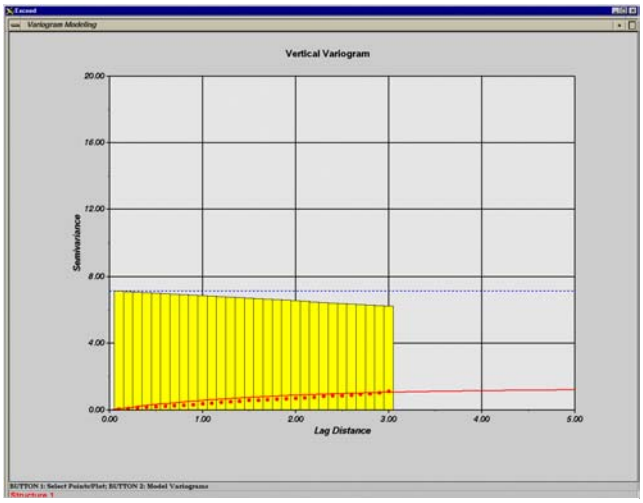

Figure 6.22: Variogram of w06

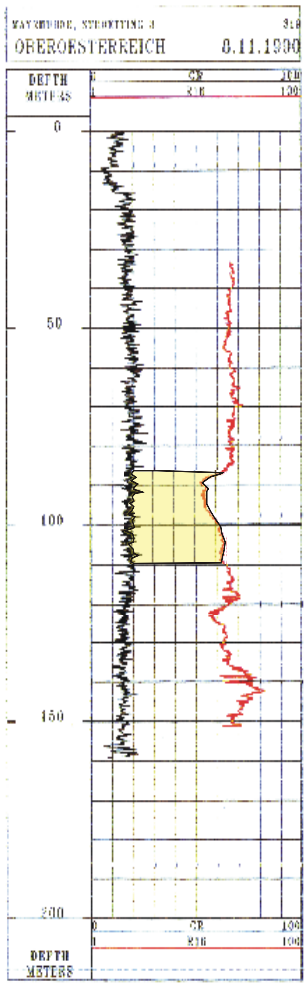

Figure 6.23: Plot of w06

6.3.3.8 Vertical variogram of Ottnanger Schlier facies at well w10

The Ottnanger clay horizon at well w10 shows very similar values as well w06 does. The same linear trend without marks of layering or inhomogenity. The range is also 5 m and the thickness about 20 m. The exponential model has been used and fits the data best with its characteristic trait (see Figures 6.24 and 6.25).

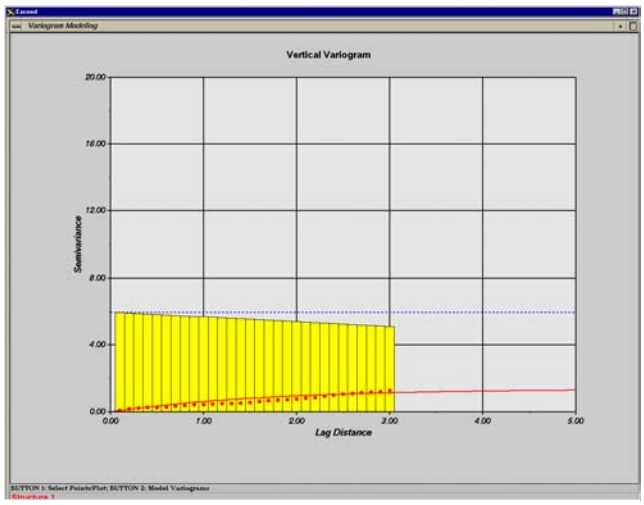

Figure 6.24: Variogram of w10

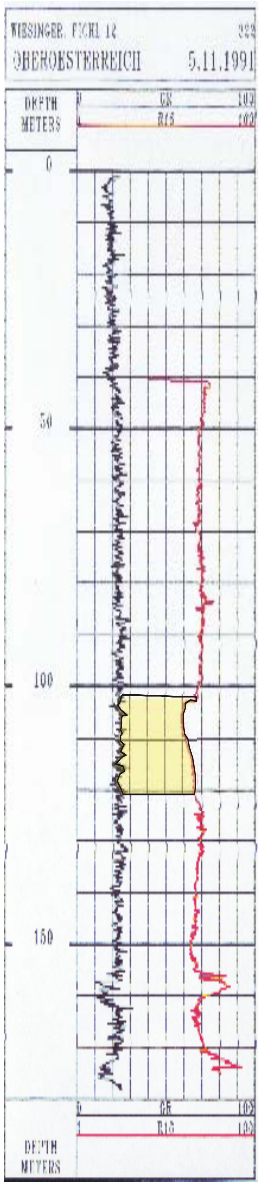

Figure 6.25: Plot of w10

6.3.3.9 Vertical variogram of Ottnanger Schlier facies at well w12

For modeling these data the gaussian model has been used, due to the fact that the data fit very nice at the beginning and then the dissimilarity increases slightly. The range is 3,2 m and the layer thickness about 19 m. The homogenity can be interpreted as very high due to the low dissimilarity values at a lag distance of 3 meters (see Figures 6.26 and 6.27).

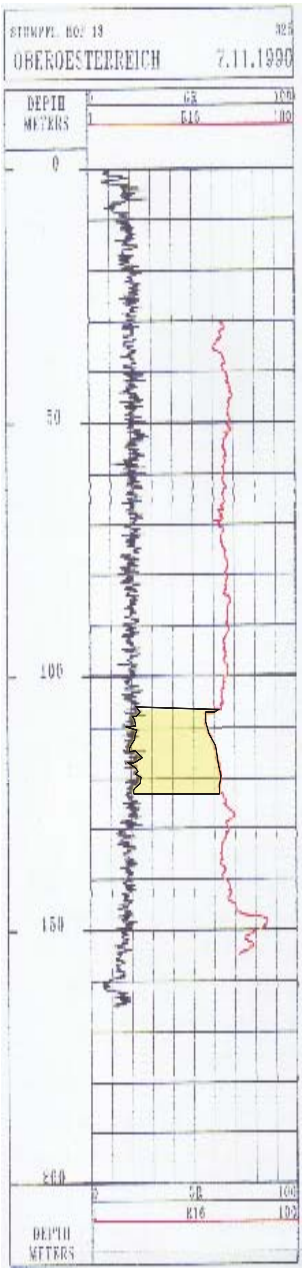

Figure 6.26: Plot of w12

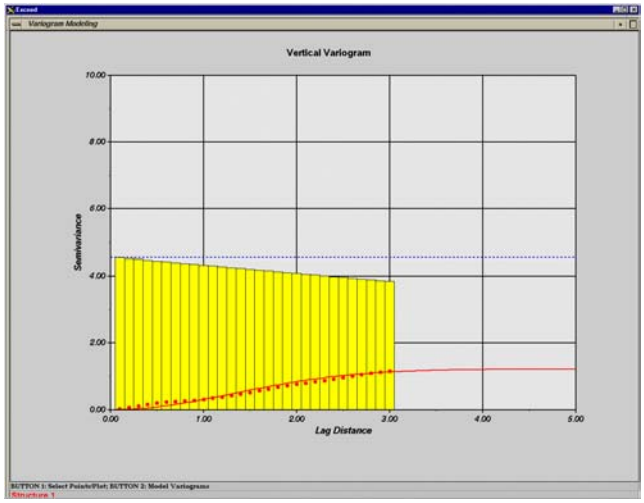

Figure 6.27: Variogram of w12

6.3.3.10 Vertical variogram of Atzbacher sand facies at well w01

The model that has been used for approaching the empirical data is an exponential one and the range is about 2,5 m. The thickness reaches a value of 31 m. As you can see from the data the values are scattering and show a little oscillation effect. For fitting the data best a nugget effect has been used and when looking at the Ottnanger clay variogram from the same well you can see that there also occurs a nugget effect. That means that the values are scattering at the very beginning distance.
Due to these results a layering of clay and sand could be interpreted and therefore the homogenity is not too high (see Figures 6.28 and 6.29).

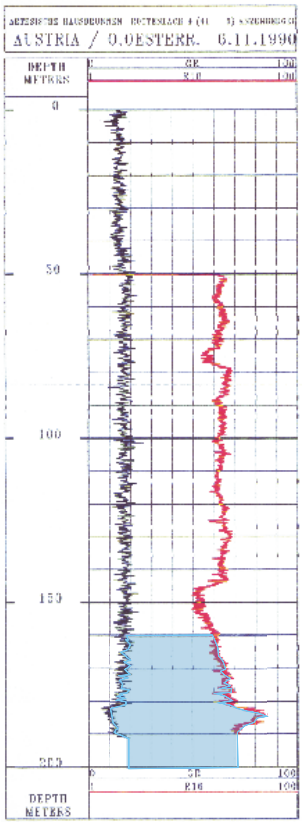

Figure 6.28: Plot of w01

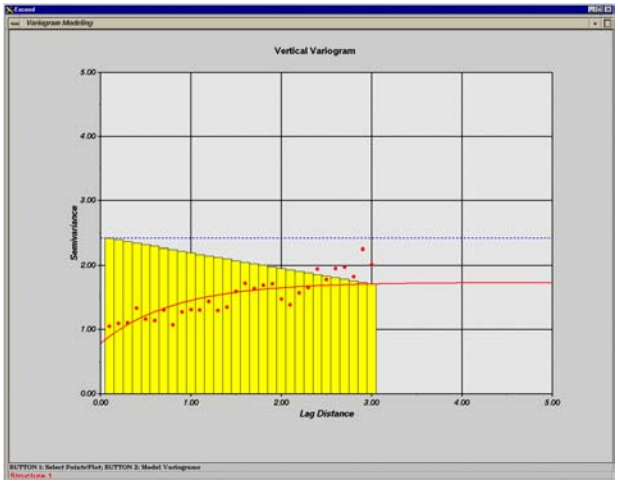

Figure 6.29: Variogram of w01

6.3.3.11 Vertical variogram of Atzbacher sand facies at well w20

For modeling these empirical data the linear model has been used and the range is 1,8 m. The thickness of the horizon reaches a value of 40 m. No oscillation effects occur and that means that there is not a high layering, but nevertheless I would interpret the strong gradient as a lithology change. That effect has nothing to do with strong interbedding of clays in the sand. It could be interpreted as changing grain sizes or changing mineral character (see Figures 6.30 and 6.31).

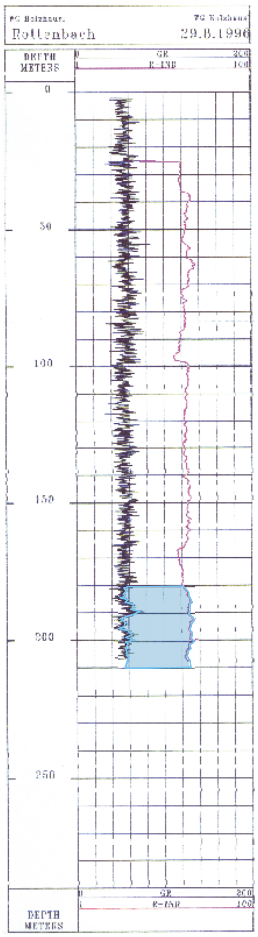

Figure 6.30: Plot of w20

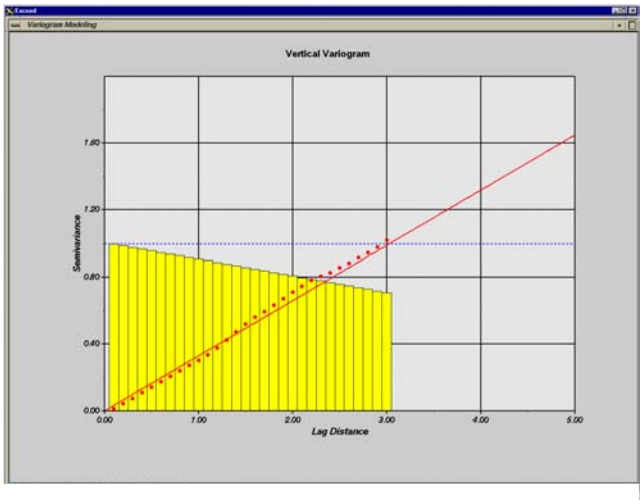

Figure 6.31: Variogram of w20

6.3.3.12 Vertical variogram of Atzbacher sand facies at well w03

At a low lag-distance there is a similarity of the lithology of the horizon, but farer away the dissimilarity increases and the exponential model has been used for fitting the first part of the

variogram best. I'm aware that this model is not the best choice for interpreting the data because the oscillation effect is not to ignore. Unfortunately the program lacks the possibility to model these data set so that I had to choose one which approaches the empirical data best. Therefore the range results in 1m and the thickness of the horizon about 35 m.
When looking at the amplitude of the oscillation compared to well w01 for instance, then the layering can be interpreted as large horizons with different lithology (see Figures 6.32 and 6.33).

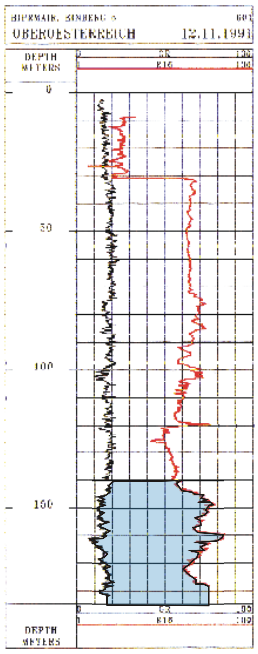

Figure 6.32: Plot of w03

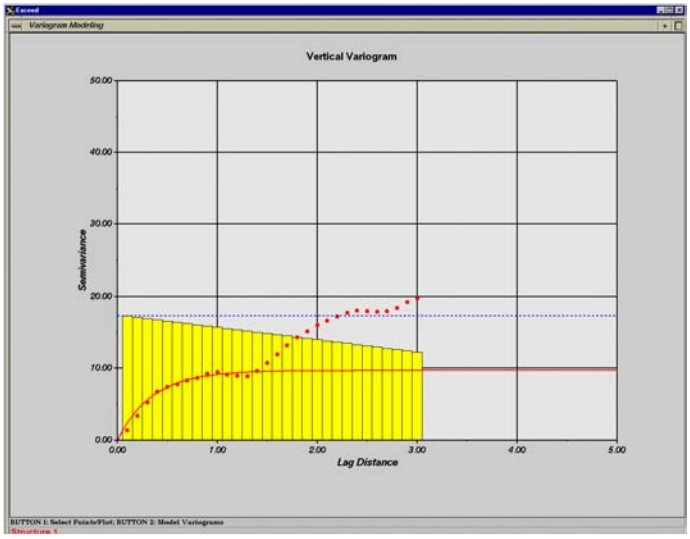

Figure 6.33: Variogram of w03

6.3.3.13 Vertical variogram of Atzbacher sand facies at well w06

At this well a similar problem as in well w03 occurs and it was not possible to choose a good fitting model, but the hole effect speaks for its self. Powerful layers of interbedding can be seen due to the large amplitude of the oscillation effect. The thickness of the layers ranges

between 1 and 2 meters and the similarity becomes larger and smaller again (see Figures 6.34 and 6.35).

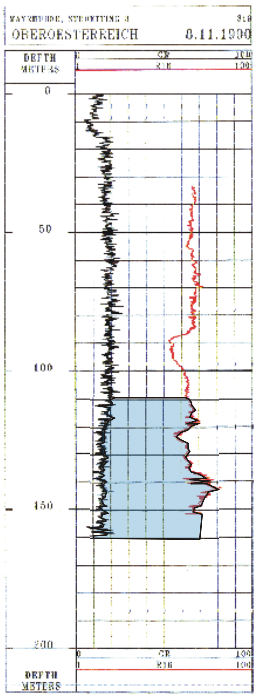

Figure 6.34: Plot of w06

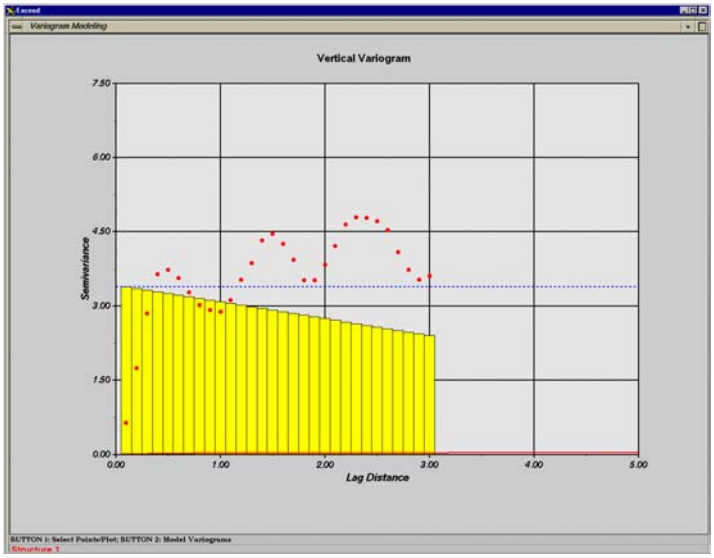

Figure 6.35: Variogram of w06

6.3.3.14 Vertical variogram of Atzbacher sand facies at well w10

The same case as in well w06 occurs in this well when looking at the hole effect of the data. Again no model can be found for approaching the empirical data. The dissimilarity is not as high with 2 as in well w06 where it reaches a value of about 4. That means that the difference with increasing lag-distance is not as high. But there is no doubt that layering of smaller thickness exists (see Figures 6.36 and 6.37).

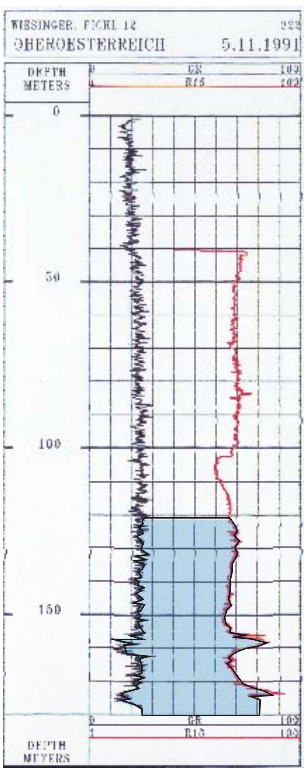

Figure 6.37: Plot of w10

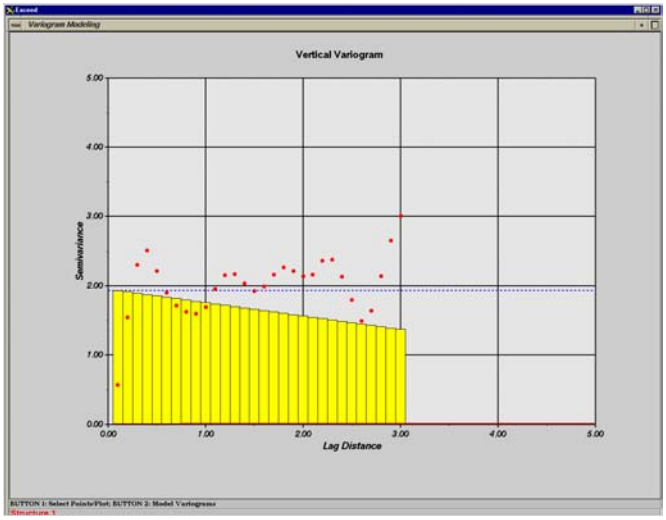

Figure 6.36: Variogram of w10

6.3.3.15 Vertical variogram of Atzbacher sand facies at well w12

With increasing distance the dissimilarity increases as well, at smaller lag-distance not as high as with larger lag-distance. Therefore the gaussian model is the best for interpreting the data

set. At a distance of about 3 meters the data show a trend for becoming similar again but the hole effect is not as clear as in well10 or in well06 (see Figures 6.38 and 6.39).

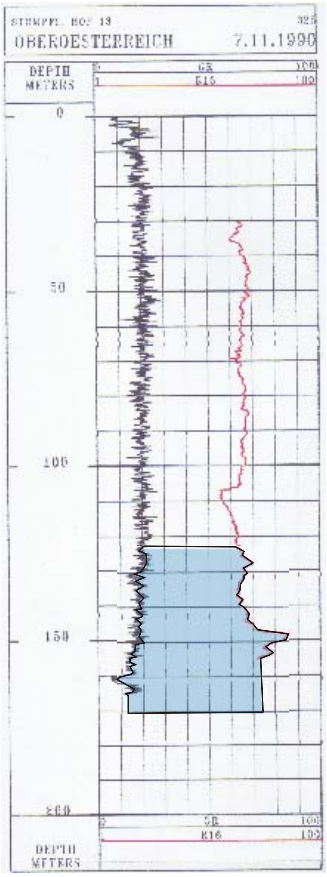

Figure 6.38: Plot of w12

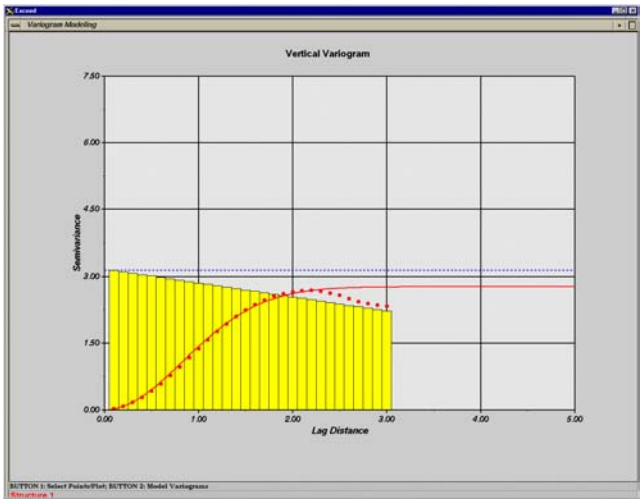

Figure 6.39: Variogram of w12

6.3.3.16 Vertical variogram of Atzbacher sand facies at well w05

The data of the variogram show again an oscillation effect. On the one hand the data correlate very well and on the other they show a high dissimilarity, depending on the lag-distance. The

explanation is a mixed-layer structure. No model has been found for approaching the empirical data. Comparing this variogram to the variogram w06, a high similarity of the data is given when only looking at the amplitude of the oscillation. The only difference is the higher dissimilarity of w06 with increasing lag-distance (see Figures 6.40 and 6.41).

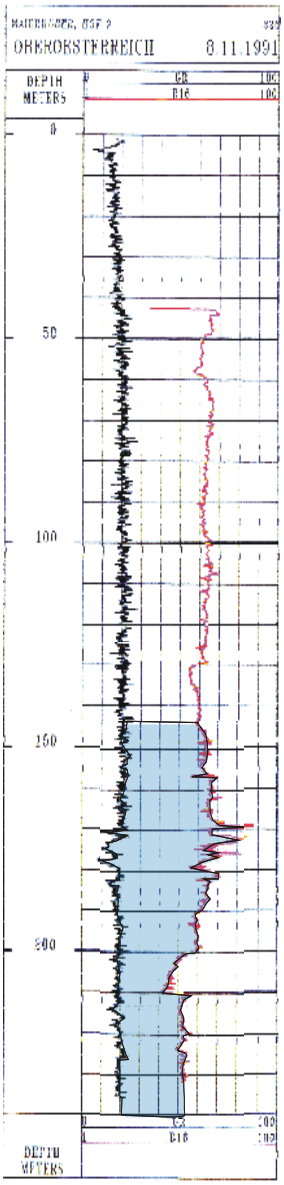

Figure 6.40: Plot of w05

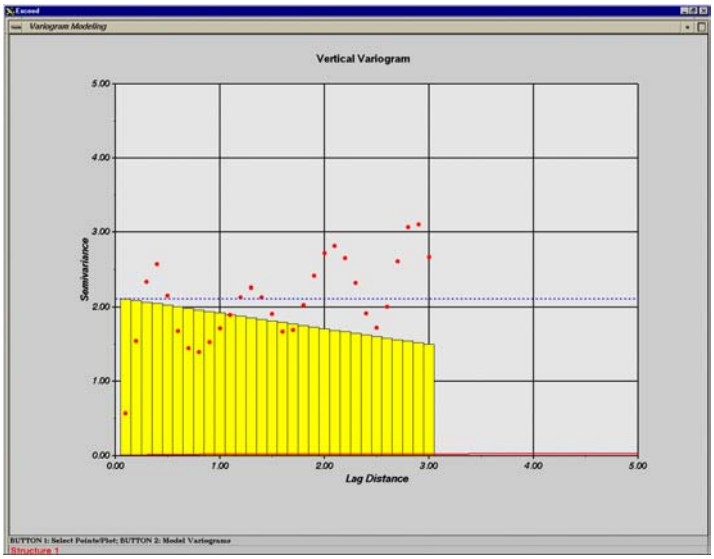

Figure 6.41: Variogram of w05

6.3.3.17 Vertical variogram of Atzbacher sand facies at well w07

The spherical model has been used for approaching the data best. The oscillation of the R16 values is not as strong compared to well w05, but nevertheless it can be seen in a slight way. The range shows a high value of 3.2 m and the abrupt rise of dissimilarity at small lag-sizes means that the lithology strongly changes within short distances (see Figures 6.42 and 6.43).

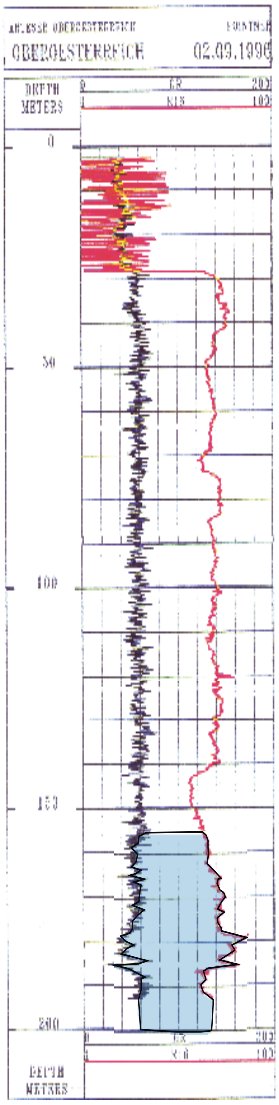

Figure 6.42: Plot of w07

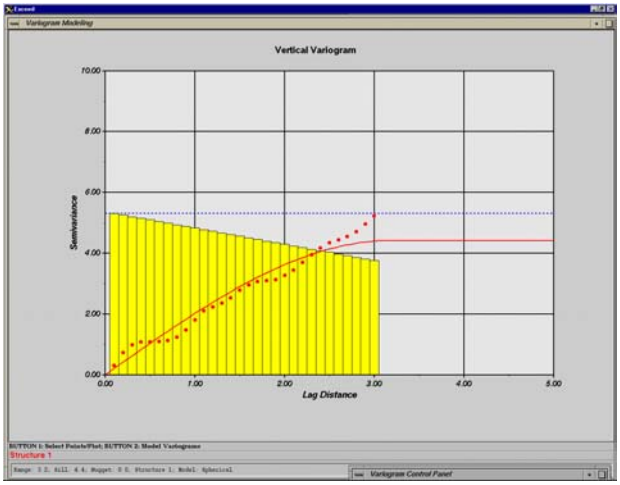

Figure 6.43: Variogram of w07

6.3.3.18 Vertical variogram of Atzbacher sand facies at well w14

The Atzbacher horizon shows no oscillation in this well anymore and the gaussian model determined a range value of 3 m. Compared to well w07, the rise of dissimilarity at small lag-sizes is much higher when comparing the values at the y-axis. The high oscillation at the resistivity log for the Atzbacher horizon shows the same trend (see Figures 6.44 and 6.45).

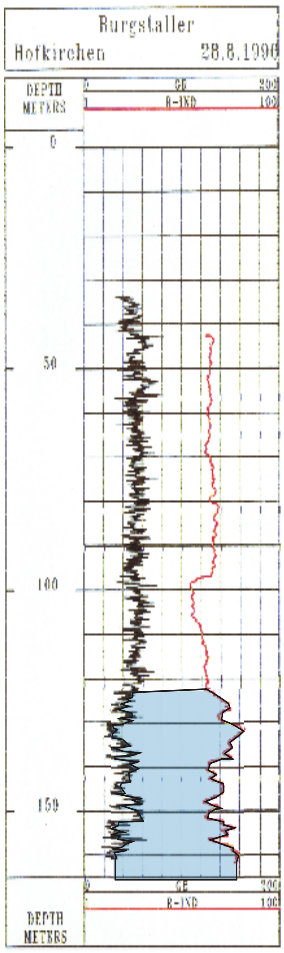

Figure 6.44: Plot of w14

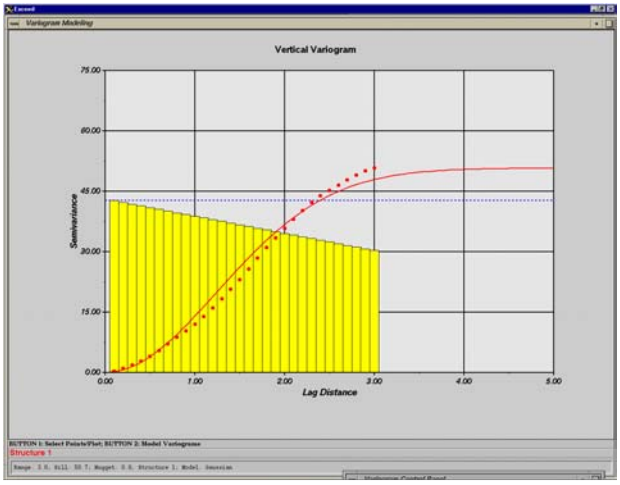

Figure 6.45: Variogram of w14

6.3.4 Results of Semi-Variogram analysis

1) The Ottnager clay and the Atzbacher Sand show a different characteristic in the Semi-Variogram analysis (see Figures 4.46 and 4.47). The Ottnanger clay is much more homogenous and shows no hole effects at all. That means that there is no strong alternating layer structure compared to the Atzbacher horizon. The whole layer mainly consists of clays and marls without a strong change of lithofacies. Regarding the

horizon of different wells, it could be seen that the clay layer does not change much and mainly shows the same character.
The Atzbacher Sand is inhomogenous because of single clay layers in the formation and so the horizon is much more effected from different lithologies.
The character of the lithology changes strongly due to large interbedding of clay layers in the packages, mainly consisting of sand. This is an evidence that the Atzbacher Sands are not as homogenous as the Ottnanger clay. Concerning the single horizons of the Atzbacher Sands in the crop, there could be seen that the sequence shows sands of generally 50 cm thickness always disturbed by clay layers. The thickness of the single different layers always changes depending on the sedimentation cycle.
The Atzbacher Sands were mainly formed in litoral area of the sea and also in the inner shelf area, strongly affected from sea floods. So there is no regularity of the builded sedimentation. The Ottnanger Schlier formation occured in the shelf and slope area of the sea, therefore the sequence is not much effected of sea floods infiltrating sands or other sediments. The theory is verfied by the variograms showing ranges of 2-3 m and very low dissimillarities, in difference to the variograms of the Atzbacher Sands. The homogenous layer of clay above the Atzbacher Sands confirms the theory that the Ottnanger sands are not connected to the Atzbacher horizon and the Atzbacher Sand is building its own horizon of groundwater without connection to the Ottnagner Schlier. Variograms of the Ottnanger clay show that the whole layer is much more homogenous and the R16 values does not show much unregularities and due to that fact I assume that the horizon does not show a regulary layering of sand and clay but at the most a mixture of grainsizes. The variograms confess this assumption due to no hole effects occur beeing an evidence for powerful layering.

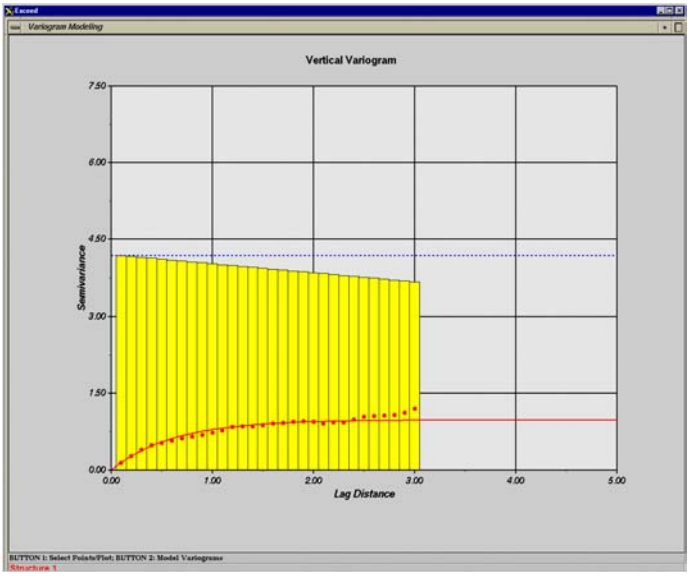

Figure 6.47: Ottnanger clay w03

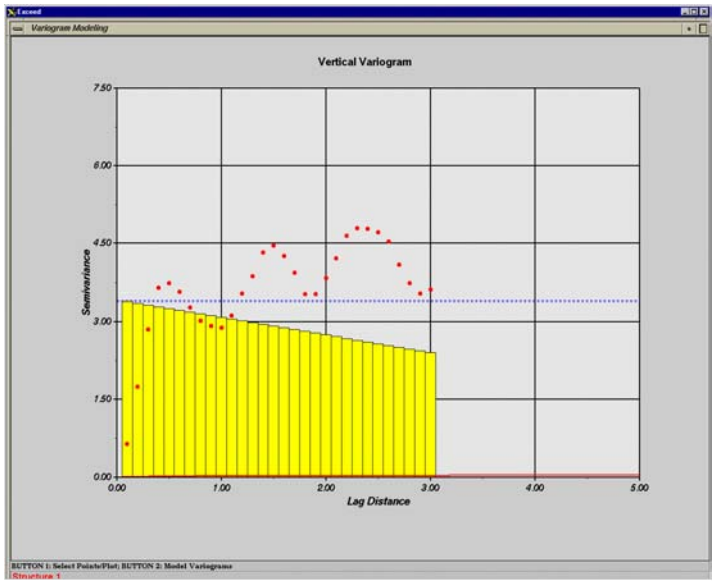

Figure 6.46: Atzbacher sand w06

2) The Ottanger clay variograms can be classified due to the dissimilarity values at a lag distance of 3m into two groups:

- Dissimilarity ranging between 2-5: w07, w014, w01

Wells	Dissimilarity value at lag-distance of 3m	Model	Nugget effect at lag-distance of 0m
W07	~ 5	gaussian	-

W14	~ 4	gaussian	-
W01	~ 2	exponential	~ 1

- Dissimilarity ranging between 0.2 and 1.5: w05, w20, w03, w06, w10, w12

Wells	**Dissimilarity value at lag-distance of 3m**	**Model**	**Nugget effect at lag-distance of 0m**
W05	~ 1	exponential	-
W20	~ 0.2	linear	-
W03	~ 1.5	exponential	-
W06	~ 1.5	exponential	-
W10	~ 1.5	linear	-
W12	~ 1	gaussian	-

3) The Atzbacher Sand variograms can be classified due to the dissimilarity values at a lag distance of 3m and a hole effect into three groups:

- Dissimilarity of ~ 20 with a hole effect: w03

Wells	**Dissimilarity value at lag-distance of 3m**	**Model**	**Nugget effect at lag-distance of 0m**
W03	~ 20	exponential	-

- Dissimilarity ranging between 1 and 5 without hole effect: w01, w20, w07

Wells	**Dissimilarity value at lag-distance of 3m**	**Model**	**Nugget effect at lag-distance of 0m**
W01	~ 2	exponential	~ 1
W20	~ 1	linear	-
W07	~ 5	sherical	-

- Dissimilarity ranging between 1 and 5 with a hole effect: w06, w10, w12, w05

Wells	**Dissimilarity value at lag-distance of 3m**	**Model**	**Nugget effect at lag-distance of 0m**
W06	~ 4	-	-
W10	~ 3	-	-
W12	~ 2	gaussian	-
W05	~ 3	-	-

7 Literature

Quoted Literature:

Clavier, C. & Coates, G. & Dumanoir, J., (1984) : The Theoretical and Experimental Bases for the Dual-water Model for Interpreation of Shaly-sands, Soc. Pet. Engrs. J., 24, 153-167, 1984

David, Michel, (1997): Geostatistical Ore Reserve Estimation, Elsevier Scientific Publishing Company, 1997

De Witte, L., (1955): A Study of Electric Log Interpretation Methods in Shaly Formations, Trans. AIME 204, 103-110, 1955

Ellis, Darwin V., (1987): Well Logging for Earth Scientists, Elsevier Science Publishing Co. Inc., New York, 532 pages, 1987

Faupl, Peter & Roetzel, Reinhard, (1987): Gezeitenbeeinflusste Ablagerung der Innviertler Gruppe (Ottnangien) in der oberösterreichischen Molassezone, Jb.Geolog.B.-A., Band 130, Heft 4, 415-447, Wien, 1987

Gillott, Jack E., (1968): Clay in Engineering Geology, Elsevier Publishing Company, Amstersdam London New York, 1968

Kezdi, A., (1969): Handbuch der Bodenmechanik, VEB Verlag für Bauwesen, Berlin, Akademiai Kiado Budabest, 1969

Krenmayr, Hans Georg, (1991): Sedimentologische Untersuchungen der Vöcklaschichten in der oberösterreichischen Molassezone im Gebiet der Vöckla und der Ager, Jb. Geolog. B.-A., Band 134, Heft 1, 83-100, Wien, 1991

Madsen, Fritz T. & Mitchell, James K., (1989): Chemical Effects on Clay Hydraulic Conductivity and their Determination, Mitteilungen des Institutes für Grundbau und Bodenmechanik Eidgenössische Technische Hochschule Zürich, Nr.135, 1989

Roetzel, Reinhard & Krenmayr, Hans Georg, (1996): Das Tertiär der Molassezone in Oberösterreich, 32-35, in Ein Querschnitt durch die Geologie Oberösterreichs Wandertagung 1996 Exkusionsführer, Österreichische Geologische Gesellschaft, Band 16, Wien, 1996

Wackernagel, Hans, (1995): Mulitvariante Geostatistics, Springer Verlag Berlin Heidelberg, 1995

Waxman, M. H. & Smits, L. J., (1967): Electrical Conductivities in Oil-bearing Shaly Sands, SPE-1863-A, presented at 42nd Annual Fall Meeting: Society of Petroleum Engineers, 1967, 8, 107-122, 1967

Additional used Literature:

Aberer, F., (1957): Die Molassezone im westlichen Oberösterreich und in Salzburg, Mitteilungen der Geologischen Gesellschaft, Band 50, 23-94, Wien, 1957

Adams, John A. S. & Gasparini, Paolo, (1970): Gamma-ray Spectrometry of Rocks, American Elsevier Publishing Company, 1970

Duivenstijn, A. J. & Venverloo, L. A. J., (1964): Praktische Gammaspektrometrie, Philips Technische Bibliothek, 1964

Dutter, Rudolf, (1985): Geostatistic, B.G.Teubner Stuttgart, 1985

Hohn, Michael Edward, (1988): Geostatistics and Petroleum Geology, Van Nostrand Reinhold, 1988

Kohl, H., (1996): Quartäre Sedimente und Landschaftsentwicklung im Welser Raum, 73-74 Exkursionshaltepunkte, 75-93, in Ein Querschnitt durch die Geologie Oberösterreichs Wandertagung 1996 Exkusionsführer, Österreichische Geologische Gesellschaft, Band 16, Wien, 1996

Manning & Hall & Hughes, (1993): Geochemistry of Clay-Pore Fluid Interactions, Chapman and Hall, London, 1993

Rögl, F. & Rupp, Ch., (1996): Stratigraphie in der Molassezone Oberösterreichs, 66-72, in Ein Querschnitt durch die Geologie Oberösterreichs Wandertagung 1996 Exkusionsführer, Österreichische Geologische Gesellschaft, Band 16, Wien, 1996

Schön, J. H., (1996): Physical Properties of Rocks: Fundamentals and Principles of Petrophysics, Handbook of Geophysical Exploration, Section 1, Seismic Exploration: V.18, PERGAMON, 583 pages, 1996

Tollmann, Alexander, (1985): Geologie von Österreich, Band 2, Franz Deuticke, Wien, 1985

Wagner, L., (1996): Die tektonisch-stratigraphische Entwicklung der Molasse und deren Untergrundes in Oberösterreich und Salzburg, 36-65, in Ein Querschnitt durch die Geologie Oberösterreichs Wandertagung 1996 Exkusionsführer, Österreichische Geologische Gesellschaft, Band 16, Wien, 1996

Winter, Peter, (1996): Untersuchungen zur Ermittlung von Kennwerten mineralischer Dichtschichten mit geophysikalischen Verfahren, Leobner Hefte zur Angewandten Geophysik, Band 5, 1-46, 1996

8 Appendix

Sample A2 measured with 6.66 gS/l:

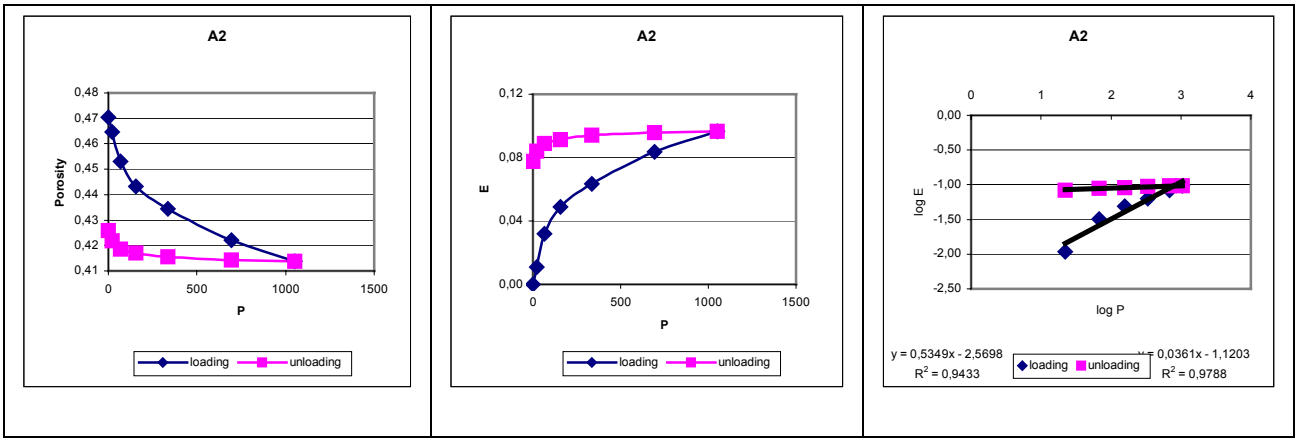

Figure 8.1: Porosity vs pressure, elasticity modulus vs pressure, log of elasticity modulus vs log of pressure for facies A2 measured with 6.66 gS/l

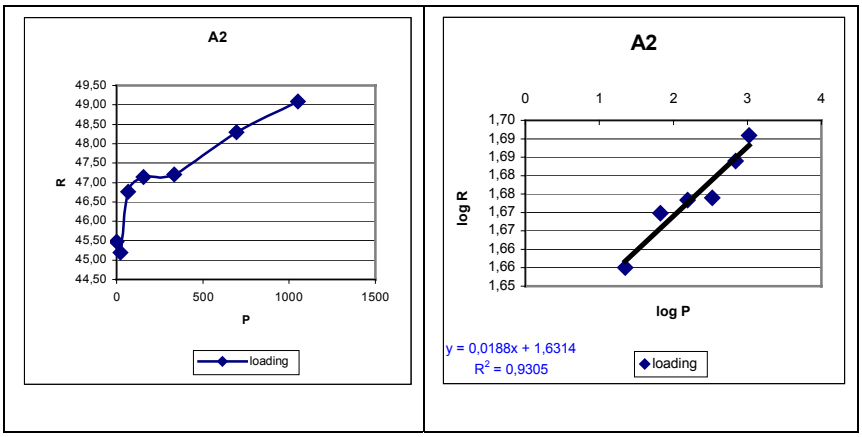

Figure 8.2: Specific electrical resistivity vs pressure, log of specific electrical resistivity vs log pressure for facies A2 measured with 6.66 gS/3l

Sample A2 measured with 13.33 gS/l:

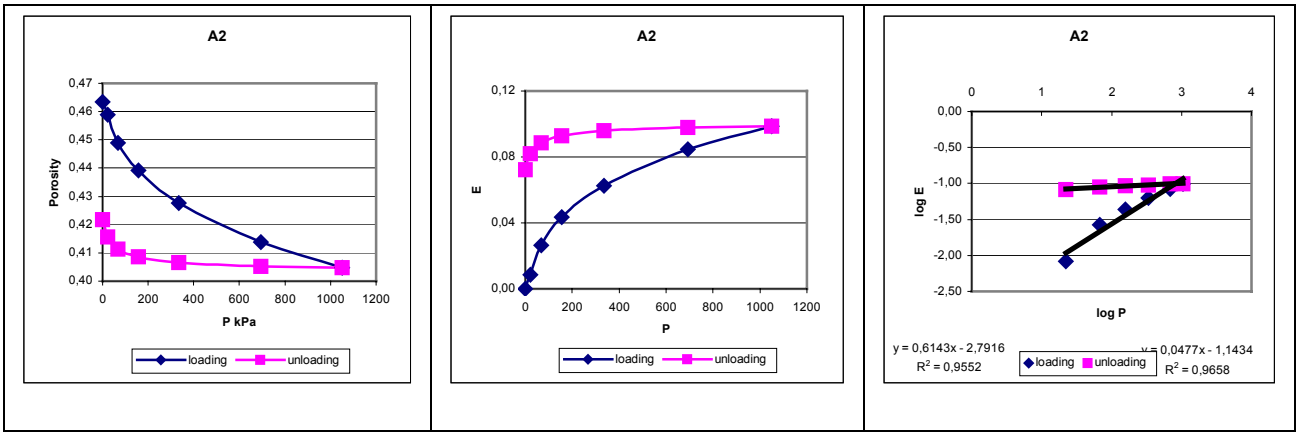

Figure 8.3: Porosity vs pressure, elasticity modulus vs pressure, log of elasticity modulus vs log of pressure for facies A2 measured with 13.33 gS/l

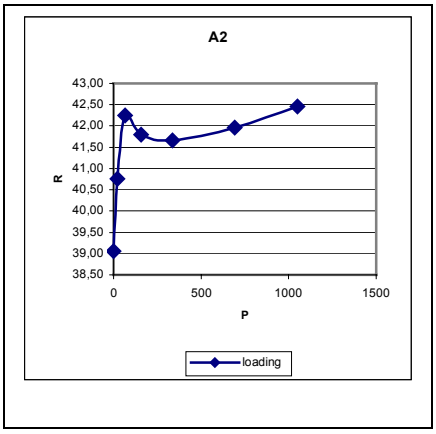

Figure 8.4: Specific electrical resistivity vs pressure for facies A2 measure with 13.33 gS/l

Sample A2 measured with 20 gS/l:

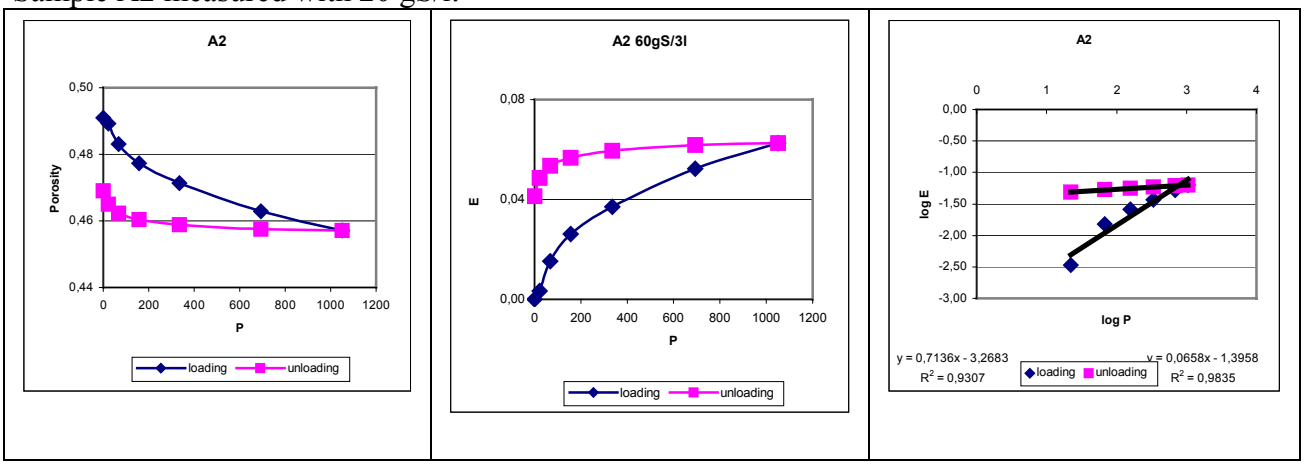

Figure 8.5: Porosity vs pressure, elasticity modulus vs pressure, log of elasticity modulus vs log of pressure for facies A2 measured with 20 gS/l

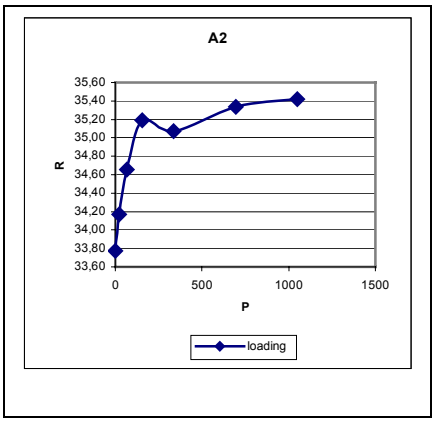

Figure 8.6: Specific electrical resistivity vs pressure for facies A2 measure with 20 gS/l

Sample A3 measured with 6.66 gS/l:

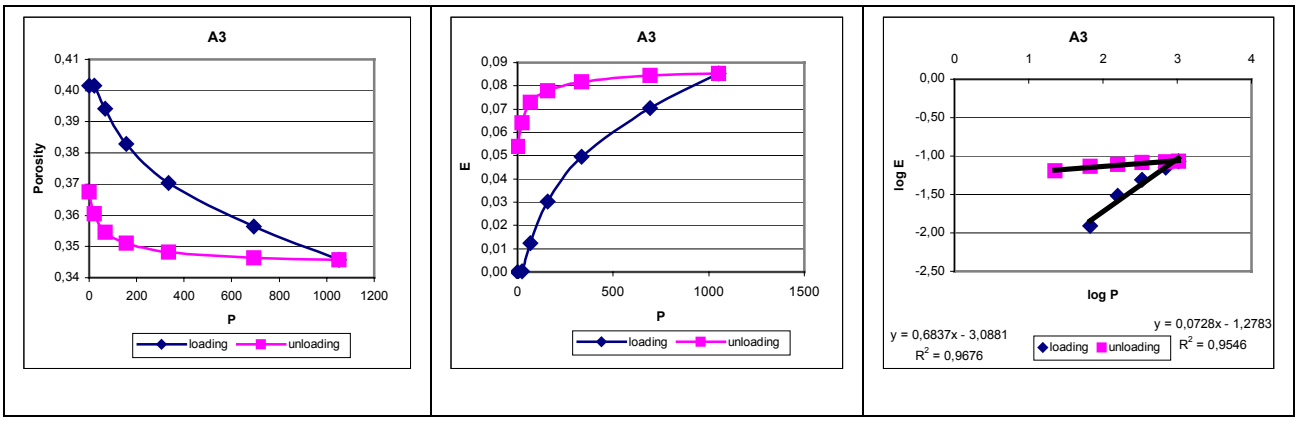

Figure 8.7:Porosity vs pressure, elasticity modulus vs pressure, log of elasticity modulus vs log of pressure for facies A3 measured with 6.66 gS/l

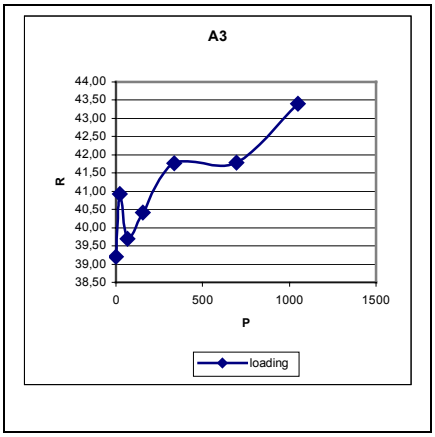

Figure 8.8: Specific electrical resistivity vs pressure for facies A3 measure with 6.66 gS/l

Sample A3 measured with 13.33 gS/l:

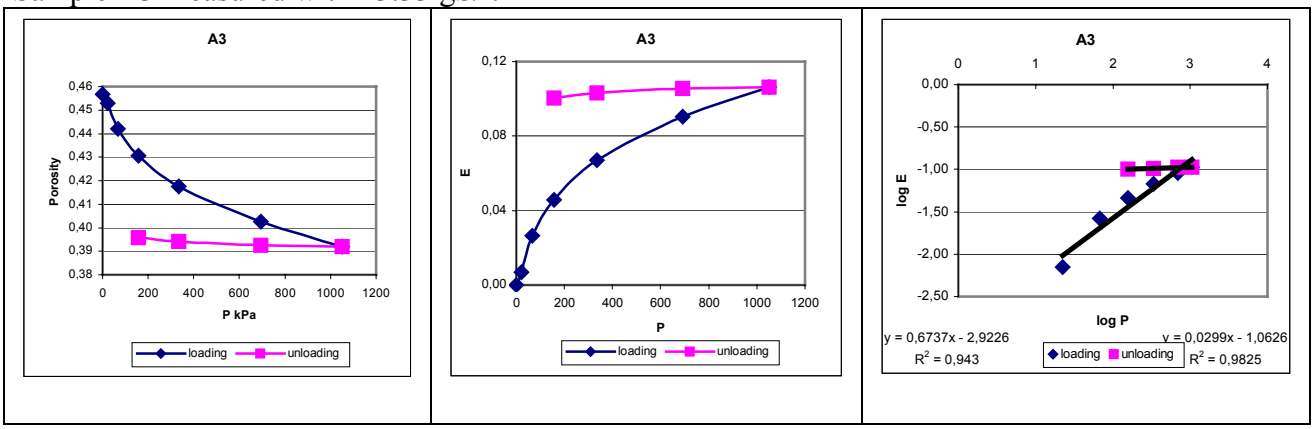

Figure 8.9: Porosity vs pressure, elasticity modulus vs pressure, log of elasticity modulus vs log of pressure for facies A3 measured with 13.33 gS/l

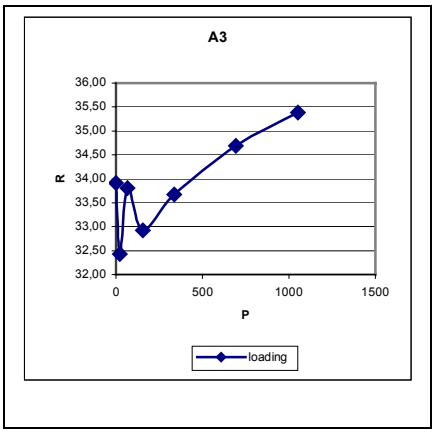

Figure 8.10: Specific electrical resistivity vs pressure for facies A3 measure with 13.33 gS/l

Sample A3 measured with 20 gS/l:

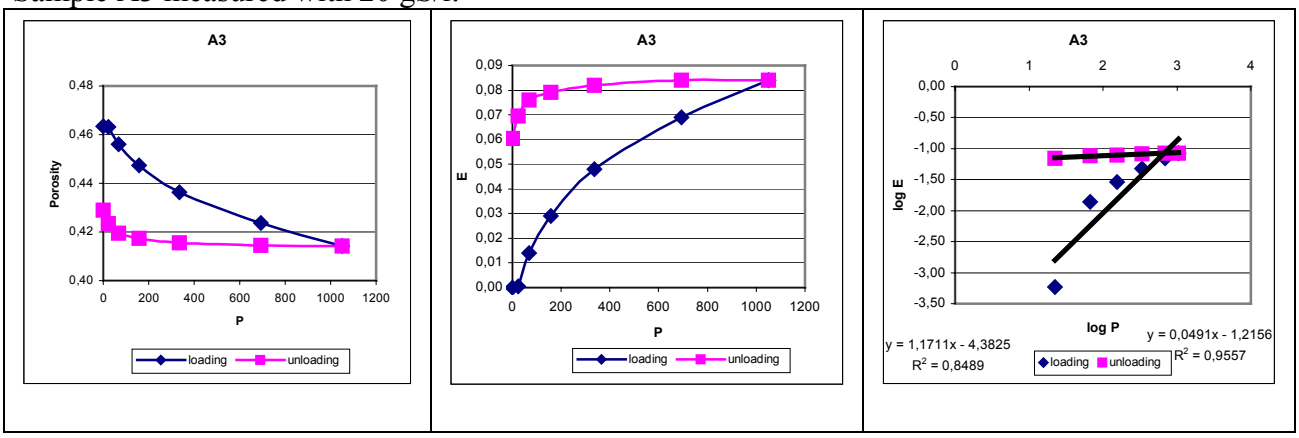

Figure 8.11: Porosity vs pressure, elasticity modulus vs pressure, log of elasticity modulus vs log of pressure for facies A3 measured with 20 gS/l

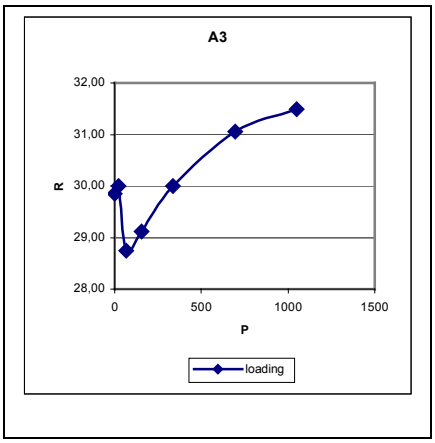

Figure 8.12: Specific electrical resistivity vs pressure for facies A3 measure with 20 gS/l

Sample A4 measured with 0.33 gS/l:

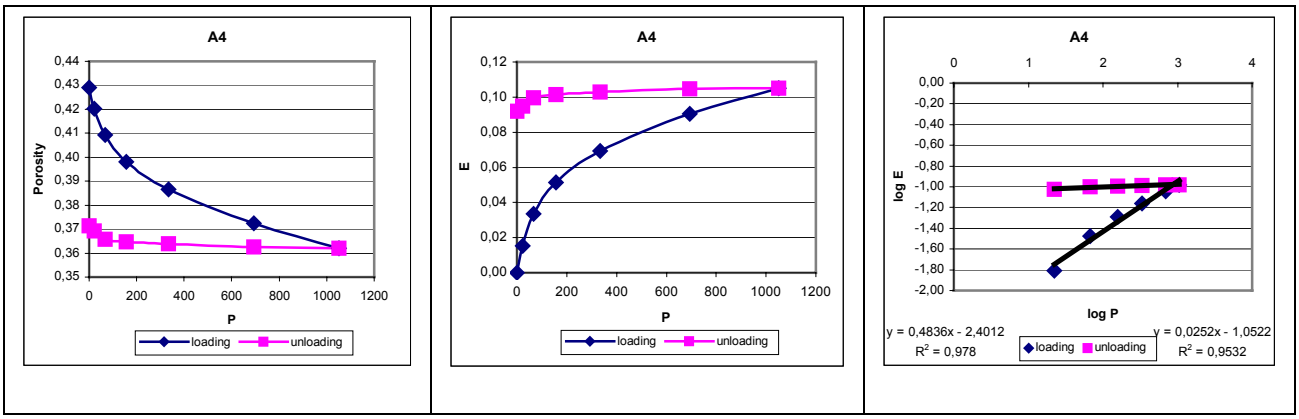

Figure 8.13: Porosity vs pressure, elasticity modulus vs pressure, log of elasticity modulus vs log of pressure for facies A4 measured with 0.33 gS/l

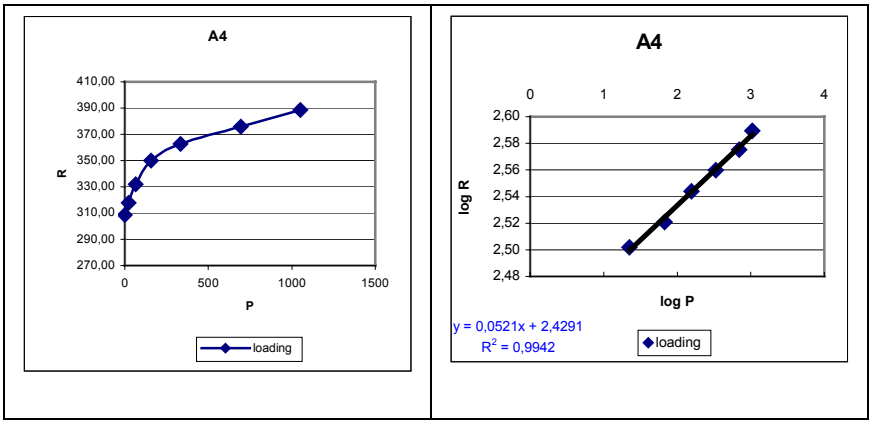

Figure 8.14: Specific electrical resistivity vs pressure, log of specific electrical resistivity vs log pressure for facies A4 measured with 0.33 gS/3l

Sample B1 measured with 6.66 gS/l:

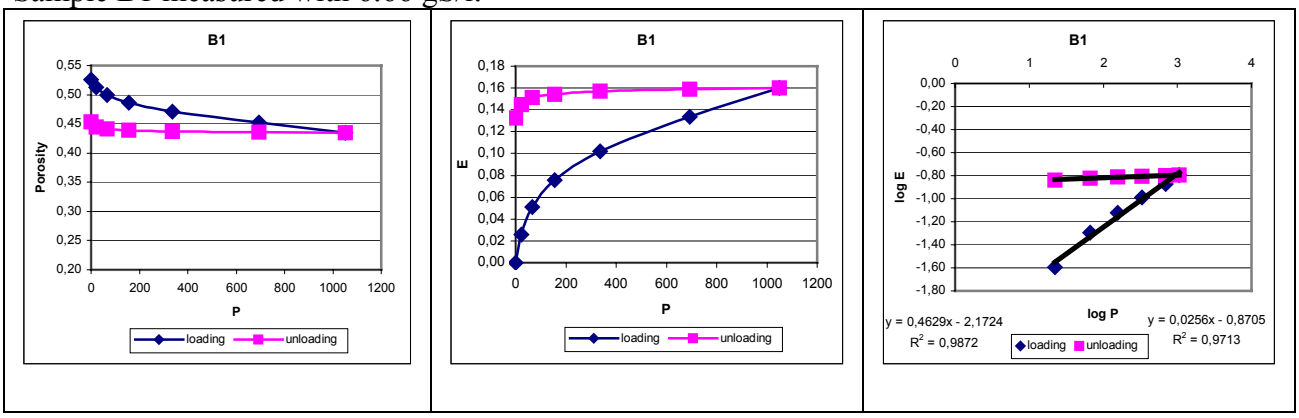

Figure 8.15: Porosity vs pressure, elasticity modulus vs pressure, log of elasticity modulus vs log of pressure for facies B1 measured with 6.66 gS/l

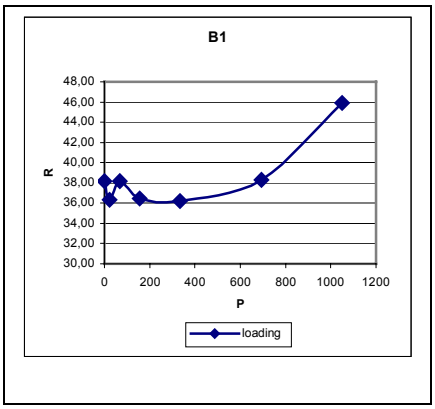

Figure 8.16: Specific electrical resistivity vs pressure for facies B1 measure with 6.66 gS/l

Sample B1 measured with 13.33 gS/l:

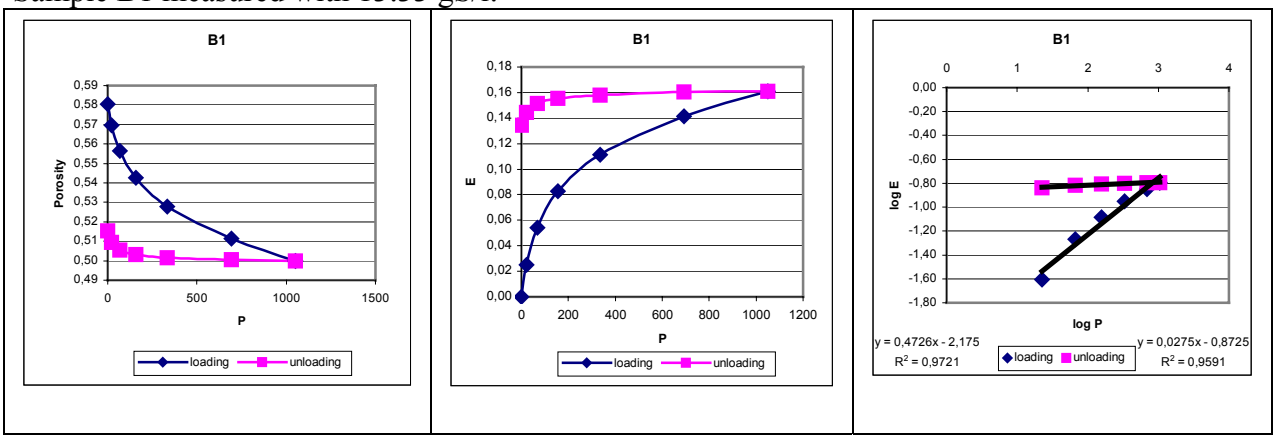

Figure 8.17: Porosity vs pressure, elasticity modulus vs pressure, log of elasticity modulus vs log of pressure for facies B1 measured with 13.33 gS/l

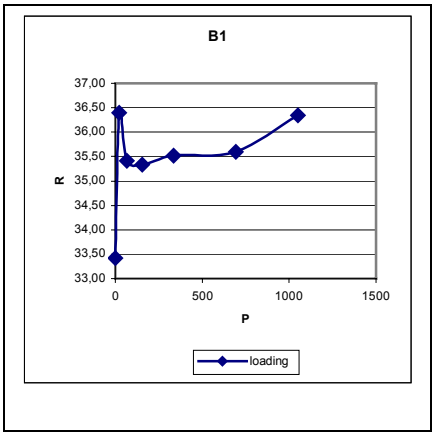

Figure 8.18: Specific electrical resistivity vs pressure for facies B1 measure with 13.33 gS/l

Sample B1 measured with 20 gS/l:

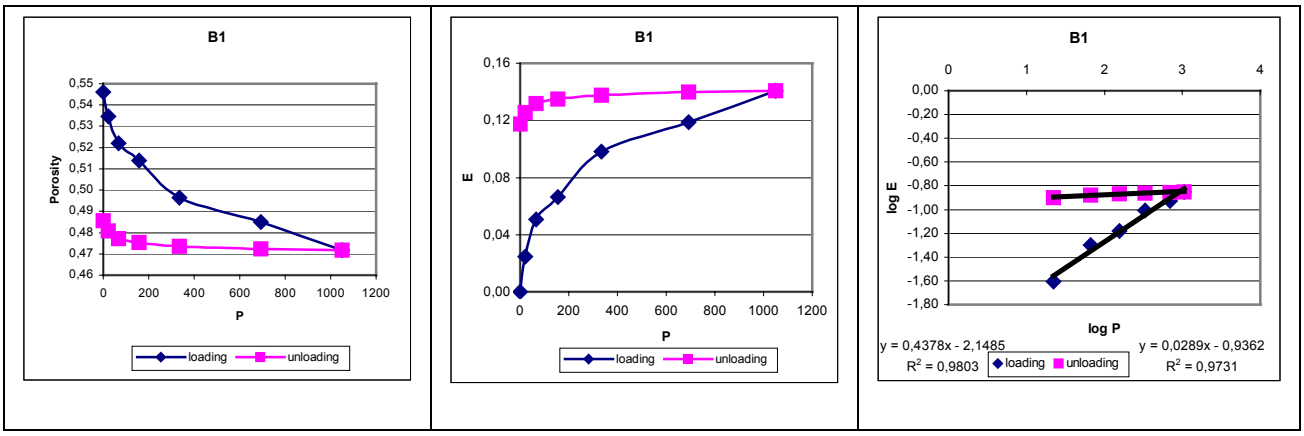

Figure 8.19: Porosity vs pressure, elasticity modulus vs pressure, log of elasticity modulus vs log of pressure for facies B1 measured with 20 gS/l

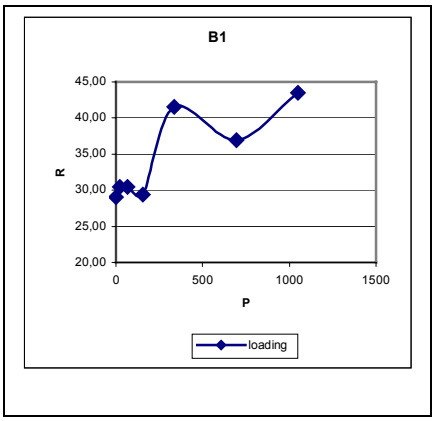

Figure 8.20: Specific electrical resistivity vs pressure for facies B1 measure with 20 gS/l

Sample B2 measured with 6.66 gS/l:

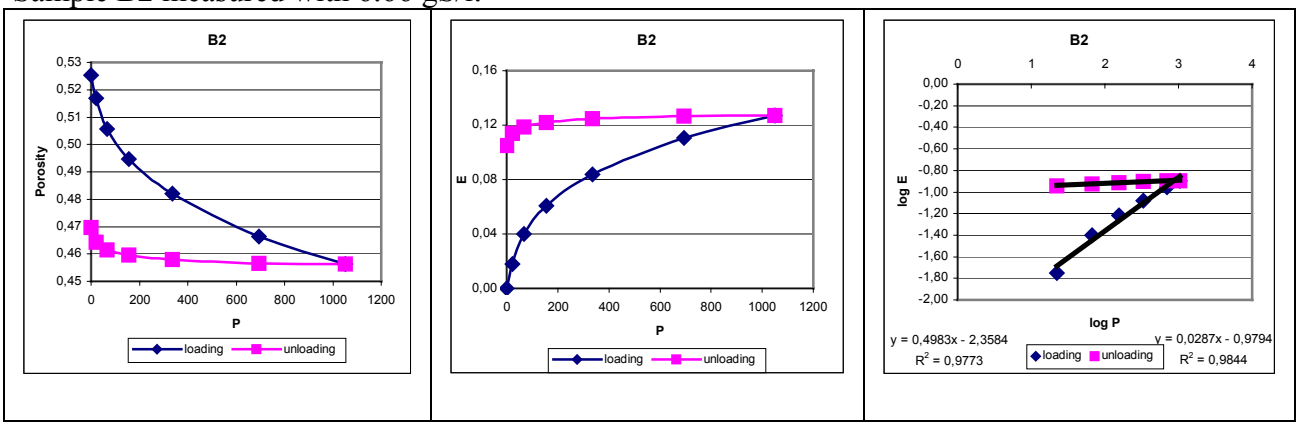

Figure 8.21: Porosity vs pressure, elasticity modulus vs pressure, log of elasticity modulus vs log of pressure for facies B2 measured with 6.66 gS/l

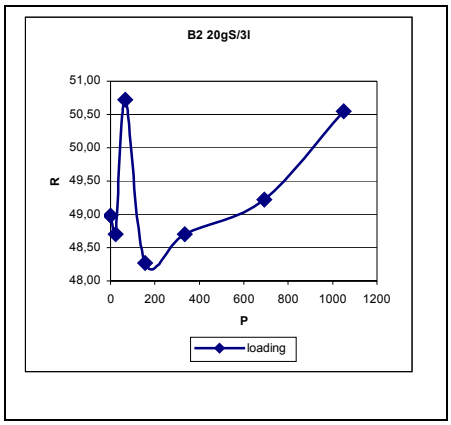

Figure 8.22: : Specific electrical resistivity vs pressure for facies B2 measure with 6.66 gS/l

Sample B2 measured with 13.33 gS/l:

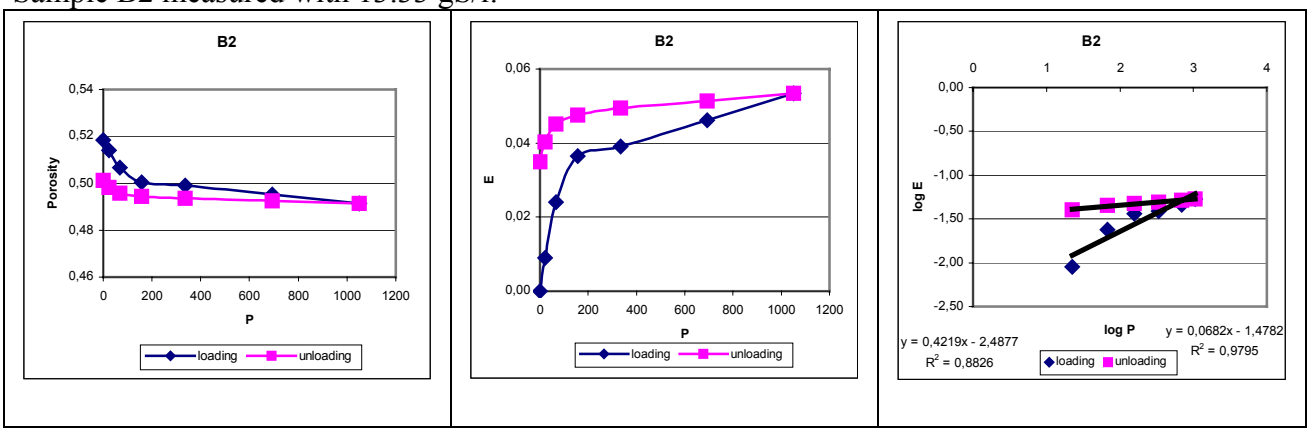

Figure 8.23: Porosity vs pressure, elasticity modulus vs pressure, log of elasticity modulus vs log of pressure for facies B2 measured with 13.33 gS/l

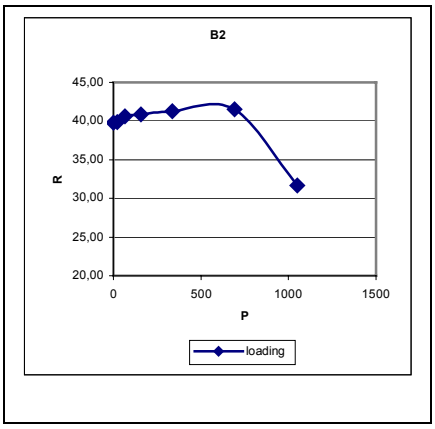

Figure 8.24: Specific electrical resistivity vs pressure for facies B2 measure with 13.33 gS/l

Sample B2 measured with 20 gS/l:

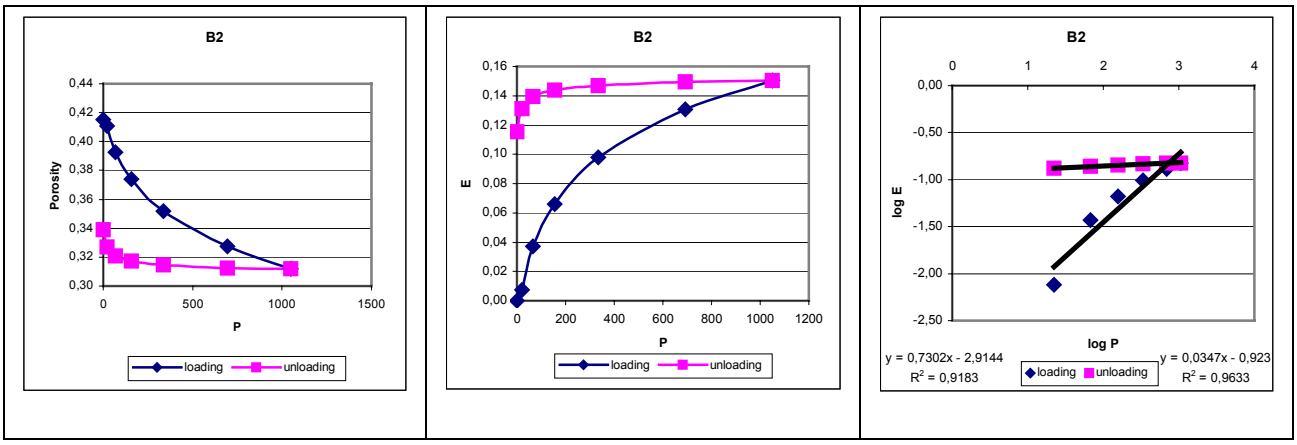

Figure 8.25: Porosity vs pressure, elasticity modulus vs pressure, log of elasticity modulus vs log of pressure for facies B2 measured with 20 gS/l

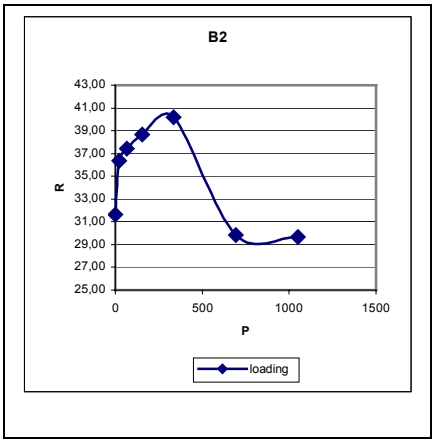

Figure 8.26: Specific electrical resistivity vs pressure for facies B2 measure with 20 gS/l

Sample C1 measured with 6.66 gS/l:

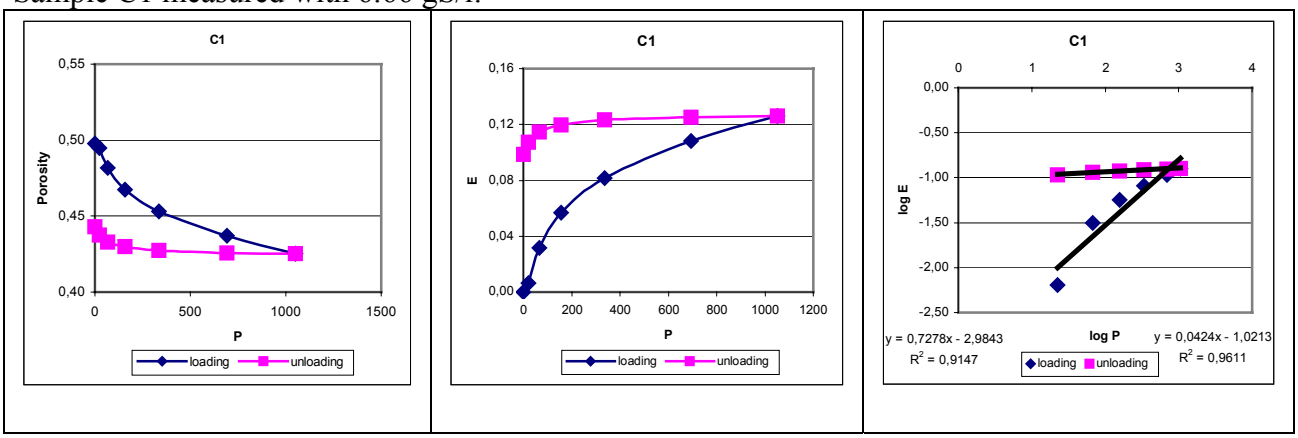

Figure 8.27: Porosity vs pressure, elasticity modulus vs pressure, log of elasticity modulus vs log of pressure for facies C1 measured with 6.66 gS/l

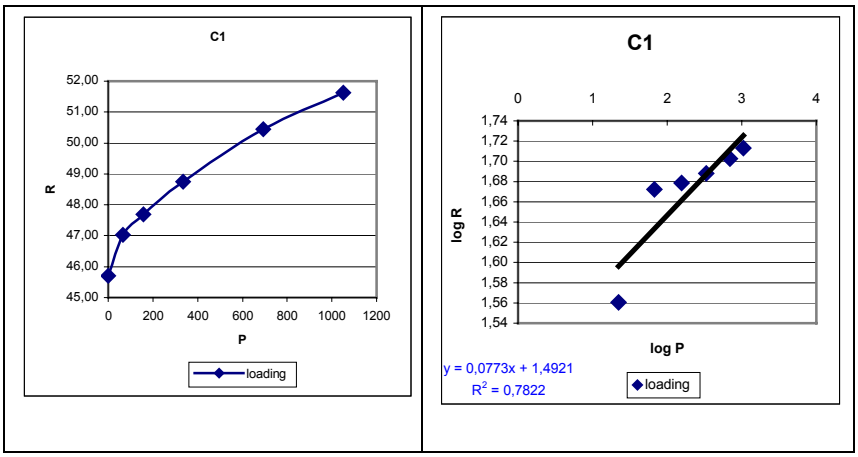

Figure 8.28: Specific electrical resistivity vs pressure, log of specific electrical resistivity vs log pressure for facies C1 measured with 6.66 gS/3l

Sample C1 measured with 13.33 gS/l:

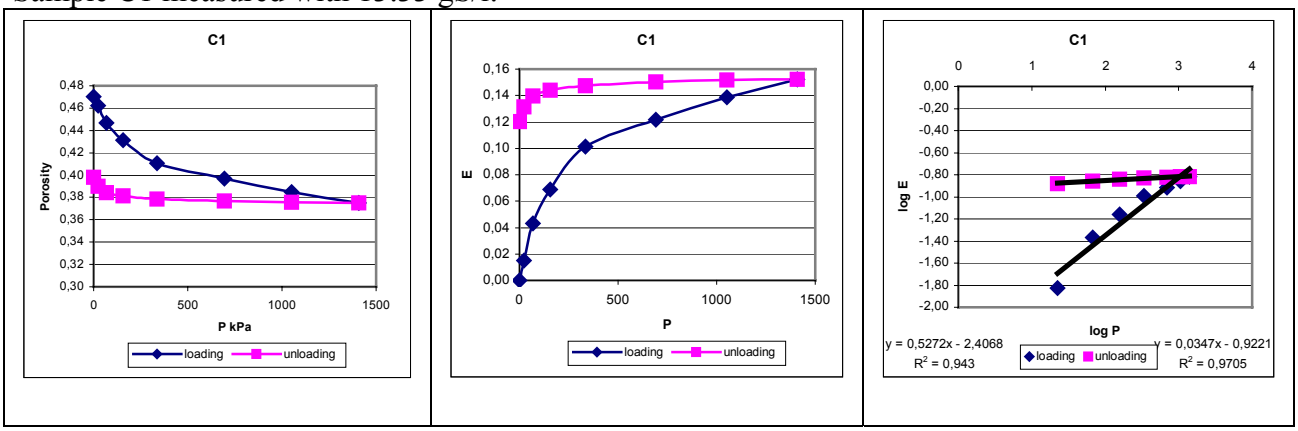

Figure 8.29: Porosity vs pressure, elasticity modulus vs pressure, log of elasticity modulus vs log of pressure for facies C1 measured with 13.33 gS/l

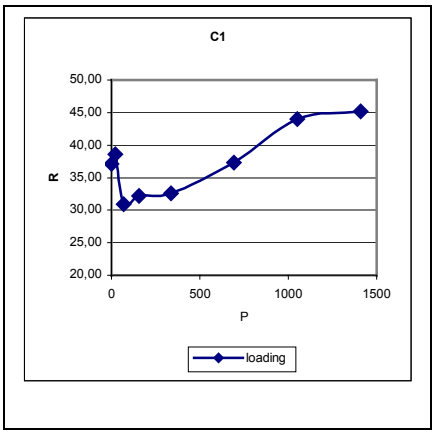

Figure 8.30: Specific electrical resistivity vs pressure for facies C1 measure with 13.33 gS/l

Sample C1 measured with 20 gS/l:

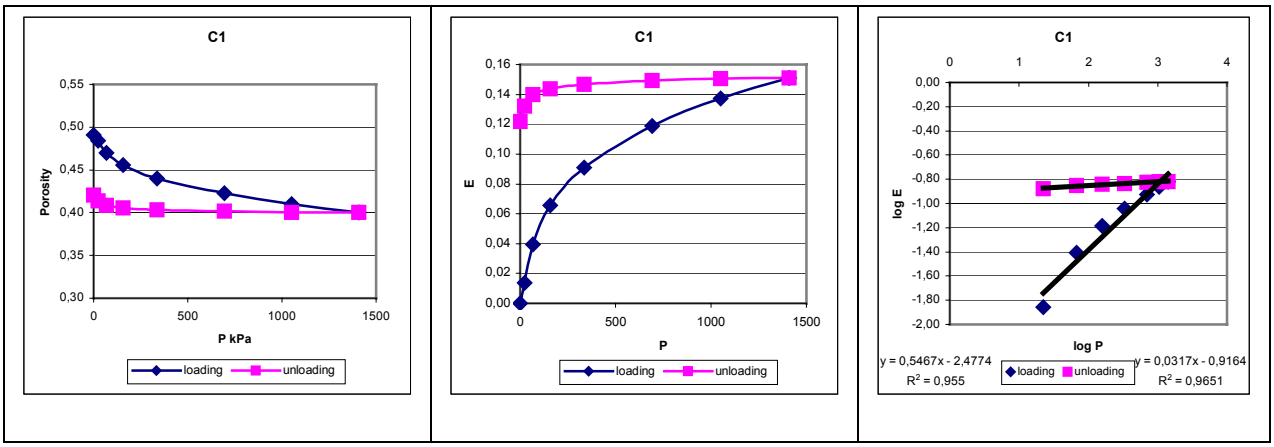

Figure 8.31: Porosity vs pressure, elasticity modulus vs pressure, log of elasticity modulus vs log of pressure for facies C1 measured with 20 gS/l

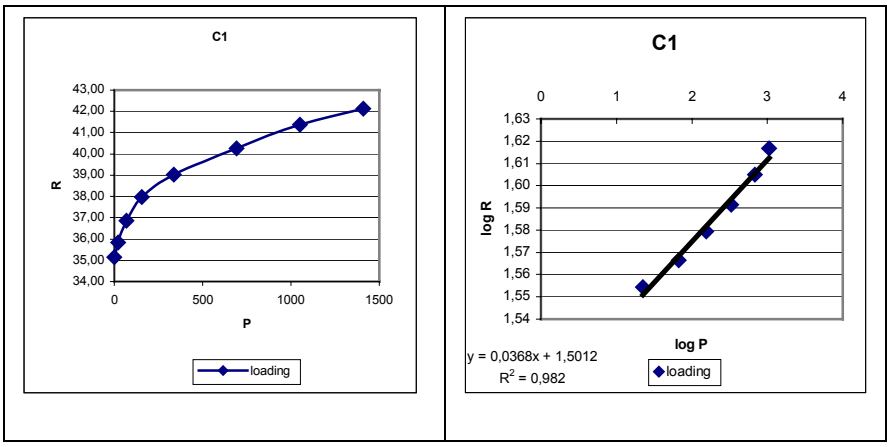

Figure 8.32: Specific electrical resistivity vs pressure, log of specific electrical resistivity vs log pressure for facies C1 measured with 20 gS/3l

Sample C2 measured with 6.66 gS/l:

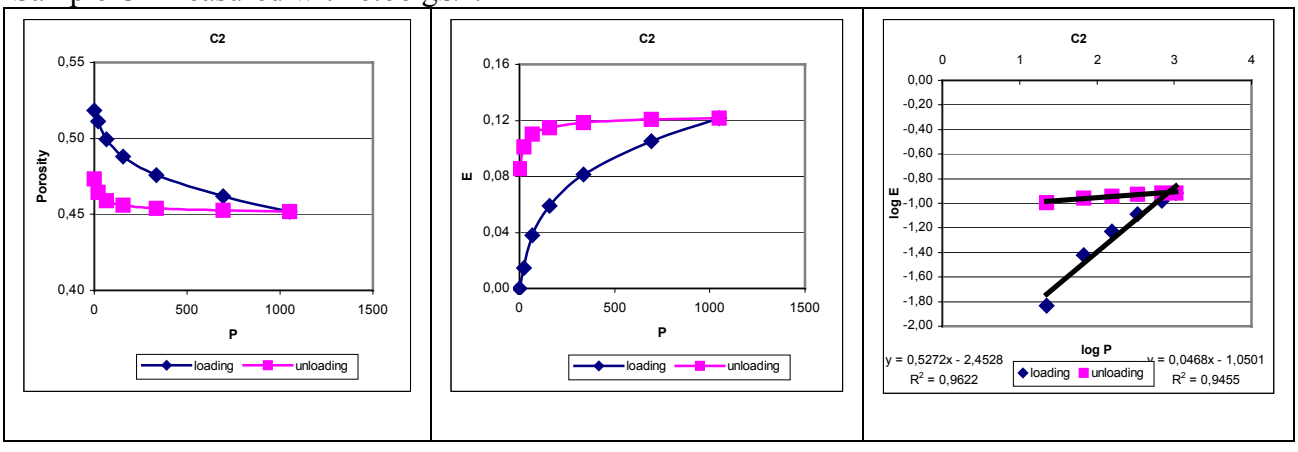

Figure 8.33: Porosity vs pressure, elasticity modulus vs pressure, log of elasticity modulus vs log of pressure for facies C2 measured with 6.66 gS/l

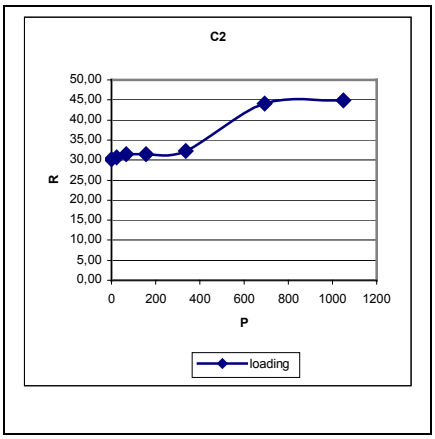

Figure 8.34: Specific electrical resistivity vs pressure for facies C2 measure with 6.66 gS/l

Sample C2 measured with 13.33 gS/l:

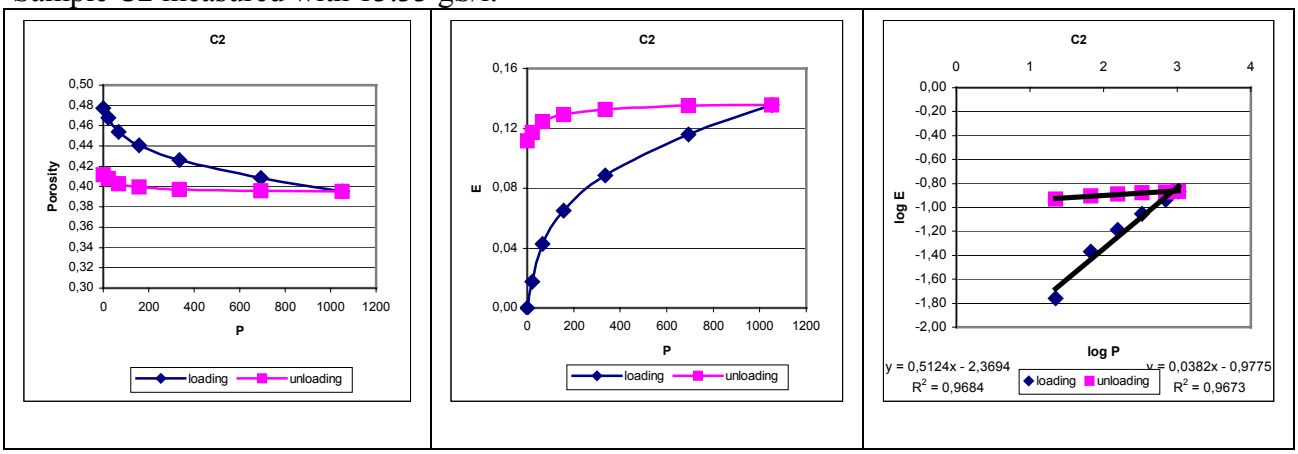

Figure 8.35: Porosity vs pressure, elasticity modulus vs pressure, log of elasticity modulus vs log of pressure for facies C2 measured with 13.33 gS/l

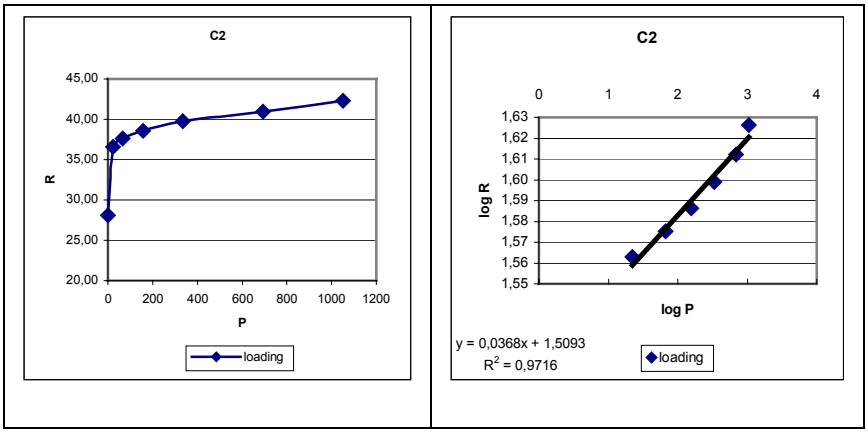

Figure 8.36: Specific electrical resistivity vs pressure, log of specific electrical resistivity vs log pressure for facies C2 measured with 13.33 gS/3l

Sample C2 measured with 20 gS/l:

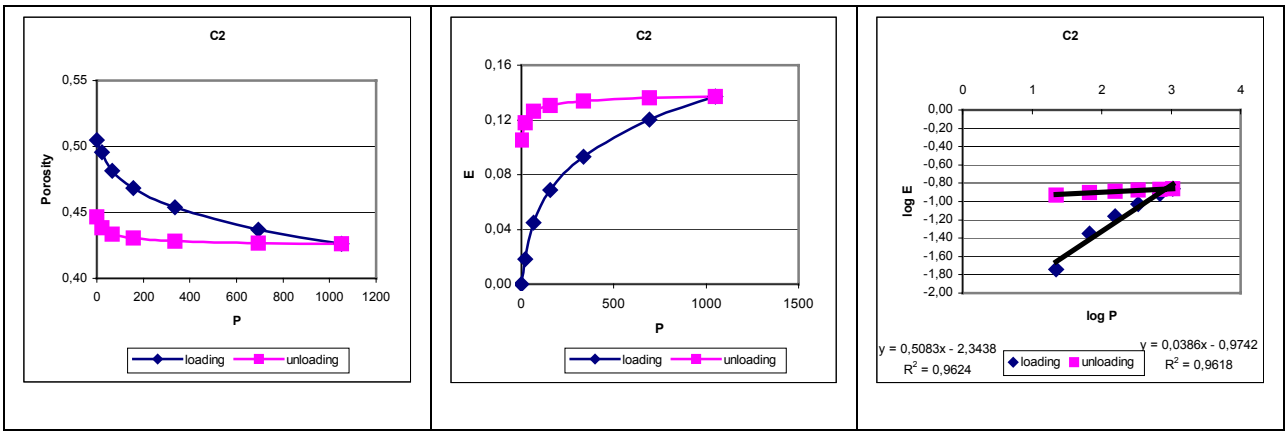

Figure 8.37: Porosity vs pressure, elasticity modulus vs pressure, log of elasticity modulus vs log of pressure for facies C2 measured with 20 gS/l

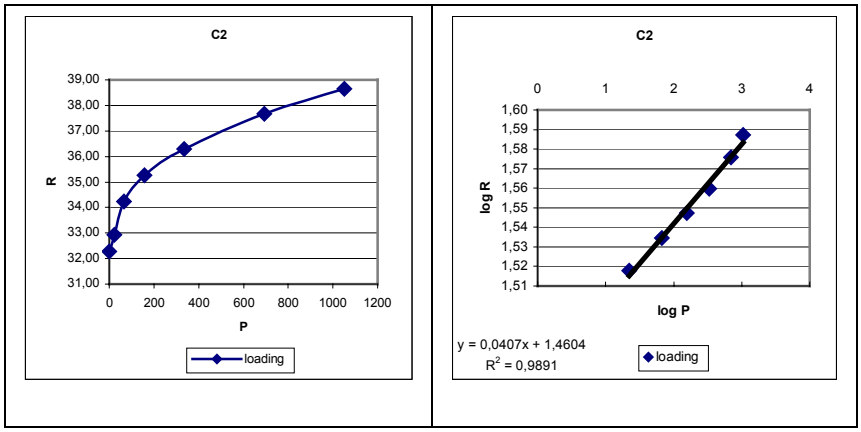

Figure 8.38: Specific electrical resistivity vs pressure, log of specific electrical resistivity vs log pressure for facies C2 measured with 20gS/3l

Sample C3 measured with 6.66 gS/l:

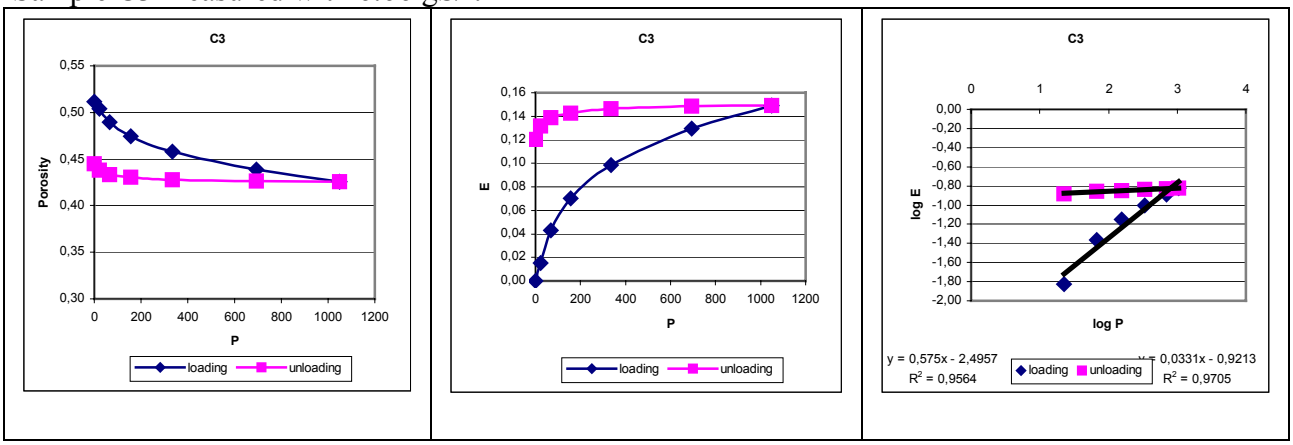

Figure 8.39: Porosity vs pressure, elasticity modulus vs pressure, log of elasticity modulus vs log of pressure for facies C3 measured with 6.66 gS/l

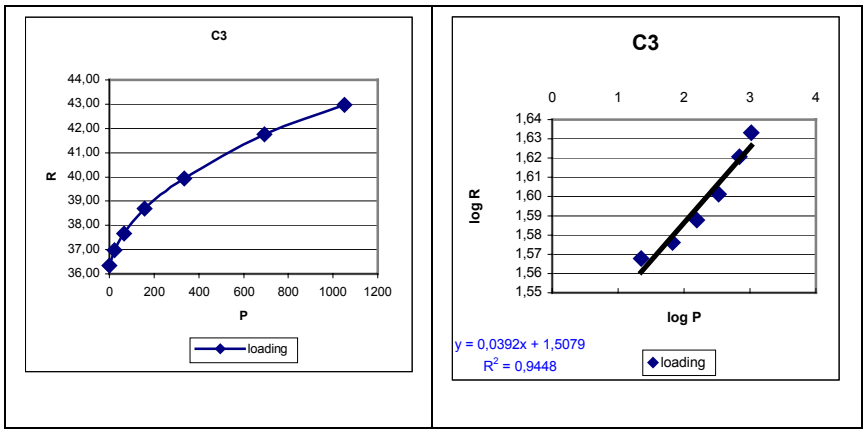

Figure 8.40: Specific electrical resistivity vs pressure, log of specific electrical resistivity vs log pressure for facies C3 measured with 6.66 gS/3l

Sample C3 measured with 13.33 gS/l:

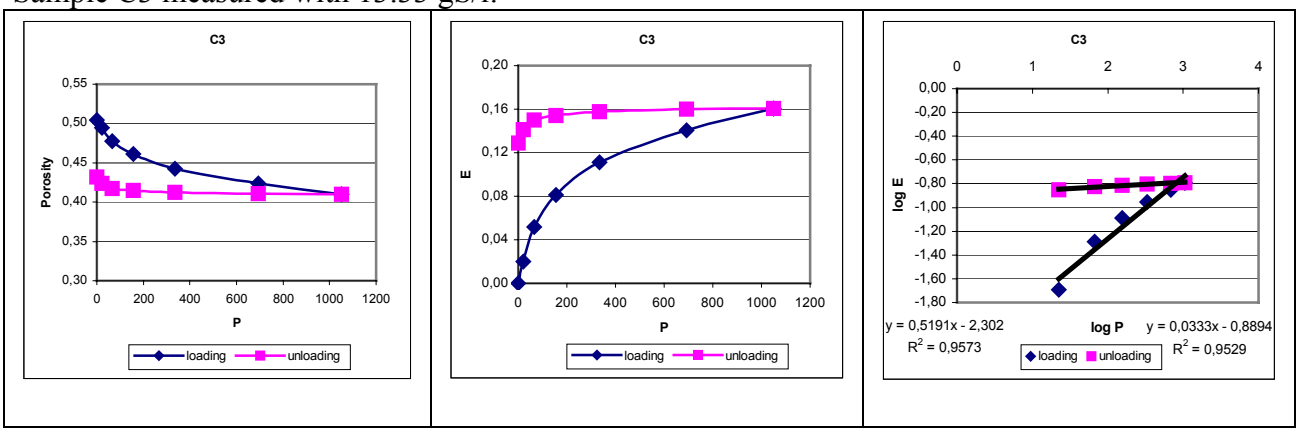

Figure 8.41: Porosity vs pressure, elasticity modulus vs pressure, log of elasticity modulus vs log of pressure for facies C3 measured with 13.33 gS/l

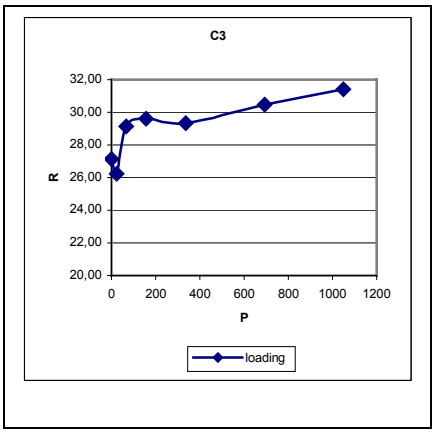

Figure 8.42: Specific electrical resistivity vs pressure for facies C3 measure with 13.33 gS/l

Sample C3 measured with 20 gS/l:

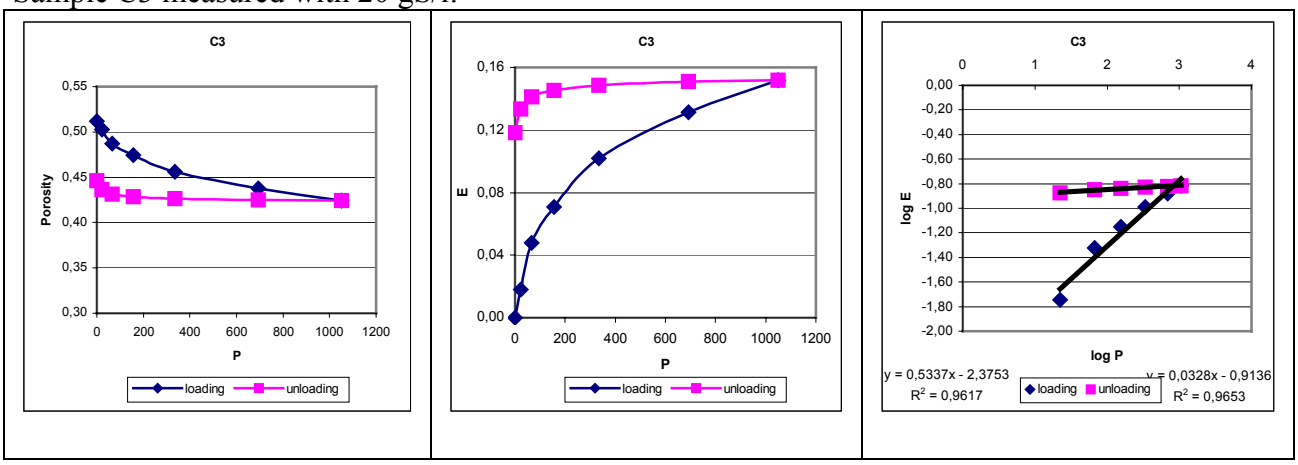

Figure 8.43: Porosity vs pressure, elasticity modulus vs pressure, log of elasticity modulus vs log of pressure for facies C3 measured with 20 gS/l

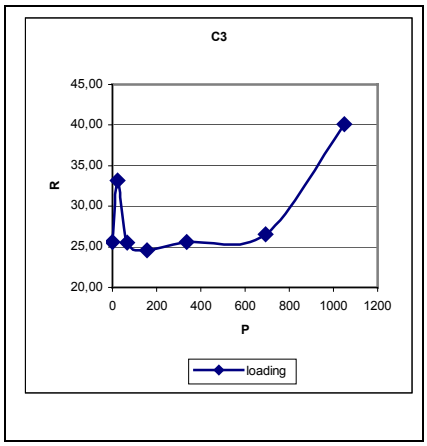

Figure 8.44: Specific electrical resistivity vs pressure for facies C3 measure with 20 gS/l

Sample Ottnanger Schlier measured with 6.66 gS/l:

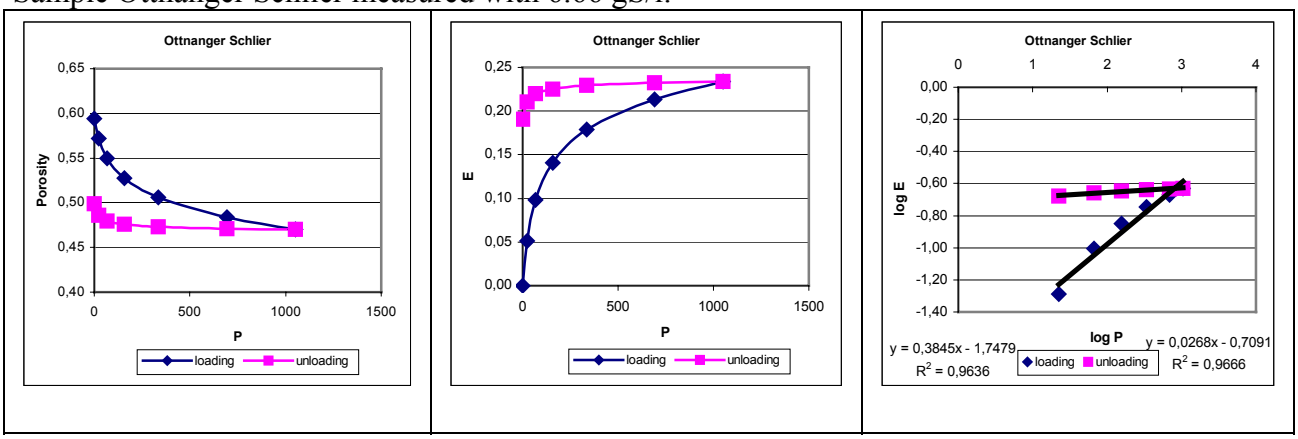

Figure 8.45: Porosity vs pressure, elasticity modulus vs pressure, log of elasticity modulus vs log of pressure for facies Ottnanger Schlier measured with 6.66 gS/l

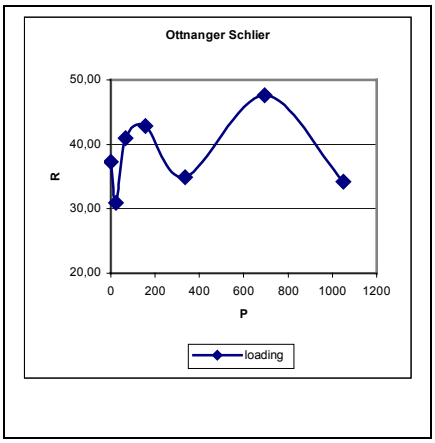

Figure 8.46: Specific electrical resistivity vs pressure for facies Ottnanger Schlier measure with 6.66 gS/l

Sample Ottnanger Schlier measured with 13.33 gS/l:

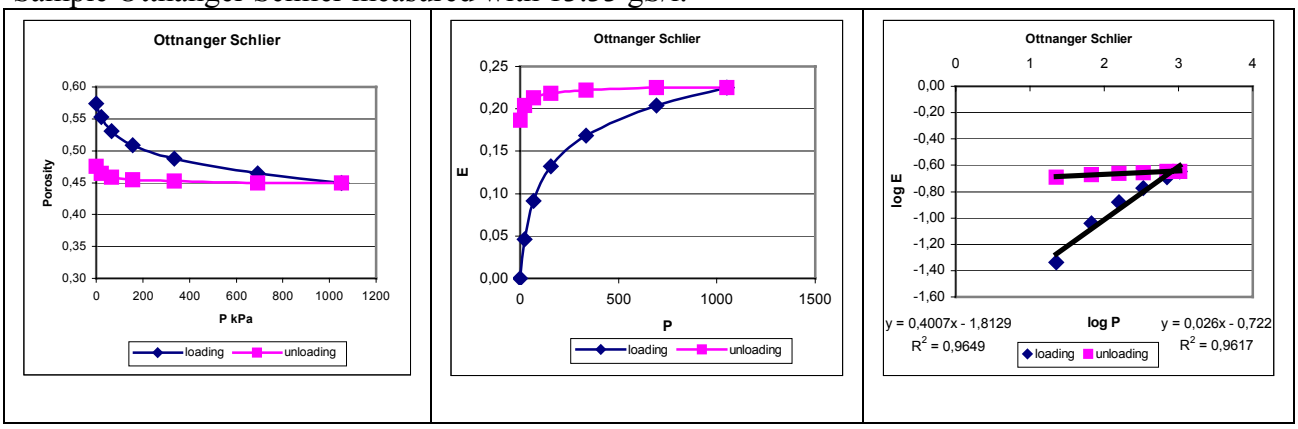

Figure 8.47: Porosity vs pressure, elasticity modulus vs pressure, log of elasticity modulus vs log of pressure for facies Ottnanger Schlier measured with 13.33 gS/l

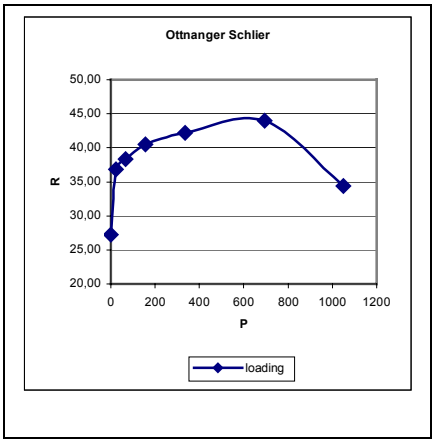

Figure 8.48: Specific electrical resistivity vs pressure for facies Ottnanger Schlier measure with 13.33 gS/l

Sample Ottnanger Schlier measured with 20 gS/l:

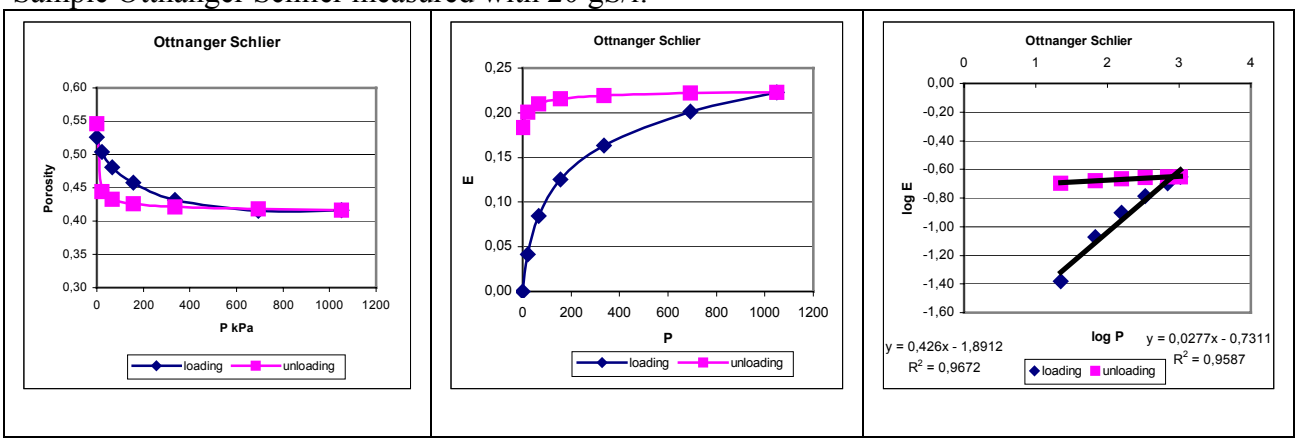

Figure 8.49: Porosity vs pressure, elasticity modulus vs pressure, log of elasticity modulus vs log of pressure for facies Ottnanger Schlier measured with 20 gS/l

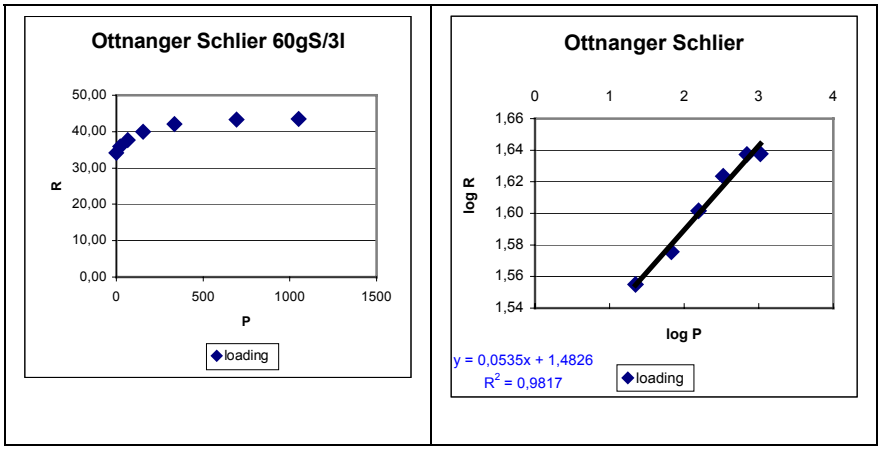

Figure 8.50: Specific electrical resistivity vs pressure, log of specific electrical resistivity vs log pressure for facies Ottnanger Schlier measured with 20 gS/3l